

**UNCOVERING THE EFFICIENCY LIMITS
TO OBTAINING WATER: ON EARTH AND BEYOND**

by

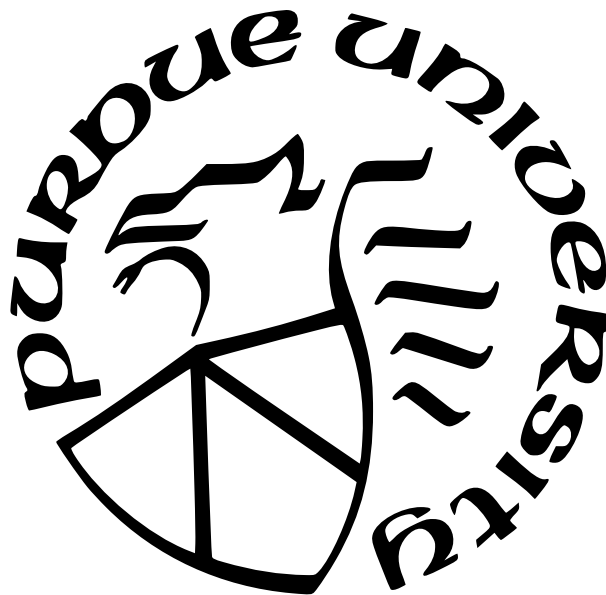
Akshay K. Rao

A Thesis

Submitted to the Faculty of Purdue University

In Partial Fulfillment of the Requirements for the degree of

Master of Science in Mechanical Engineering



School of Mechanical Engineering

West Lafayette, Indiana

May 2022

**THE PURDUE UNIVERSITY GRADUATE SCHOOL
STATEMENT OF COMMITTEE APPROVAL**

Dr. David M. Warsinger, Chair

School of Mechanical Engineering and Birck Nanotechnology Center

Dr. Luciano Castillo

School of Mechanical Engineering

Dr. Jose Garcia-Bravo

School of Engineering Technology

Dr. Ilias Bilonis

School of Mechanical Engineering

Approved by:

Dr. Nicole L. Key

To the leagues of giants, whose shoulders we stand upon.

ACKNOWLEDGMENTS

Special thanks to my thesis advisor, David Warsinger, for his mentorship, academic inspiration, and support over the past four years. Thanks to my committee members: Luciano Castillo, Jose Garcia-Bravo, and Ilias Bilonis, for their guidance towards my academic interests. Thanks to my family and Emeraldal Fong for their constant support. Specific thanks to all the student collaborators of this work: Andrew J. Fix, Abhimanyu Das, Yun Chi Yang, and Owen R Li, as well as all members of the Warsinger Water lab. Finally, thanks to the Purdue University department of Mechanical Engineering, Digested Organics, Bob Boulware, the United States National Renewable Energy Lab (NREL), and the United States Bureau of Reclamation for financial support.

TABLE OF CONTENTS

LIST OF TABLES	7
LIST OF FIGURES	9
LIST OF SYMBOLS	18
ABBREVIATIONS	19
ABSTRACT	20
1 INTRODUCTION	21
1.1 Water scarcity	21
1.2 Common water technologies	21
1.3 In-situ resource utilization in Outer Space	24
1.4 Efficiency metrics in water	25
2 UNCOVERING THE ENERGY EFFICIENCY LIMITS OF OBTAINING WA- TER IN THE SOLAR SYSTEM	27
2.1 Chapter overview	27
2.1.1 Extraterrestrial water sources	27
2.1.2 Extended least work	28
2.2 Results	29
2.3 Conclusions	33
2.4 Methods	34
2.4.1 Least work derivation	35
2.4.2 Property models	37
2.4.3 Validation and error	38
2.4.4 Model limitations	39
2.5 Chapter acknowledgements	40
2.6 Chapter author contributions	40

3	THERMODYNAMIC LIMITS OF ATMOSPHERIC WATER HARVESTING . . .	41
3.1	Chapter overview	41
3.1.1	Atmospheric water harvesting	41
3.1.2	Current water harvesting technologies	42
3.1.3	Energy comparisons	44
3.2	Methods	45
3.2.1	Numerical model	45
3.2.2	Modelling framework	46
3.2.3	Mapping and computing	47
3.2.4	Model validation	48
3.2.5	Assumptions and limitations	48
3.3	Results	50
3.3.1	Energy requirements and process efficiencies	50
3.3.2	Fog and saturated humid air mixtures	53
3.3.3	Energy-optimal water recovery	54
3.3.4	Realistic energy comparison	56
3.3.5	Geospatial analysis	58
3.3.6	Field-wide challenges	59
3.4	Chapter conclusions	61
3.5	Chapter acknowledgements	63
3.6	Chapter author contributions	63
4	CONCLUSIONS	64
4.1	Contributions	64
4.2	Overarching takeaways	64
4.3	Future work	65
	REFERENCES	66
A	APPENDIX: OBTAINING WATER IN THE SOLAR SYSTEM	76
B	APPENDIX: ATMOSPHERIC WATER HARVESTING	92

LIST OF TABLES

A.1	Water-Ice ranges of conditions	87
A.2	Liquid water ranges of conditions	88
A.3	Water vapor ranges of conditions. Vapor pressure is used to represent mixing fraction and ambient pressure due to the ideal gas relationship. The depth is considered for both accessing water at the mean planetary solid surface and the 1bar pressure level. Due to the extreme low pressure on Mars, water is able to stay in the vapor state below 273.15K.	89
A.4	All simulations, except for ZnSO ₄ , use the FREZCHEM thermochemistry database provided by Professor David Catling. Zinc solutions are simulated using the LLNL database. Each trial is simulated at 0.5 molality and 300 K. Trends are validated with prior literature on NaCl and ZnSO ₄ studies of least work and compared to the least work trends of five other relevant binary electrolyte solutions: KCl, MgCl ₂ , CaCl ₂ , Na ₂ SO ₄ , MgSO ₄ . This comparison can be found in Figure 11 of Mistry, Hunter, Lienhard (2013) [21].	90
A.5	Compressibility factor validation. The calculation of the compressibility factor for sub-freezing temperatures is compared to the compressibility factor presented in Wexler (1997) [91]. The maximum percent difference between the two is 0.01%	91
B.1	RH _{desorb} is the relative humidity needed to induce desorption, W _{max} is the maximum water uptake for the MOF, and Δh _{adsorb} is the enthalpy of adsorption for a given MOF. RH _{inflection} is the relative humidity “inflection point” at which the water uptake is 50% of the maximum water uptake (W _{max}). Given the added complexity of considering numerous MOFs, our modeling framework assumes a step-wise increase in water uptake from near-zero to W _{max} at RH _{inflection} . This enables easy modification of the model for new MOF materials so other researchers can make use of the model. It also presents an idealized scenario for the MOFs. All information and assumptions are used from prior work [30], [80].	94
B.2	Comparison of assumptions to prior literature	103

B.3 One calculation that is carried out in the same manner between both models is the minimum desorption temperature. Both models can take a known/assumed absolute humidity of the incoming air stream and determine the temperature for which that absolute humidity is 10% relative humidity. This work heats ambient air to attain the desorption relative humidity, whereas Kim et al. (2020) uses a saturated air stream at 25°C from the recirculation process. By setting the ambient condition to 25°C and 100% RH in our model, we confirmed that our model would calculate a desorption temperature of 71°C, which is the minimum temperature determined by Kim et al. (2020). While this is only a small portion of the models, it is nonetheless a shared calculation between the two models which were matched. Furthermore, the cycle model for the single-cycle recirculation system presented by Kim et al. (2020) was replicated for MOF-801 B.7. The foundational assumptions about operating conditions for both models match and can reproduce results of the prior published work. 106

LIST OF FIGURES

1.1	Overview of separation technologies used for water, according to the required pore size. This figure was used from [8] and was originally created by [9]	22
1.2	Overview of AWH technologies (outer circle) and fundamental process categories (inner circle). Images in the inner circle include: Dropwise condensation on a tube (Dew, [12]); SEM Polysulfone–graphene oxide composite membrane (Membrane, [13]); SEM graphene structured fog net (Fog, [14]); Optical microscope MOF-303 (Sorbent, [15]).	23
1.3	The energy requirements and sources of water available on a representative set of planetary bodies within the solar system. The phase available refers to the thermodynamic state of the available water source (i.e., water-ice, saline liquid brines, and water vapor). The average conditions are informed by literature of planetary spectroscopy measurements and planetary formation models. The thermodynamic framework and detailed energy calculations are described further in Ch. 2.	25
2.1	Least work of water harvesting. a , The two plots describe an upper and lower bound for the least work of desalination for liquid water mixtures of relevant two-component electrolyte solutions in the solar system. The lower and upper bounds are found by comparing the least work of ten binary aqueous solutions that are relevant to existing liquid water sources in the solar system [21]. The axis bounds were limited to provide a meaningful comparison, since solubility varies for each species. b , The contour of least work is shown for isothermal water extraction from water vapor in a planet body’s atmosphere. The relative humidity represents the vapor pressure as a fraction of the saturation pressure at a given temperature. The axes maximize the range of validity of the thermodynamic models. The blue-green-yellow color contour (0–12 kJ/kg) numerically matches values in part A. c , Least work required to obtain water from pure ice is shown as a function of the ambient temperature. The desired temperature is assumed to be 300K (near the average temperature on Earth). Each sub-figure considers the case where the water source is on the surface of the planet (in this, the change in gravitational potential is negligible).	30

2.2	<p>Comparison of least work on planetary bodies with known conditions. A. The least work energy consumption, modeled by Eq. 2.1 for each considered source, is plotted on a logarithmic scale, with the expected value shown. The averages for water-ice and water vapor sources are depicted in light blue and orange, respectively. Each colored bar is separated into up to three components (heating, separation, and gravitational energy), representing the energy contributions, to the total least work energy. When a source is not available on a given planet or an energy component of least work is zero, the respective color or bar is left out. The data points (black) represent the minimum, maximum, and median, as given by the Latin hypercube sampling approach. The error bars are overlaid to represent the population standard deviation, accounting for the sample size. Variation in dynamic weather conditions uses uniform distributions of parameters within observed ranges (Materials and Methods, Table B.1). B. The original sources of data are classified into categories based on the type of vehicle that was used.</p>	32
3.1	<p>A comparison of experimental atmospheric water harvesting technologies including fog [63], [72], [73], dew [16], [62], [74], membrane [16], [75], [76], and sorption [16], [26], [77], [78]. ^aCloud seeders and chillers do not have a unified metric for area, SEC, or SWP. ^b Passive systems are denoted as SEC = 0. In reality, the energy is supplied by natural energy harvesting, bypassing electrical energy conversion.</p>	44
3.2	<p>Energy requirements for water harvesting vary based on the driving force and ideal processes. a. The minimum least work ($W_{\text{least,min}}$) or thermodynamic minimum energy requirement irrespective of the process, is plotted as a contour variable on the psychrometric chart (B.1). The intermediate white lines represent constant relative humidity ranging from 10% to saturation. The least work assumes an infinitesimal recovery ratio (the amount of water removed from the available water in the air), which represents the minimum thermodynamic change to the environment. Near the top left corner (RH = 100%), the least work approaches 0 kJ/kg. b. The second law efficiency (η_{II}), of an ideal dew collection device (B.3) is found as the minimum energy consumption of dew divided by the least work. The energy consumption of dew harvesting is evaluated at the optimal recovery ratio, described in Fig. 3.3. The intermediate white lines represent constant relative humidity ranging from 10% to saturation. c. The efficiency of an ideal open-system membrane water harvesting device with the Claridge-Culp-Liu configuration (B.10). The recovery is set at 65% to maintain consistency with the sorbent process. d. The efficiency of an ideal MOF process (B.5) consisting of four MOF materials is found as the minimum energy consumption for the MOF process divided by the least work. The dotted line denotes the shift between two sets of desorption conditions (B.8). All cooling and heating are provided using Carnot devices and pumping is shown as isentropic.</p>	51

3.3	<p>Optimal recovery for ideal dew harvesting systems. a, The recovery ratio shows the amount of water that is collected in the liquid phase, as a fraction of the total amount of water in the ambient air. The energy requirement of dew harvesting is shown as a function of the recovery from the ambient air for various ambient conditions, where the optimal recovery occurs at the minimum of each frontier. The horizontal axis is stopped at 0.5 to avoid frost-inducing conditions ($T_{\text{cond}} < 273.15K$). b, The optimal recovery ratio to minimize energy consumption for dew harvesting is shown on the contour axis of the psychrometric chart. Each point aims to minimize the function shown in a, subject to constraints: $0 < R < 1$ and $T_{\text{cond}} > 273.15K$. R is the recovery ratio and T_{cond} is the condensation temperature (Shown as T_3 in S3). The labelled white lines represent constant relative humidity.</p>	55
3.4	<p>The energy-optimal AWH technology, under realistic component-level assumptions, varies with the ambient conditions. a, The modelled energy requirements are shown for the three active water harvesting processes, under ideal-component efficiency assumptions. The comparison is shown near room temperature (300K), on a logarithmic scale. The minimum energy requirement (black) refers to the least work at the ambient condition. a, The dew, membrane, and sorbent energy consumptions are shown under realistic component-level assumptions with heat transfer COPs of 3, vacuum pump efficiencies of 20%, and compressor efficiencies of 65%. c, The ideal processes are compared on the basis of maximum exergy-efficiency, where the membrane process is limited at $r = 65\%$. d, The energy-optimal deployment is compared under realistic assumptions.</p>	57
3.5	<p>The least work for 2021 is computed using hourly satellite reanalysis data. This map shows the geographic distribution of the energy requirements for atmospheric water harvesting. The light-blue shade represents geographic regions where water harvesting may encounter barriers with frost accumulation (average temperature < 274 K). The map uses the surface air temperature, humidity, and pressure in hourly increments at 2m from January 1, 2021 to December 31, 2021. The raw data has a resolution of $0.625^\circ \times 0.5^\circ$ and is from the NASA MERRA-2 reanalysis project [82]</p>	60
A.1	<p>Extended least work model visualization: The least work can be modeled as a staged, fully reversible process. The input and reject streams represent the feed and brine. These are evaluated the natural temperature of the source. The pure water from the input mixture is separated, isothermally using the minimum separation work. It is then brought to the Earth standard conditions, via the work due to heating. A third stage can be similarly added when gravitational potential is applicable.</p>	76

A.2	PHREEQC model validation: A comparison of activity coefficient values to validate the thermochemical property models in PHREEQC is shown [CITE 1,2]. The activity of water, Na+, and Cl- are compared to prior literature for the thermochemical databases used in this study. The comparison was done at 300K and 0.596M (seawater salinity). The PHREEQC (default) and Livermore National Lab (LLNL) databases are publicly available at USGS. The Frezchem database is provided by Professor David Catling and Dr. Jon Toner [20], [23], [46]. Experimental values are provided at M = 0.6 from Chirife and Resnik (1984). . . .	77
A.3	Equation of state specific Gibbs free energy validation. The analytical EOS represents the property calculations based on the compressibility factor correlations, presented in methods. The CoolProp database of properties is validated against ASHRAE property standards [57].	78
A.4	Equation of state least work of separation validation. The calculation assumes an isothermal process at the thermodynamic dead state temperature (300K) to isolate the separation energy. The analytical equation of state (blue) and CoolProp property database (orange) are used for pure water vapor. The CoolProp database for humid air properties (green) is additionally used for comparison [57].	79
A.5	Equation of state least work of heating validation. The calculation assumes an isobaric process at saturation (RH = 100%). The analytical equation of state (blue) and CoolProp database (orange) are used for pure water vapor. Regardless of the equation of state, the least work approaches zero at the thermodynamic dead state.	80
A.6	Equation of state least work of heating validation. The calculation considers the total least work at ambient conditions that are well defined by the CoolProp database [57]. The relative error is calculated by $err = 100 \left(\frac{W_{analytical} - W_{CoolProp}}{w_{analytical}} \right)$. The majority of the error may be attributed to the compressibility factor correlations since a 1st order Taylor series expansion in pressure was used. As shown by Wexler (1977) [91] this error is reduced to less than 1% at temperatures below 273K, and therefore the range of this plot show the conditions of maximum model error.	81
A.7	Water harvesting from air and pure water vapor mixtures. This considers the full parametric sweep for water harvesting. The single-component version (left) assumes Dalton's law and ignores other components in the mixture. The air version (right) assumes water is in a standard air mixture and accounts for energy interactions between mixture components. Nearly inert water vapor mixtures, like air, can behave as an ideal gas at low humidity. Water vapor on other planets is often found at low vapor pressures and concentrations. This suggests that the least work at low temperatures and humidity behaves similarly when computed with full mixture properties and water vapor partial properties. . . .	82

A.8	Extended model of NaCl brine separation. Axes bounds represent the range of model validity. NaCl properties resemble water solutions on Earth and fall in between the upper and lower bounds shown in the manuscript Fig 2.1. For reference, most conventional waters on Earth are less than 1m.	83
A.9	Extended model for magnesium sulfate brine separation. Axes bounds represent the range of model validity. White space signifies supersaturation. Magnesium sulfate solutions fall in between the upper and lower bounds shown in the manuscript.	84
A.10	Irreversibility of transient heating in physical mixtures like regolith. The heat capacity contribution of water encompasses the relative mass and specific heat capacity of water and the other species in the physical mixture.	85
B.1	a, Process schematic describing ambient air (1) flow being dehumidified (2) through an ideal atmospheric water device. The definition of the thermodynamic minimum represents a steady state, isothermal process. The thickness of each arrow qualitatively represents the relative magnitude of the mass flow rate. The color of each arrow represents the amount of water in the given stream, with more saturated colors signifying more water. The graph qualitatively describes the temperature (vertical axis) along the ideal process (horizontal axis). b, The thermodynamic state of the air stream is described on the psychrometric chart. Beginning at high humidity, and isothermally moving to low humidity. The change in absolute humidity between states 1 and 2 corresponds to the mass of water collected.	98
B.2	The least work trends are similar to those shown in previous analyses in desalination and with thermal-MOF systems [21], [24], [30]. The minimum least work is evaluated with the limit as recovery goes to zero. This trend varies significantly by the relative humidity.	99
B.3	a, The process schematic describes an ideal dew water harvesting device. Ambient air enters at the ambient temperature (1), is cooled to the dew point for condensation (2) (by a Carnot-like device), and then exits at a saturated state at the condenser temperature (3). The graph qualitatively describes the temperature of the air (vertical axis) along the dew harvesting process (horizontal axis). b, The dew process for the humid air stream is visualized on the psychrometric chart. The difference in humidity between (1) and (3) represents the mass of water collected.	100

- B.4 The figure shows the recovery associated with subcooling a humid air mixture to the frost accumulation temperature. The lower bound of condenser temperature is limited by frost accumulation, and here is set to 273.15K. Lower condenser temperatures, or larger subcooling, induces higher recoveries and yields. In the case of a constant COP with respect to temperature, maximizing the recovery also maximizes the process efficiency. However, as shown by Fig 3.3 in the main text, when the COP is inversely proportional to the temperature difference, as is the case with a Carnot-device and many practical cooling systems, there is a trade-off between maximizing yield and efficiency. 101
- B.5 a, The MOF process aims to concentrate water vapor within a structure in cycles, to increase the humidity for more efficient condensation. The psychrometric chart represents the humid air states in the process. Ambient air (1) is heated to a low relative humidity (2) where it can desorb the water contained within the MOF. To facilitate desorption, the MOF must be heated to a pre-defined relative humidity. The humidified air (3) is then sent to a condenser to extract water similar to the dew harvesting process. The graph qualitatively describes the temperature (vertical axis) along the desorption and condensation process (horizontal axis).
 b, The humid air states of the MOF process are described on the psychrometric chart. The process begins at an arbitrary inlet ambient air temperature and humidity. The collected mass of liquid water corresponds to the difference in humidity between (4) and (5). 102
- B.6 a, The MOF process aims to concentrate water vapor within a structure in cycles, to increase the humidity for more efficient condensation. The psychrometric chart represents the humid air states in the process. Ambient air (1) is heated to a low relative humidity (2) where it can desorb the water contained within the MOF. To facilitate desorption, the MOF must be heated to a pre-defined relative humidity. The humidified air (3) is then sent to a condenser to extract water similar to the dew harvesting process. The graph qualitatively describes the temperature (vertical axis) along the desorption and condensation process (horizontal axis).
 b, The humid air states of the MOF process are described on the psychrometric chart. The process begins at an arbitrary inlet ambient air temperature and humidity. The collected mass of liquid water corresponds to the difference in humidity between (4) and (5). 104
- B.7 The open system was chosen as it is the simpler option that is more robust and flexible to adapt to different MOF's and operating conditions. Additionally, it is the most comparable system to the other AWH systems modeled in this work (dew, membrane, and least work). So, while the two systems are different in several aspects, they also share many similarities as discussed above. The framework developed in this work is developed with a very similar approach. . . 107

- B.8 We further demonstrate this with the plots below. These plots show the specific energy consumption of water harvesting at an ambient temperature of 300K. The left plot employs the MOF assumptions exactly, whereas the right plot employs a constant desorption relative humidity to each MOF. It can be seen that when all MOFs use the same desorption relative humidity, the energy consumption across the range of humidity values is nearly identical. In the main text, we use all 4 MOFs while employing a constant desorption humidity across all MOFs. 108
- B.9 A sensitivity analysis was conducted with assumed parameters in the MOF model, to show the relative effects on the energy consumption. The default analysis conditions include the ambient relative humidity of 50%, the specific heat capacity (1 kJ/kg K), and recovery ratio of 65%, and MOF-specific properties in presented previously. As can be seen, the specific heat capacity, adsorption energy, and maximum water uptake of the MOF have very minimal impact on the specific energy consumption. However, these variables may significantly impact the non-normalized energy consumption, which may be important in practical systems with size and form factor constraints. The most significant factor affecting the specific energy consumption for water harvesting is the desorption relative humidity. Due to the integral method used to determine the outlet humidity ratio from the desorption process, even small increases in the desorption relative humidity led to significant increases in the outlet humidity ratio. Thus, for a constant recovery ratio, a significant increase in desorption outlet humidity ratio leads to a higher condenser temperature and cooling COP, greatly improves the specific energy consumption of the system. 109
- B.10 The membrane process employs a membrane to isothermally concentrate water vapor before condensation. This is a depiction of the original Claridge-Culp-Liu dehumidification process [69]. The psychrometric chart represents the humid air states in the process. Ambient air (1) is concentrated (2) where now it has a lower energy requirement for condensation. The water vapor is condensed and then is pumped back to atmospheric pressure. Note: only the air states are shown in the psychrometric chart. Since the membrane is assumed to be perfectly selective, only water vapor enters the condenser. b, The humid air states of the membrane process are described on the psychrometric chart. The process begins at an arbitrary inlet ambient air temperature and humidity. The collected mass of liquid water corresponds to the difference in absolute humidity between 1 and 2 minus the amount of excess vapor that is rejected from the system. 110

- B.11 The fraction of water condensed represents the recovery ratio at the condenser of the membrane. The system pressure ratio represents the ratio between the system operating pressure and the ambient vapor pressure of water. This calculation is done for 30°C and $\text{RH} = 70\%$. A perfectly ideal membrane system will have a system pressure approaching 1 (infinitesimal flux) and a recovery ratio nearing 100%. For the analysis in this work, the recovery ratio, or fraction of water condensed, is set to 65% to create a fair comparison with the other processes. Optimizing this process with recirculation could artificially increase the true recovery ratio, thus enabling higher efficiencies. 111
- B.12 The breakeven recovery represents the recovery ratio at which the membrane must operate to be energy-equivalent to dew harvesting. In the membrane system, it is always optimal to condense all the water vapor that passes through the membrane. In the case that this happens, the membrane system will require less energy than dew. However, achieving high recovery through heat exchangers may have practical limitations such as scaling and frost. 112
- B.13 The breakeven efficiency refers to the isentropic efficiency of the vacuum pump in the membrane system that allows the membrane to be energy-equivalent to the dew harvesting process. The figure on the left assumes a compressor efficiency of 50%, while the figure on the right sets the compressor efficiency to 90%. The sub-saturated region in white represents the area where dew is better than the membrane even with isentropic vacuum pumping. This white region becomes larger with lower compressor efficiency and lower recovery. The default recovery for the membrane system is 65%, which was chosen to create a fair comparison on the basis of yield with the MOF-sorbent process. 113
- B.14 Dew harvesting, membrane, and sorbent processes are modeled with cooling and heating coefficient of performances of 3 and pump isentropic efficiencies of 65% (compressor) and 20% (vacuum pump) [61], [70], [81]. This represents a first order estimate of current heating and cooling technologies, although in practice larger temperature differences will yield lower efficiency components and technologies for near-saturation pumping may encounter additional issues. The contour axis is represented on a log scale in units of kJ/kg 114

B.15 Ideal processes are compared on the basis of energy efficiency. All heating and cooling are assumed to be conducted by a Carnot-like device. Fog harvesting (yellow) is optimal in supersaturated conditions. Dew harvesting (red) is optimal in high-humidity conditions. Membrane processes (blue) are optimal in low relative humidity conditions. Ideal sorbent systems are always sub-optimal when compared to membrane systems, however the dashed region shows where sorbent processes are better than dew harvesting. Furthermore, as the COP decreases (real systems may be 3 or less), the membrane processes become optimal at higher relative humidity. Additionally, the region where sorbent systems outperform dew harvesting also increases in area on the temperature-humidity plane. This analysis is conducted for open system processes and only consider thermodynamic optimality. Other factors may influence deployment such as technology cost and accessibility. 115

B.16 The air temperature at 2m above the surface is mapped, based on the monthly NASA MERRA2 database [82]. The median and standard deviation are taken from monthly mean temperatures (January 2019 to January 2021). 116

B.17 The specific humidity at 2m above the surface is mapped, based on the monthly NASA MERRA2 database [82]. The median and standard deviation are taken from monthly mean temperatures (January 2019 to January 2021). 117

B.18 The number of months in a year where the monthly average surface temperature is above 274K is mapped, based on the monthly NASA MERRA2 database [82]. This is averaged over 2019 and 2020. The evidence of global temperature rise should be noted [89]. 118

LIST OF SYMBOLS

α	Chemical activity
b	Molality
B'	1 st Virial coefficient
c_p	specific heat capacity
η	Isentropic efficiency
η_{II}	2 nd law efficiency
g	Specific Gibb's free energy
G	Gibbs free energy
h	Specific enthalpy
M_w	Molecular weight
p	Pressure
q	Intensive heat transfer
r	Recovery ratio
R	Universal gas constant
s	Specific entropy
T	Temperature
v	Specific volume
w	Intensive thermodynamic work
ω	Humidity ratio
z	Altitude
Z	Compressibility factor

ABBREVIATIONS

ASHRAE	American Society of Heating, Refrigerating and Air-Conditioning Engineers
AWH	Atmospheric water harvesting
COP	Coefficient of performance
CPU	Central processing unit
ED	Electrodialysis
GHG	Green house gas
GOR	Gained-output ratio
ISRU	In-situ resource utilization
LW	Least work
MOF	Metal organic framework
NF	Nanofiltration
NASA	National Aeronautics and Space Administration
RH	Relative humidity
RO	Reverse osmosis
SEC	Specific energy consumption
SWP	Specific water production
UF	Ultrafiltration

ABSTRACT

Inclement challenges of a changing climate and humanity's desire to explore extraterrestrial environments both necessitate efficient methods to obtain freshwater. To accommodate next generation water technology, there is a need for understanding and defining the energy efficiency for unconventional water sources over a broad range of environments. Exergy analysis provides a common description for efficiency that may be used to evaluate technologies and water sources for energy feasibility. This work uses robust thermodynamic theory coupled with atmospheric and planetary data to define water capture efficiency, explore its variation across climate conditions, and identify technological niches and development needs.

We find that desalinating saline liquid brines, even when highly saline, could be the most energetically favorable option for obtaining water outside of Earth. The energy required to access water vapor may be four to ten times higher than accessing ice deposits, however it offers the capacity for decentralized systems. Considering atmospheric water vapor harvesting on Earth, we find that the thermodynamic minimum is anywhere from 0x (RH = 100%) to upwards of 250x (RH < 10%) the minimum energy requirement of seawater desalination. Sorbents, modelled as metal organic frameworks (MOFs), have a particular niche in arid and semi-arid regions (20-30%). Membrane-systems are best at low relative humidity and the region of applicability is strongly affected by the vacuum pumping efficiency. Dew harvesting is best at higher humidity and fog harvesting is optimal when super-saturated conditions exist. Component (e.g., pump, chiller, etc.) inefficiencies are the largest barrier in increasing process-level efficiency and strongly impact the regions optimal technology deployment. The analysis elucidates a fundamental basis for comparing water systems energy efficiency for outer space applications and provides the first thermodynamics-based comparison of classes of atmospheric water harvesting technologies on Earth.

1. INTRODUCTION

1.1 Water scarcity

Obtaining water is a crucial challenge to sustaining life, as we know it. Particularly in extreme environments, the ability to obtain fresh water can become a limiting factor to habitability. A prime example of this predicament is in outer space. Astronauts must either reuse every ounce of water that is taken from Earth or have the capacity to obtain and purify water on another planetary body. Although water is found in some form (solid, liquid, vapor) on every planet in the Solar system, it is not directly clear how we might access these extraterrestrial water sources. This motivates a need for understanding how to compare different approaches of obtaining water across a wide range of conditions.

Water scarcity is also becoming a limiting factor to habitability on Earth. As of 2020, two-thirds of the global population lives in water stress at least one month out of the year, and the issue is particularly concentrated in arid regions ($RH < 30\%$) [1], [2]. Furthermore, climate change induced desertification [3] and widespread groundwater resource exhaustion [4] motivate the need for new approaches for obtaining water.

The Earth holds approximately $1.4 \times 10^{18} \text{ m}^3$ of water. 96.5% is found in Oceans, Seas, and Bays. 1.74% of Earth's water is found in ice or snow. 0.76% of all water is easily treatable groundwater. Finally, 0.001% is found in the atmosphere and 0.0002% is found in rivers [5]. With global groundwater depletion and pollution, the effects of water scarcity can be especially detrimental in remote, inland regions. Furthermore, the cost of water transportation and distribution constrains the applicability of many current approaches to centralized water production.

1.2 Common water technologies

Methods of treating water sources (e.g., freshwater, river water, groundwater, seawater) are strongly coupled to the contaminants in the water source, as shown in Fig. 1.1. Disinfection and chemical treatment are cheap and effective methods for treating nearly pure water sources that may have biological contamination. Low-pressure filtration like UF, NF can be

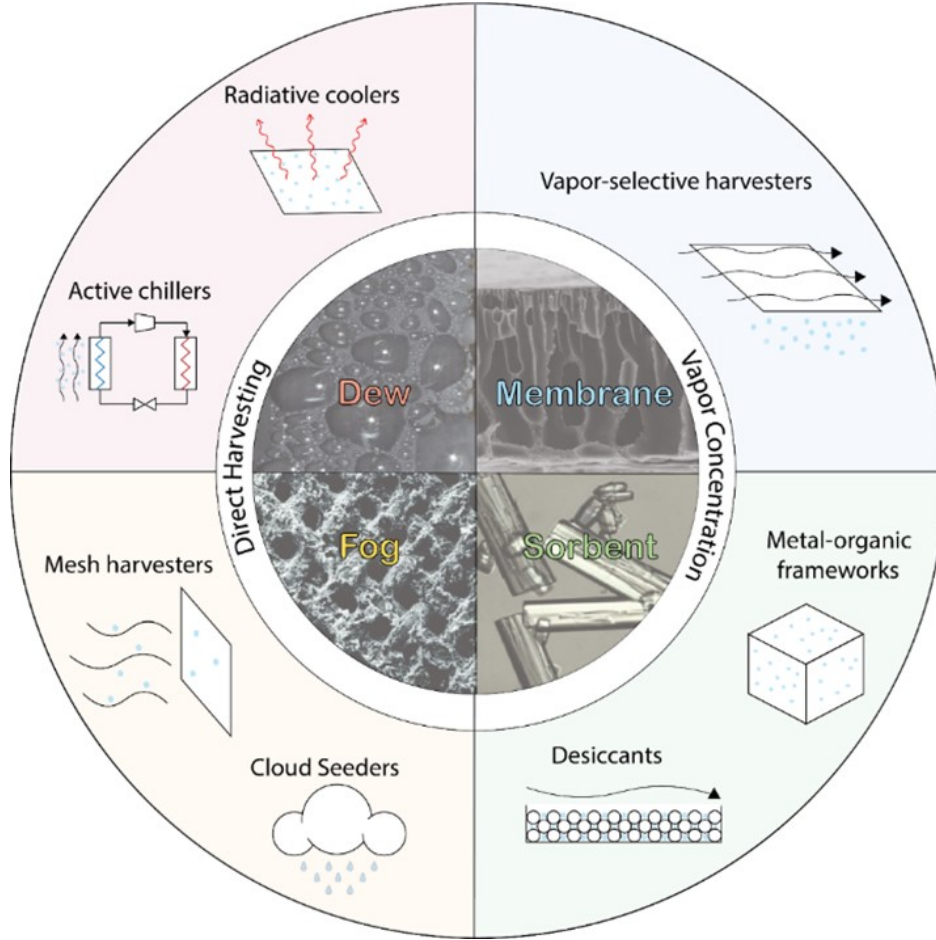


Figure 1.2. Overview of AWH technologies (outer circle) and fundamental process categories (inner circle). Images in the inner circle include: Dropwise condensation on a tube (Dew, [12]); SEM Polysulfone–graphene oxide composite membrane (Membrane, [13]); SEM graphene structured fog net (Fog, [14]); Optical microscope MOF-303 (Sorbent, [15]).

decentralized water purification with relatively little need for pretreatment. Air- and water-borne pathogens and worsening pollution will require some post-treatment for AWH to be used for drinking water [10]. However, this treatment is likely less difficult than filtering trace contaminants, such as Arsenic and Boron, that are found in oceans and rivers [11].

Current systems can be organized into categories based on the physical mechanisms and driving forces that are employed, as shown by Fig. 1.2. Direct harvesting aims to capture water vapor from the ambient air-water mixture. Vapor concentration uses novel materials to separate the water from the ambient air before condensing to liquid. This categorization is

described further in Ch. 3. Prior categorizations consider integrated systems and sub-classes of adsorbent technologies [16]–[18].

The primary challenge for AWH is that energy needs, in most situations, are orders of magnitude higher than even seawater desalination. Furthermore, these systems are developed for Earth-based environments and are strongly affected by the ambient temperature, pressure, and humidity. This motivates the need to understand the fundamental energy requirements and limiting factors of AWH to improve efficiencies and identify the best use cases for current technologies.

1.3 In-situ resource utilization in Outer Space

Water technologies on Earth have been developed for thousands of years under the assumption of Earth-standard conditions (near 300K and 100kPa). Obtaining water in space-based environments encounters technological challenges due to the extreme environments.

Although water is present on every planet and many moons in the Solar system, as shown by Fig. 1.3 the temperature, pressure, and water source composition are much different than the water sources encountered on Earth. This difference results in significant energy considerations, but also implies that the water treatment mechanisms on Earth may not necessarily function the same way. Atmospheres and oceans in outer space have much different compositions (e.g., sulfuric acid vapor on Venus [19], perchlorate brines on Mars [20], etc.) than traditional water sources on Earth [21]. High salinity brines and low vapor pressures are fundamentally the most difficult separations and are an active area of research. Furthermore, due to low pressures ($< 10\text{kPa}$) and temperatures ($< 270\text{K}$) on many planetary bodies, water commonly exists in a vapor-solid phase regime which creates practical issues with obtaining liquid water such as refreezing and vaporization. Current ISRU approaches to extract water-ice on the Moon and Mars are constrained to polar ice deposits [22], [23].

There is a significant need to develop tailored ISRU technologies for a specific environment (i.e., temperature, pressure, composition). Studying the thermodynamic limits of extra-terrestrial water systems is motivated by the diversity of available options and may be useful for guiding trajectories of technology development.

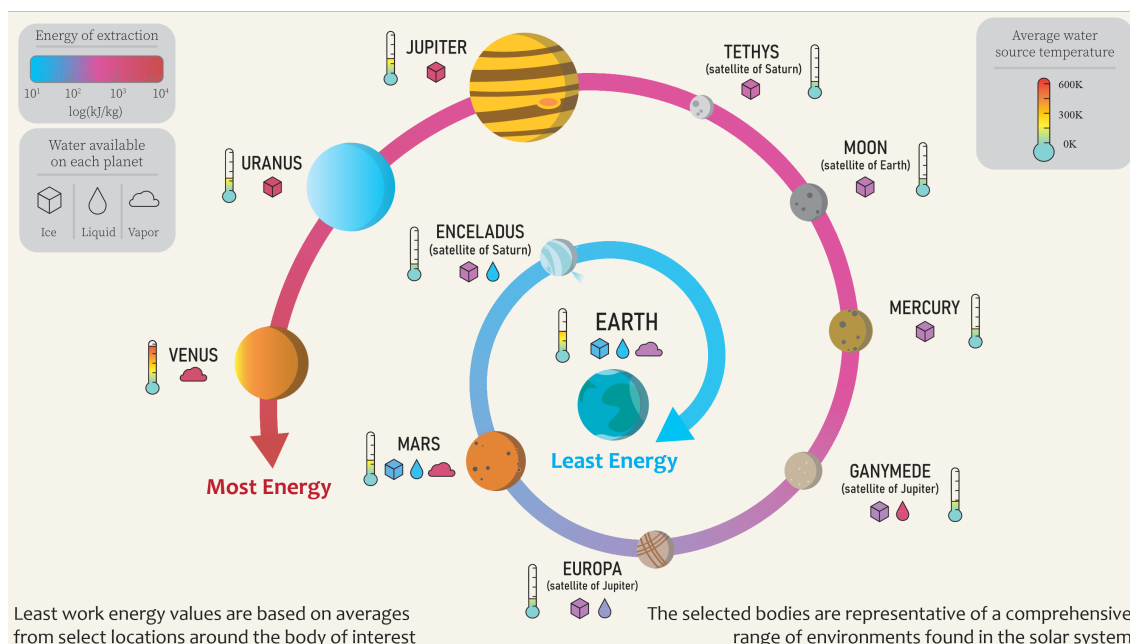


Figure 1.3. The energy requirements and sources of water available on a representative set of planetary bodies within the solar system. The phase available refers to the thermodynamic state of the available water source (i.e., water-ice, saline liquid brines, and water vapor). The average conditions are informed by literature of planetary spectroscopy measurements and planetary formation models. The thermodynamic framework and detailed energy calculations are described further in Ch. 2.

1.4 Efficiency metrics in water

The relationship between consumption and yield is quantified by thermodynamic efficiency. There are many methods to describe the efficiency in water systems; the most commonly used approaches are the gained output ratio (GOR), hydraulic law efficiency, and exergy efficiency [CITE WARSINGER THERMO]. GOR is the ratio of the process heat transfer to the enthalpy of vaporization. This measures how much better a process is compared to directly evaporating or condensing water and is primarily used for thermal processes. The hydraulic, or 1st law efficiency, compares the energy consumption of a real process to the energy required for the process. The 1st law efficiency is commonly used to quantify the impact of component-level inefficiencies on overall process energy consumption. Exergy analysis, also known as least work analysis or 2nd law analysis, considers the energy

requirement and the quality of available energy with respect to the ambient environment. 2nd law analysis is used to identify sources of inefficiency in a process and quantify the minimum possible energy requirement [24]–[26]. The minimum energy requirement is calculated only with information about the environment, and therefore is technology agnostic. This feature makes 2nd law analysis particularly useful as a fundamental basis for comparing technologies and use cases.

Examples of applying 2nd law analysis span various industries [cite] and have found significant success in evaluating water technologies. Lienhard formalized the least work framework for generalized chemical processes and non-ideal solutions. This framework was then used to identify specific components and mechanisms of entropy generation in reverse osmosis desalination processes. [6] used the least work framework to compare the efficiency of open and closed reverse osmosis processes, which proved the energy benefit from transient desalination systems. This approach was then used to design high-efficiency processes for high recovery desalination [27] and high efficiency wave-powered desalination [28]. Qin et al. (2019) compared different desalination processes to elucidate the trade-offs between continuous reverse osmosis (RO) and electrodialysis (ED) [29]. Kim et al. (2020) brought 2nd law analysis to the AWH field by analyzing impacts of MOF materials on process efficiency and quantifying gains due to multiple staged processes [30].

2. UNCOVERING THE ENERGY EFFICIENCY LIMITS OF OBTAINING WATER IN THE SOLAR SYSTEM

A version of this chapter has been prepared for submission to Science Advances. Akshay K. Rao, Abhimanyu Das, Owen R Li, David M. Warsinger

2.1 Chapter overview

Water systems are governed by thermodynamics and experience a fundamental trade-off between efficiency, energy consumption, and yield. Here, we use thermodynamic theory to outline the energy efficiency limits of harvesting water and apply it to a representative set of water sources in the Solar System. Our method provides a perspective on the relative effects that the water source has on the energy requirements and can potentially be used as a tool for comparing the energy efficiency of different water harvesting approaches. Furthermore, our study may help enrich the understanding of how to develop and deploy water processes for extreme environments.

2.1.1 Extraterrestrial water sources

Stable sources of water in the Solar System generally exist as saline liquid water brines, water vapor in the ambient air, or as water-ice [19], [20], [22], [31]–[43]. In many cases, liquid water sources solely exist deep underground and are combined with a variety of complex salts [20]. Water vapor can be found in many atmospheres, but generally occurs in sparse quantities [34], [38], [39]. Water-ice, on the other hand, is the most common form. It can be found in ice caps, craters, clouds, or small bodies in space. Space exploration and research has derived estimates of water temperature, pressure, and mixture composition on various bodies in the Solar System. Prior literature has examined the water vapor properties including enthalpy [44], but this is limited in describing energy requirements in the context of energy quality. On Earth, we have a robust understanding of the minimum energy requirements, but it is limited to air mixtures at Earth-standard temperatures and pressures [45]. Understanding the properties of water in extreme environments, where it exists as highly

saline mixtures, in high pressure environments (>100 MPa), and at high ($> 1000\text{K}$) and low ($< 50\text{K}$) temperatures, is still an ongoing research objective in astrophysics and physical chemistry [46]. Overall, water in the Solar System is commonplace, yet thermodynamically complex, and the analysis of pure water extraction consequently varies significantly.

2.1.2 Extended least work

The least work framework is derived from the combination of the first and second laws of thermodynamics [21], [24]. It quantifies the exergy, or thermodynamic minimum energy, required to do a process and is computed using the properties of the water source that is used.

$$W_{\text{least}} = \lim_{r \rightarrow 0} (G_p + G_b - G_f) + (G_{\text{Earth}} - G_p) + \int_{\text{source}}^{\text{surface}} g_{\text{planet}} dz \quad (2.1)$$

Eq. 2.1 describes an extension to the least work framework that considers systems that require separation, heating, and significant change in gravitational potential. W_{least} represents the minimum energy requirement, or least work, needed to obtain water from a given water source. G is the Gibbs free energy, or embodied thermophysical energy, of water in a given environment or mixture. The Gibbs free energy is a function of the temperature, pressure, and chemical activity. The isothermal separation step is defined by the feed (input), permeate (pure water), and brine (reject). Subscript f refers to the feed (f) – or naturally occurring – water-mixture. p refers to the permeate, or pure water. b refers to the brine (b) – or reject – water-mixture after pure water is removed. The subscript Earth denotes the desired final state of liquid water at: Earth standard temperature (300K) and pressure (1 bar). r signifies the fractional recovery of pure water from the bulk, feed mixture. g_{planet} and z respectively signify the acceleration due to gravity and relative position between the source and the surface of a given planetary body. The three grouped terms represent isothermal separation, heating of homogenous composition, and a change in gravitational potential.

$$\eta_{II} = \frac{W_{\text{least}}}{W_{\text{real}}} \quad (2.2)$$

Eq. 2.2 defines the 2nd law efficiency, η_{II} , as a function of the least work and a given system or process. Here, W_{real} represents the energy consumption of a real system. W_{least} is process agnostic and quantifies the energy change in the environment.. Therefore, η_{II} can be used to compare the efficiency of a given process relative to the environment in which it is deployed.

2.2 Results

In this work, we consider the least work of harvesting water from its existing state on a planetary body to the desired state at the given surface with Earth-standard temperature and pressure, as shown by Fig. 2.1. Extending this framework, we apply water mixture property models for extreme conditions (low temperatures, high salinities, high pressures) to understand energy viability for water harvesting in extraterrestrial environments.

The material phase of the source (solid, liquid, vapor) is the dominant factor for the energy requirements of pure water extraction, as described by Fig. 2.1. The energy requirement for extracting pure water from concentrated liquid mixtures is generally one to two orders of magnitude lower than extracting from water-ice or water vapor. The energy requirement for extracting water from water vapor vastly ranges from near 0 (humid) to over 600 kJ/kg (arid).

As the temperature of the ambient environment approaches the desired temperature (assumed to be Earth standard 300K), the heating requirements decrease exponentially. Liquid source energy requirements are not as sensitive to temperature as they are to composition. This is due to the fact that water at Earth’s average temperature (300K) naturally exists as a liquid, and therefore have lower heating requirements (< 10 kJ/kg).

The molar concentration of a liquid water mixture is the primary factor in determining the energy requirement of extraction. The species of salt present has only a small impact, by less than a factor of two, as shown by the difference between the plots in Fig. 2.1A. This is explained by the variation in ion activity according to the Debye–Hückel theory and the Pitzer-Kim model [21], [47]. As a result, increasing the brine salinity, irrespective of which salt, proportionally increases the least work, within the range of conditions investigated. The

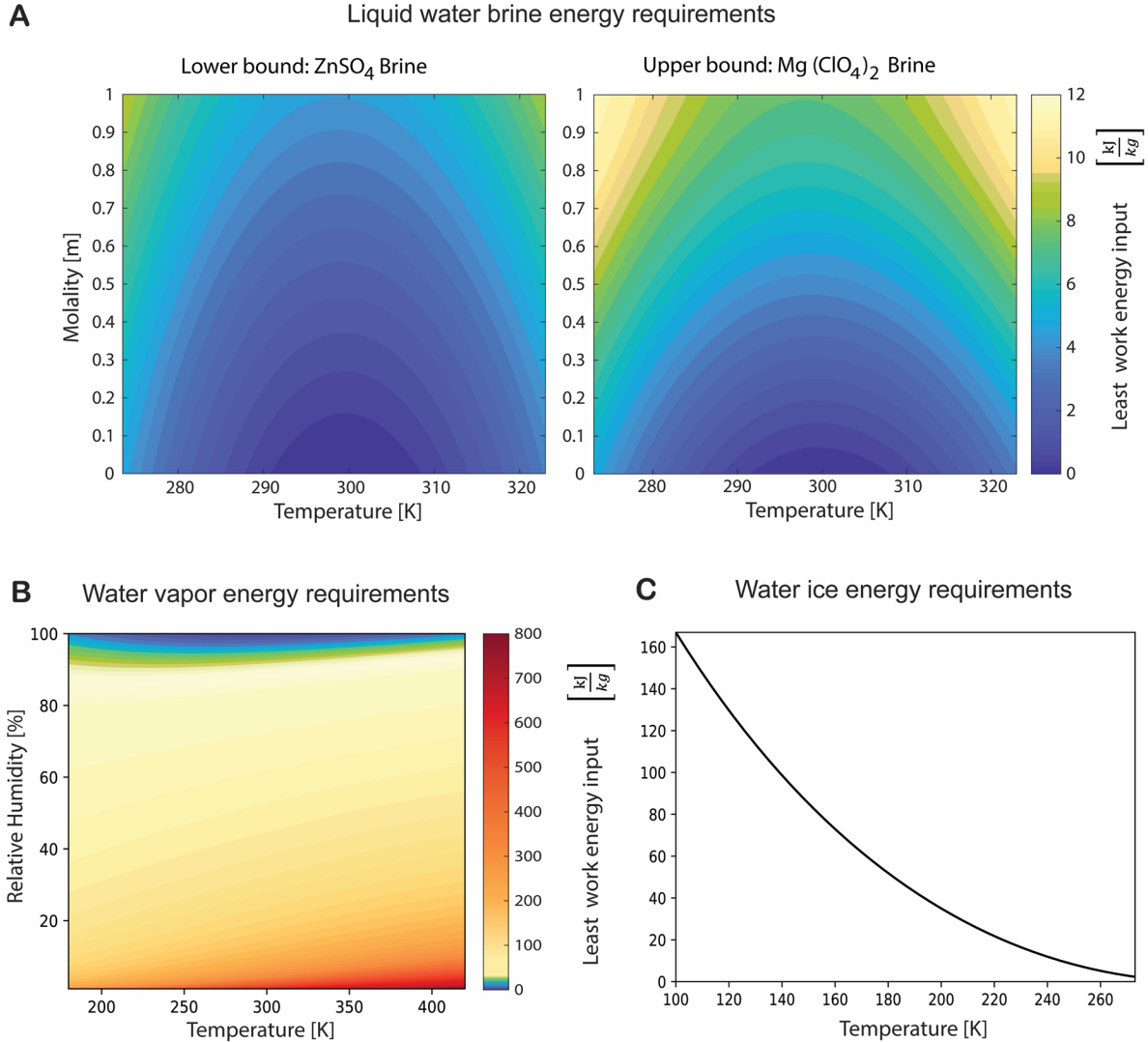


Figure 2.1. Least work of water harvesting. **a**, The two plots describe an upper and lower bound for the least work of desalination for liquid water mixtures of relevant two-component electrolyte solutions in the solar system. The lower and upper bounds are found by comparing the least work of ten binary aqueous solutions that are relevant to existing liquid water sources in the solar system [21]. The axis bounds were limited to provide a meaningful comparison, since solubility varies for each species. **b**, The contour of least work is shown for isothermal water extraction from water vapor in a planet body’s atmosphere. The relative humidity represents the vapor pressure as a fraction of the saturation pressure at a given temperature. The axes maximize the range of validity of the thermodynamic models. The blue-green-yellow color contour (0–12 kJ/kg) numerically matches values in part A. **c**, Least work required to obtain water from pure ice is shown as a function of the ambient temperature. The desired temperature is assumed to be 300K (near the average temperature on Earth). Each sub-figure considers the case where the water source is on the surface of the planet (in this, the change in gravitational potential is negligible).

separation energy for solutions increases non-linearly at high molalities, as shown by the increasing contour slope at high salinities. For most cases, the energy required to separate salts from liquid water mixtures is a larger proportion of the total energy requirement, especially for near Earth-standard conditions. This analysis does not account for the influence of organic materials which may be found in various bodies of water.

For water vapor, near-saturation conditions lead to the lowest separation energy requirements, with the least work approaching zero at saturation ($RH = 100\%$). The separation energy requirement increases significantly below a relative humidity of approximately 20% and above 300K, as shown by Fig. 2.1.

The absolute pressure of the water source and its environment mostly influence the phase-change regime (solid-liquid, solid-vapor, liquid-vapor). Changes in pressure within each regime have negligible effects in liquids and solids due to incompressibility. However, extreme pressures in liquid brines yield high solubility and ion activity, which may increase the least work [47]. Ice is nearly incompressible, however extreme pressures (>100 MPa) may slightly decrease the required work.

The depth, or elevation, was considered for specific cases where the water source is not at the surface of the planetary body (Europa, Ganymede, Enceladus, etc.) or the elevation of the surface is unclear (Jupiter, Uranus). Gravitational potential energy is a significant factor in the energetics and is independent of the phase. As shown by Fig. 2.2, this energy requirement is most significant for Ganymede, where the thickness of the ice shell layer may be 800km thick [48]. The gravitational energy requirement varies significantly, up to two orders of magnitude. The acceleration due to gravity on the moons with liquid water is approximately $0.1 - 1.5$ m/s^2 , while the gravitational acceleration on Uranus and Jupiter are approximately 9 and 25 m/s^2 , respectively. The location of the water source, relative to the surface, is unique to each planet. For example, the thickness of an ice layer (10-800km), depth of a brine deposit, or altitude of a cloud layer are influenced by a number of factors including the dynamics of planetary formation, internal heat fluxes, and weather [49]. We note that in niche circumstances, a theoretically ideal system may be able to bypass gravitational pumping requirements. This would include transporting liquid from the bottom of an ocean or vapor through an atmosphere, assisted by a natural pressure gradient.

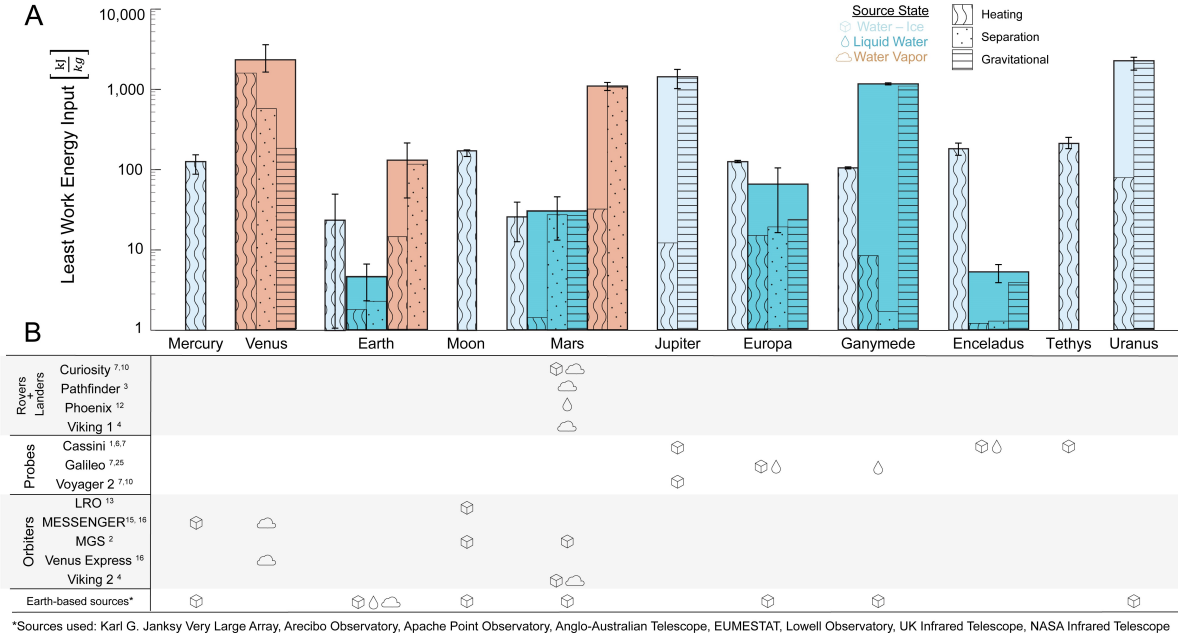


Figure 2.2. Comparison of least work on planetary bodies with known conditions. A. The least work energy consumption, modeled by Eq. 2.1 for each considered source, is plotted on a logarithmic scale, with the expected value shown. The averages for water-ice and water vapor sources are depicted in light blue and orange, respectively. Each colored bar is separated into up to three components (heating, separation, and gravitational energy), representing the energy contributions, to the total least work energy. When a source is not available on a given planet or an energy component of least work is zero, the respective color or bar is left out. The data points (black) represent the minimum, maximum, and median, as given by the Latin hypercube sampling approach. The error bars are overlaid to represent the population standard deviation, accounting for the sample size. Variation in dynamic weather conditions uses uniform distributions of parameters within observed ranges (Materials and Methods, Table B.1). B. The original sources of data are classified into categories based on the type of vehicle that was used.

Since the modeled desired state is set to average Earth conditions (300K, 1bar), the most energetically viable source of water is liquid water on Earth, as shown by Fig. 2.2. Similarly, on planetary bodies where liquid sources are available, liquid water is usually the most viable. These bodies include Mars (as sparse subsurface brines) and the moons of Jupiter and Saturn (as subsurface oceans). Ganymede is the exception due to its thick ice shell (800 km) posing a large contribution to the gravitational energy requirement. Other rocky bodies – the Moon, and Mercury – are limited in what may be extracted, since water-ice is the primary form that is available. Furthermore, Venus is fundamentally the least favorable, as water vapor is the only water option. However, acquiring such water may still be desirable, as the least work of such intensive vapor extraction is still significantly less than the energy required for deep space transport by rockets.

A lower bound for the theoretical minimum energy to take an object into space is the kinetic energy associated with escape velocity. On Earth, this is 11.19 km/s or approximately 62,600 kJ/kg payload. Modern chemical rockets require significant amounts of additional fuel mass [50], which effectively increases the energy per payload mass. In contrast, the energy required per mass of water carried by a deep space rocket may be anywhere from 10 to over 10,000 times greater than *in-situ* resource utilization from the water sources investigated in this work.

2.3 Conclusions

The case studies of least work analysis uncover trends in the fundamental energetics of water extraction. It describes the theoretically ideal physics, agnostic of any specific technology. The framework considers the energy change of the sample of water itself. The abundance of available thermodynamic work in the solar system, such as sunlight, may be harnessed to satisfy the energy budget. Realizable engineering systems will include both process and path specific requirements on top of the thermodynamic minimum. Examples of such practical inefficiencies include frictional and heat losses and limitations of energy reuse [51]. The implementation of such extraterrestrial systems may be faced with “astronomical” infrastructure challenges [52], [53]. Accessing sources of water at great depths and filtering

complex salts at high concentrations will pose continued issues [54]. Additional study is needed to understand the infrastructure requirements to establish Earth-like conditions on the surface of another planet. When current limitations are surpassed, the ability to access water on other worlds will unlock a vast range of possibilities for the exploration of the Solar System.

While the presented results discuss a widely applicable range of conditions observed on Earth and other planets, more states of liquid water exist and are yet to be thoroughly characterized. Specifically, at extremely high ($>10,000$ K) and low (<50 K) temperatures and high pressures (> 100 MPa), characterizing the free energy of water treads into unknown territory. Supercooled liquid states and salt-glass are relevant to many cold planets and are created by path-specific cooling that has further complexities [23].

The least work framework, for the minimum energy to obtain pure water, helps prioritize water sources by their macro properties. The parametric study of energetics (Fig. 2.1) and discrete case studies (Fig. 2) provide a new perspective for prioritizing the exploration of known and theoretical worlds. This work serves as a basis for modeling resource harvesting in harsh and unknown environments. Further investigation should help more clearly quantify degrees of habitability for humans based on the energy requirement of obtaining water. The input parameters for the models presented in this paper can be verified with a more in-depth characterization of the given sources of water. The exploration of the engineering constraints of systems can provide a means for quantifying tradeoffs between the accessibility and energetics of water extraction. This understanding will help to drive the future decisions concerning water harvesting and resource (oxygen and fuel) reformation.

2.4 Methods

To analyze the energetics of water extraction in the Solar System, we mapped the least work with respect to input conditions are common to water sources in the Solar System. Using the macro properties of various water sources, we conducted a case study to compare the energetics of water harvesting from each source. Data was obtained from various space exploration initiatives (referenced in main text). Models referenced established thermochemistry

databases with Engineering Equation Solver (EES) and PHREEQCi [55]. Property models were additionally validated with CoolProp and EES, which are ASHRAE and NIST validated thermal fluid property databases [56], [57]. To quantify uncertainty, we used a Latin hypercube approach to sample evenly across the range of conditions. This method is commonly used to quantify uncertainty in higher dimensions with a limited number of samples.

2.4.1 Least work derivation

For each existing body of water of known pressure, temperature and composition, a black box is used to represent input (i.e. feed) and output streams, (i.e. brine and permeate) with the corresponding energy input. By solving the first and second laws of thermodynamics for a both internally and externally reversible system, the minimum energy for obtaining drinkable water simplifies to a change in Gibbs free energy between the input and output states plus any change in gravitational potential. This calculation assumes the final destination of the water is at the world’s surface. For systems without a clearly defined surface or extremely high surface pressures, such as the gas giants, ice giants, and Venus, the final destination occurs at an elevation associated with 1bar of pressure. The initial elevation is taken to be the approximated location of the water source, via measurement or models.

$$G(T, P, C) = H(T, P) - T_0 S(T, P) + \sum_i C_i \mu_i \quad (2.3)$$

Where G, the Gibbs free energy is defined as a function of the thermodynamic state. H represents the enthalpy of the defined state, the subscript o represents the dead state temperature, or ambient temperature, S represents the entropy at the defined state, μ_i represents the chemical potential, T is the solution temperature, P is the solution pressure, and C is the fractional composition of each constituent. The least work is defined as a balance of Gibbs free energy, shown in Eq. 2.1.

$$W_{\text{least}} = W_{\text{sep}} + W_{\text{heat}} + W_{\text{grav}} \quad (2.4)$$

The least work is divided into three contributions: the separation, the heating, and the gravitational potential.

$$w_{\text{sep}} = \lim_{(r \rightarrow 0)} g_{\text{p}}(T_0, P_0, 0) - \frac{1}{r} g_{\text{f}}(T_0, P_0, C_0) + \frac{1-r}{r} g_{\text{b}}(T_0, P_0, C_0^*) \quad (2.5)$$

The separation energy requirement on a mass of pure water basis, w_{sep} , represents removal of water from the bulk source mixture at the thermodynamic dead state. The intensive property for Gibbs free energy is denoted by the lower case g . The subscripts: sep, heat, and grav, represent thermodynamic work, heating, and gravitational potential energy. Where r is the fraction of ambient water that is converted to pure water and C_0^* is calculated based on C_0 and r .

For liquid-salt mixtures, water sources that are chemically combined with salts, the separation component of least work can be expanded further with the Pitzer formulation of Gibbs free energy [21].

$$w_{\text{sep}} = \frac{1-r}{r} \frac{RT_0}{1 + \sum b_i^* M_i} (\sum b_i^* \ln(\alpha_i^*) + \frac{1}{M_w} \ln \alpha_w^*) - \frac{1}{r} \frac{RT_0}{1 + \sum b_i M_i} (\sum b_i \ln(\alpha_i) + \frac{1}{M_w} \ln \alpha_w) \quad (2.6)$$

The activities of a species and its molality are represented by α and b . Solutes are denoted by the subscript i , while water on a per mass basis is denoted by w . The solute concentrations, solute activities and solvent activity of the brine depend on the recovery ratio (r_i) of the separation process. $R_i, T_0,$ and M_i denote the universal gas constant, temperature of the source. The superscript $*$ denotes that the property is calculated after recovery, thus representing the brine stream. Separation work values are evaluated at small recovery ratios ($r = 0.075, 0.05, 0.025$) and extrapolated to zero to obtain the minimum least work at infinitesimal recovery [24].

$$W_{\text{heat}} = G_{\text{Earth}}(300\text{K}, 100\text{kPa}, 0\text{M}) - G_{\text{p}}(T_0, P_0, 0) \quad (2.7)$$

The heating step represents a temperature change from the dead-state (T_0, P_0) to the near-Earth conditions (300K, 100kPa). This step assumes heating occurs after the separation

mechanism, as to minimize the energy input. For generality, the desired state or Earth-state, can be replaced by any desired conditions. For this analysis, we are concerned with obtaining freshwater at conditions similar to Earth.

$$w_{\text{grav}} = \int_{\text{source}}^{\text{surface}} g' dz \quad (2.8)$$

In Eq. 2.8 g' with no subscript, denotes the acceleration due to gravity. The variable z represents the altitude along the path from the source location to the defined surface.

2.4.2 Property models

Property relationships for liquid water are extracted from PHREEQC with the FREZCHEM database for electrolyte solutions [20], [23], [46]. Property relationships for ice and vapor are derived analytically from Maxwell's relations. The analytical equations of state are then compared to experimental data for validation.

For water vapor, the standard form of a real gas with a compressibility factor (Z) is used. Eq. 2.9 shows the two-term Virial equation-of-state.

$$\frac{Pv}{RT} = Z = 1 + B'P \quad (2.9)$$

Where Z is the compressibility factor, which represents deviation from ideal gas behavior. v is the specific volume and R is the gas constant for water vapor. B' is represents temperature-dependent deviation from ideal behavior.

$$B' = \left[\frac{0.44687}{T} - \frac{565.965}{T^2} \times 10^{\frac{100800}{34900+T^2}} \right] 10^{-5} \quad (2.10)$$

$$\left. \frac{\partial v}{\partial T} \right|_P = \frac{ZR}{P} \quad (2.11)$$

The differential forms for changes in entropy and enthalpy for pure substances are simplified with the compressibility factor.

$$ds = \frac{c_p}{T} dT - \left. \frac{\partial v}{\partial T} \right|_P dP = \frac{c_p}{T} dT - \frac{ZR}{P} dP \quad (2.12)$$

$$dh = T ds - v dP = c_p dT \quad (2.13)$$

s and h are intensive descriptions of entropy (Eq. 2.12) and enthalpy (Eq. 2.13), respectively. c_p is the specific heat capacity at constant pressure.

Combining these equations yields a differential form of Gibbs free energy for pure water vapor with respect to a dead state (T_0, P_0) .

$$dg = dh - T_0 ds = c_p dT - \frac{c_p T_0 dT}{T} + \frac{ZRT_0 dP}{P} \quad (2.14)$$

For pure vapors, Raolt's law is assumed to apply and the substance pressure is equivalent to its vapor pressure. This assumption is reasonable, especially in low-temperature and low-pressure regimes, since the interactions between water and other mixture components may be negligible. The saturation vapor pressure is found via the Buck correlations over liquid water or ice [58].

To model the free energy of water ice, the sample is assumed to be incompressible, which simplifies the Gibbs equation to only a function of temperature. The associated specific heat for ice is used.

$$dg = c_p dT - \frac{c_p T_0 dT}{T} \quad (2.15)$$

2.4.3 Validation and error

The variable conditions of each planet are considered with a sensitivity analysis. A Latin hypercube sampling method was used to reduce the number of calculations needed to capture high dimensional uncertainty. The built-in MATLAB Latin hypercube tool, lhsdesign, was used to choose the sample conditions based on a given range. Using the range, the tool splits the high dimensional space into a n-by-n grid and samples a random point such that each row and column is equally distributed. The model computes the least work as a

function of the chosen input source conditions. Then, the expectation and sample standard deviation are computed for each source. The ranges of model input conditions are listed in Tables A.1, A.2, and A.3. A limitation in this analysis is that ranges of conditions for each planet are considered to be static and uniform, rather than either spatially or temporally weighted. Therefore, the described uncertainty analysis has uniform probability and error in this case represents a range of possible values rather than a statistical interpretation. This analysis is meant to represent statistically significant trends among planets. The equation of state formulation for vapors is validated against the CoolProp property database. CoolProp contains water vapor and air properties and is thoroughly validated against ASHRAE standards. The activity values from PHREEQC are compared across various database files and the least work for saline brines are similarly compared with [24]. Error analysis is described in Figs A.3, A.4, A.6, A.7.

2.4.4 Model limitations

Limitations in the models are largely associated with estimates in thermodynamic properties of water. To generalize to planets with unknown atmospheres, we assumed water is inert in the vapor mixture and used partial properties to simplify property models. Validating this assumption, we find that water vapor generally exists in low temperature or low humidity environments. At low vapor pressures and temperatures, such as those considered in this work, water vapor behaves nearly like an ideal gas. For real mixtures with highly volatile gases, the inter-species bonding energy will lead likely to a slightly higher least work prediction in saturated and high temperature environments. Fig. 2.1 is most accurate at lower temperature and humidity. The error may be near 5% at low concentrations ($RH < 40\%$), as shown by a comparative study with real air mixtures (Fig. A.7). Additionally, to generalize property models in liquid brine mixtures, we considered binary salt mixtures at varying concentration. To understand extraction energy requirements for more complex, tertiary, and quaternary salt mixtures, the specific composition of the mixture is required. Further experimental study is needed for accurate predictions of the thermodynamic properties of such mixtures. Finally, the property models for water-ice consider ice in its pure form.

This is a reasonable assumption in many cases, like the icy moons of Saturn and Jupiter. The thermodynamic state is also limited in that it cannot capture the energetics of physically mixed substances like regolith-water-ice. For liquid and ice sources that naturally exist in clathrates or other physically absorbent structures, such as regolith, zeolites, or metal organic frameworks, the structure-specific adsorption energy barrier is an additional consideration [CITE 39]. A framework for incorporating physical mixtures as an additive term in the minimum energy calculation is shown in Fig. [A.10](#) with a focus on Lunar regolith.

2.5 Chapter acknowledgements

The authors thank Dr. David Catling and Dr. Jonathon Toner for permission to use their suite of models on the chemistry of brines and high salinity sources on other planets. The authors also thank James Zampa, Sophia Gripp, Anirwin Yekkala, and Jiyeon Im for assistance in data analysis, acquisition, and visualization. Additionally, the authors thank Dr. Alison Bramson, Dr. Felice Frankel, and Dr. Michael McDonald, Xavier Morgan-Lange, and Debraliz Isaac-Aragones for feedback through the drafting process. The authors acknowledge Purdue University EVPRP and Purdue University Mechanical Engineering.

2.6 Chapter author contributions

Akshay K. Rao: Methodology, Software, Validation, Formal Analysis, Investigation, Writing, Visualization, Project Administration. Abhimanyu Das: Methodology, Software, Validation, Investigation, Writing. Owen R Li: Validation, Investigation, Writing, Visualization. David M. Warsinger: Conceptualization, Methodology, Resources, Writing, Supervision, Funding Acquisition.

3. THERMODYNAMIC LIMITS OF ATMOSPHERIC WATER HARVESTING

A version of this chapter has been submitted to Energy Environmental Science for review.
Akshay K. Rao, Andrew J. Fix, Yun Chi Yang, David M. Warsinger

3.1 Chapter overview

Intensifying global water scarcity calls for a diverse set of water technologies, including atmospheric water harvesting (AWH) – a process that uses energy to extract water from the air. These technologies provide exceptionally pure water from the surrounding environment with simple systems. While there are many different technologies for AWH, it is difficult to compare them on a fair basis. In this chapter, we critically evaluate each mechanism type – dew, fog, membrane, and sorbent, using the 2nd law of thermodynamics. We show the minimum energy requirements of each type of process over a range of temperature and humidity conditions. Additionally, we map the minimum energy requirement of water harvesting across the globe using atmospheric data. From this understanding, we show how specific improvements in the design of systems and processes can reduce the energy required per amount of water of current methods by over an order of magnitude. This AWH study is the broadest analysis by technology, environmental conditions, and geography. This comprehensive approach reveals technology niches and guidance for the industrial development and deployment of AWH.

3.1.1 Atmospheric water harvesting

Atmospheric water harvesting (AWH) technology seeks to efficiently access the highly pure water that is available in the ambient air. Water in the atmosphere is widely available and may be free from salt and mineral contaminants. This creates an opportunity for decentralized water purification with relatively little need for pre-treatment. Air- and water-borne pathogens and worsening pollution will require some post-treatment for AWH to be used for drinking water [10]. However, this treatment is likely less difficult than filtering

trace contaminants, such as Arsenic and Boron, that are found in oceans and rivers [11]. The primary disadvantage is that energy needs for AWH in most situations are orders of magnitude higher than even seawater desalination. This motivates the need for a robust understanding of the fundamental energy requirements to determine limiting factors and identify the best use cases.

There are several performance metrics that are used to evaluate AWH technologies in terms of energy requirements and yields. The most common metrics include the specific water production (SWP) and the specific energy consumption (SEC) [24]. SWP quantifies yield on an area or mass of water basis. SEC describes the energy input of a process, per mass of water collected. In a similar vein, the moisture harvesting index quantifies the energy needs as a fraction of the liquid-vapor phase change energy ($\frac{Q_{in}}{h_{fg}}$) [59].

While these metrics consider thermodynamic principles, they do not provide a fundamental understanding of the absolute limitations, agnostic of process and energy source, and lack a rigorous connection to thermodynamic laws. In contrast, the least work framework quantifies the thermodynamic minimum energy requirement to obtain liquid water from a given water source. This is described by Eq. 3.1 in Methods.

3.1.2 Current water harvesting technologies

AWH technology can be partitioned into direct harvesting and vapor concentration methods, as described by the graphical abstract. Direct harvesting aims to capture liquid water by physically trapping droplets or cooling the ambient air-water mixture. Vapor concentration uses novel materials to separate water molecules from other air components before condensing to liquid.

Dew harvesting processes are the primary method of direct harvesting. Dew water systems cool air until the saturation pressure meets the vapor pressure of water (dew point temperature) and water condenses [59]. This can be accomplished using active or passive (radiative) heat transfer and various grades of thermal energy. Active technologies are not constrained by the energy supply, but common cooling technologies, such as heat pumps or chillers, are anywhere from 3-30% efficient [60], [61]. Passive methods, such as solar powered

devices or radiative cooling, are largely limited by ambient forces like convective losses and cloud cover and may only produce water in higher humidity regions [62]. Dew harvesting in lower humidity regions or for high recovery must employ an active technology to meet high energy requirements.

Fog harvesting, the alternative direct harvesting approach, requires environments in which liquid droplets exist in the ambient air. These systems collect small droplets using a fine mesh or use alternative methods to induce super-saturated conditions [63]. It can harvest large volumes of water at a time, but it is largely limited to a specific climate regions and high humidity seasons [64]. Recent advances in materials and nanoscale manufacturing have created new opportunities for higher yields [65].

Sorbent systems concentrate water vapor by trapping water molecules in low surface-energy structures. Commonly used technologies include silica gels, zeolites, hygroscopic materials, and more recently, metal organic frameworks (MOF) [16]. In this paper we focus on MOFs since they have been shown to be the most thermodynamically efficient sorbet method [66]. Since diffusion is the driving force, these systems are limited to a MOF-dependent humidity range [67]. Key limitations include total water capacity (yield), energy barrier for water release, water release and capture speed, and the material stability over time [17], [65]. Membrane separation processes use a partial vacuum to pull water vapor across a vapor-selective membrane. Implementing membranes in conventional dew processes has shown dramatic (nearly 50%) reductions in energy consumption [68]. Similarly, many studies have staged such membranes in HVAC systems and other processes to reduce the energy requirement for cooling and dehumidification of air-water mixtures [69]–[71].

3.1.3 Energy comparisons

Method	Fog		Dew		Membrane	Sorption
Driving Force	Ambient air flow		Cooling		Vacuum Pressure	Diffusion and heat transfer
Technology	Mesh Harvester	Cloud seeder ^a	Active chiller ^a	Passive radiative cooler	Membrane harvester	Sorbent materials
Challenges to Scalability	Limited to specific regions	Limited to specific regions	Energy efficiency	Low cooling power	N ₂ , O ₂ selectivity, H ₂ O permeance	Large volumes, material degradation
Practical Inefficiencies	Biological contaminants	NA	Low COP devices	Ambient heat losses	Pump efficiency, membrane selectivity and permeance	Low COP devices, material stability, parasitic convection
Inefficiencies of ideal processes	NA	NA	Temperature gradients, finite recovery	Temperature gradients, finite recovery	Uncontrolled mixing, finite recovery	Temperature gradients, uncontrolled mixing, finite recovery
Operating Humidity	>100%	45 – 100%	$> 4 \frac{\text{g}}{\text{kg}}$	40 – 100 %	25 – 100 %	10 – 90 %
Specific Energy Consumption	0 ^b	NA	$830 - 25,000 \frac{\text{kJ}}{\text{kg}}$	0 ^b	$580 - 830 \frac{\text{kJ}}{\text{kg}}$	$0^b - 23,000 \frac{\text{kJ}}{\text{kg}}$
Specific Water Production	$0 - 10 \frac{\text{kg}}{\text{m}^2 \text{day}}$	NA	$20 - 200,000 \frac{\text{kg}}{\text{day}}$	$0.03 - 0.85 \frac{\text{kg}}{\text{m}^2 \text{day}}$	$0.7 - 16.8 \frac{\text{kg}}{\text{m}^2 \text{day}}$	$0.1 - 8.7 \frac{\text{kg}}{\text{kg day}}$

Figure 3.1. A comparison of experimental atmospheric water harvesting technologies including fog [63], [72], [73], dew [16], [62], [74], membrane [16], [75], [76], and sorption [16], [26], [77], [78]. ^aCloud seeders and chillers do not have a unified metric for area, SEC, or SWP. ^b Passive systems are denoted as SEC = 0. In reality, the energy is supplied by natural energy harvesting, bypassing electrical energy conversion.

As described by 3.1, the environmental requirements of each approach refer to operating humidity ranges of each process. Scalability requirements are derived from current techno-

logical and operational limitations. Ideal inefficiencies represent process level considerations that cause entropy generation, such as heat transfer or mixing fluids of different composition. Practical inefficiencies also induce entropy generation but can be mitigated by improvements at the component level (e.g. pump efficiencies, pipe friction, etc.). None of the water harvesting methods are mature technologies, however improvements in process design may address significant practical issues.

Each technology employs a different method to drive the process, shown by Fig. 3.1, thus resulting in trade-offs in scalability, ideal process efficiencies, and key practical limitations. Active technologies generally have higher yields but come with the trade-off of high electricity consumption. Fog, and dew harvesting are generally used in higher humidity regions, while sorption systems can generally be operated at lower humidity regions. Passive MOF systems may use day-night temperature variation to efficiently produce water but suffer from low yields [67]. The analysis of processes in this paper considers the thermodynamic energy requirements that can be generalized to active or passive systems.

3.2 Methods

3.2.1 Numerical model

The least work framework is a process agnostic approach to analyze fundamental limits of any water acquiring process, according to the 2nd law of thermodynamics. This framework is commonly used in desalination to compare the performance of processes with different driving forces, that accomplish the same task. Models are computed using the humid air properties in EES [79] and the CoolProp library in Python [57]. The properties from both databases are thoroughly validated against ASHRAE thermodynamic property standards. Material properties for adsorbent materials, such as water uptake and heat capacities, are taken directly from experimental results [30], [80]. The complete set of equations can be found in the supplemental methods section. Code for each process model can be found on GitHub upon publication: <https://github.com/Warsingerlab/published-models/>

3.2.2 Modelling framework

The primary equations for each process are listed as a function of the ambient temperature and humidity.

The thermodynamic minimum, or least work, is found as a function of the ambient temperature and humidity [24]. The limit represents an infinitesimal change to the environment, or the recovery ratio approaching zero. For isothermal systems, this mimics the separation portion of Eq. 2.1, found in Ch.2

$$w_{\text{least, min}} = \lim_{r \rightarrow 0} \left(\tilde{e}_{\text{water}}(T) + \tilde{e}_{HA}(T, \omega^*) \frac{1 - \Delta\omega}{\Delta\omega} - \tilde{e}_{HA}(T, \omega) \frac{1}{\Delta\omega} \right) \quad (3.1)$$

$w_{\text{least, min}}$ is the minimum energy requirement per mass of water collected ($\frac{\text{kJ}}{\text{kg}}$). ω is the ambient humidity ratio, $d\omega$ is the change in humidity ratio through the process, and ω^* is the dehumidified humidity ratio. \tilde{e} is the flow exergy of a given fluid stream. T is the ambient temperature. Subscripts water and HA, represent pure water and humid air, respectively.

All ideal process models assume a Carnot device for heating and cooling, as well as isentropic pumps and compressors. Realistic component-level assumptions include $\text{COP} = 3$ and $\eta_{\text{vac}} = 20\%$, $\eta_{\text{comp}} = 65\%$ [61], [81].

As an extension of the least work, the dew energy requirement uses the species exergy formulation but accounts for the change in temperature below the dew point.

$$w_{\text{dew}} = \tilde{e}_{\text{water}}(T_{dp}) + \tilde{e}_{HA}(T_{dp}, \omega^*) \frac{1 - \Delta\omega}{\Delta\omega} - \tilde{e}_{HA}(T, \omega) \frac{1}{\Delta\omega} \quad (3.2)$$

w_{dew} signifies the energy requirement for dew water collection. T_{dp} represents the dew point temperature of the ambient air. The limit is dropped, as the minimum energy for dew processes does not occur at infinitesimal recovery. The equivalence of the species-exergy formulation and the macroscopic Carnot-device formulation is only valid for the ideal system with no explicit entropy generation.

The sorbent energy requirement, modeled as a MOF, conducts a similar exergy analysis on a basis of a cycle [30].

$$w_{textMOF} = \frac{q_{des}}{COP_h} + \frac{q_{cond} + q_{regen}}{COP_c} \quad (3.3)$$

w_{MOF} represents the energy requirement for water collection via the MOF system. It is comprised of a desorption term (q_{des}), a condensation term (q_{cond}), and a regeneration term (q_{regen}). Each of these heat transfer components are described on a per mass of water basis. Each heat transfer term is divided by a coefficient of performance, or COP, for heating (h) or cooling (c). This framework is adapted from prior work on a closed-cycle MOF process [30].

The membrane process energy consumption, like the MOF, is calculated by the sum of the work input and heat transfer divided by their respective efficiencies [69].

$$w_{membrane} = w_{vac} + w_{comp} + \frac{q_{cond}}{COP_c} \quad (3.4)$$

$w_{membrane}$ represents the energy requirement for water collection via an open system membrane process. In this analysis, we consider a Claridge-Culp-Liu process that features a membrane configuration in an open system [CITE 29]. Subscripts *vac* and *comp* represent the vacuum pump and compressor used by the system.

$$r = \frac{\dot{m}_w}{\omega \dot{m}_{HA}} = \frac{\Delta\omega}{\omega} \quad (3.5)$$

For all processes, the recovery ratio (r) is defined as the amount of water removed from the air, as a fraction of the humidity ratio of the ambient air. One exception is for the membrane process. Since the membrane process condenser is exposed to a pure water vapor stream, without air, the recovery ratio relates to the condensed water to the total water vapor flow entering the condenser.

3.2.3 Mapping and computing

The modelling framework was applied global weather data from the NASA MERRA2 project [82]. The database provided temperature, pressure, and humidity of surface air in 1hr increments from January 01, 2021, to December 31, 2021. The spatial resolution of data

was 0.5° in latitude and 0.625° in longitude. The mapping approach computed the least work at each coordinate for every time step, resulting in over 1.8 billion model evaluations. The calculation was conducted using AMD Epyc 7662 “Rome” CPUs at 3.1GHz for a total of 432 hours of compute time.

3.2.4 Model validation

A previously published MOF cycle model was replicated and compared against the published results to ensure the foundation of the present model was based on an accepted framework [30], [80]. The assumptions and sensitivity analyses regarding the MOF properties are presented in B.6, B.7, B.8, and B.9,. The membrane model is based on prior published models [68], [69]. The ideal dew model is an extension of the least work framework that is novel to this work.

3.2.5 Assumptions and limitations

The limitations of this model are primarily derived from the process-agnostic description of least work, the range of the thermodynamic property database, the high sensitivity of the MOF model to the desorption relative humidity, and the focus on open system analysis. Additionally, the nucleation dynamics of fouling, icing and fog are not captured in this model.

The least work framework allows for precise description of a system’s maximum efficiency, but the minimum energy requirement is not practically achievable. A reversible (100% efficient) process is reliant on asymptotic requirements such as isothermal separation and infinitesimal recovery. Real processes must operate at a finite recovery to meet practical yield or capacity constraints.

Exergy analysis shows characteristics of ideal systems, but practical considerations may limit the feasibility of achieving such conditions and alter the optimality conditions. For example, entropy generation due to heat transfer in dew plates may significantly impact the overall system efficiency and optimal recovery ratio. However, such impacts may only be predicted by understanding the locations and dynamics of device-specific entropy generation. Furthermore, it is important to note that technology deployment is only in-part driven

by energy. Techno-economic and social considerations may conflict with thermodynamic optimality.

The CoolProp, thermodynamic property database for humid air mixture is limited in its range of validity. Data is exclusively for conditions where the humidity is greater than $4 \frac{g_w}{kg_{air}}$, or the dewpoint is greater than the freezing point. Further, the study was done assuming sea-level atmospheric pressure as a standard. While assumption hold well on most of the Earth, a better understanding of water properties in sub-freezing conditions and low pressures, will allow us to understand water harvesting in more extreme environments, like the arctic or outer space.

The MOF process model assumed ideal MOF isotherm behaviour based on four representative MOF materials, focusing on the adsorption energy, desorption relative humidity, and maximum water uptake. The properties were chosen from an exhaustive review on existing MOFs to provide a range of humidity operating conditions [80]. Path specific uptake and the uptake dynamics of specific MOFs were not considered to maintain generalizability for comparison. However, an integral method is used to determine the desorption outlet humidity, as has been done in literature [30].

This work considers the open system version of these technologies for fair comparison. In most cases, closed systems, hybrid systems, and systems with multi-staging may be more efficient. However, these processes widely vary by configuration and are under-explored in the water harvesting literature. Future work should look to unifying the thermodynamics of closed systems to bridge the gap between current technology and the minimum least work. Efficient process design is discussed further in the Field-wide challenges section.

The exergy-based models that are used in this study are not able to account for nucleation phenomena such as fouling and icing. System dynamics are process specific but may significantly alter energy consumption when ambient air is not homogenous, or weather conditions are rapidly fluctuating. Surface phenomena such as fouling and icing are also highly specific to individual devices or processes. Along with model limits, this study assumed that any sub-freezing temperature has the potential for frost accumulation and therefore is not viable for water harvesting. Dynamic surfaces [83] and superhydrophobic surfaces [84] have been shown to allow for condensers to avoid icing with low energy consumption. In

desalination, hydrophobic surfaces also have been shown to mitigate the fouling propensity of membranes [85].

In this study, we consider only radiative or advective fog. This assumes the droplet composition is pure water or only contains aerosols that are not chemically combined with water, such as dust. Fog that is induced by reactive particles, for example salt in sea fog or aerosols in valley fog, may require small additional considerations associated with chemical bonding energy. Further, water harvesting from more impure fog events may not uphold the same assumptions of minimal post-treatment, as other AWH methods imply.

3.3 Results

3.3.1 Energy requirements and process efficiencies

The 2nd law efficiency of any process can be defined by the ratio between the least work (environment dependent) and the process energy requirement (process dependent) since the least work is thermodynamically ideal. For any process (dew, sorbent, fog, etc.), the second law efficiency represents the maximum efficiency limit or the thermodynamic losses that are built into the process. The least work, shown by Figure 1a may be used to evaluate the efficiency of any water harvesting process.

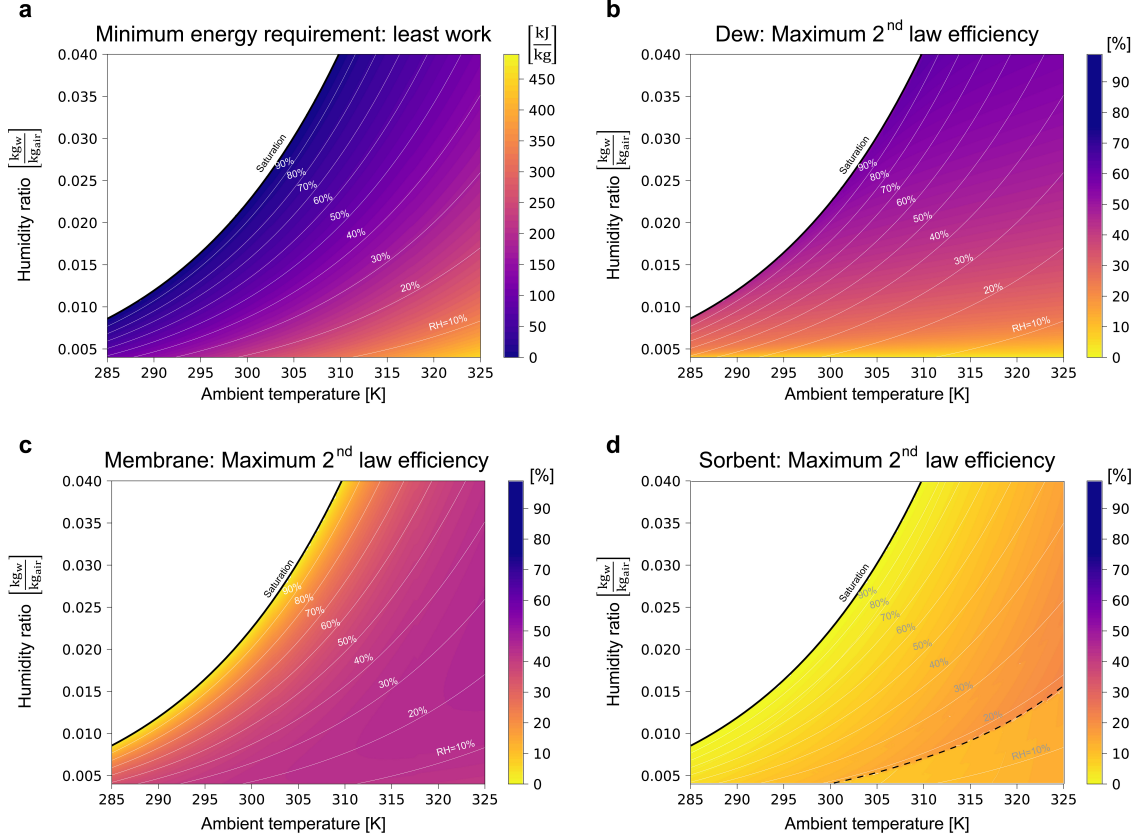


Figure 3.2. Energy requirements for water harvesting vary based on the driving force and ideal processes. **a.** The minimum least work ($W_{\text{least,min}}$) or thermodynamic minimum energy requirement irrespective of the process, is plotted as a contour variable on the psychrometric chart (B.1). The intermediate white lines represent constant relative humidity ranging from 10% to saturation. The least work assumes an infinitesimal recovery ratio (the amount of water removed from the available water in the air), which represents the minimum thermodynamic change to the environment. Near the top left corner ($\text{RH} = 100\%$), the least work approaches 0 kJ/kg. **b.** The second law efficiency (η_{II}), of an ideal dew collection device (B.3) is found as the minimum energy consumption of dew divided by the least work. The energy consumption of dew harvesting is evaluated at the optimal recovery ratio, described in Fig. 3.3. The intermediate white lines represent constant relative humidity ranging from 10% to saturation. **c.** The efficiency of an ideal open-system membrane water harvesting device with the Claridge-Culp-Liu configuration (B.10). The recovery is set at 65% to maintain consistency with the sorbent process. **d.** The efficiency of an ideal MOF process (B.5) consisting of four MOF materials is found as the minimum energy consumption for the MOF process divided by the least work. The dotted line denotes the shift between two sets of desorption conditions (B.8). All cooling and heating are provided using Carnot devices and pumping is shown as isentropic.

The least work (minimum energy requirement) is strongly controlled by the ambient relative humidity. At saturation ($\text{RH} = 100\%$), the least work for isothermal water harvesting approaches zero. Below this humidity, the least work exponentially increases, reaching nearly 500 kJ/kg at extremely arid conditions ($\text{RH} < 10\%$). It is important to note that the least work is defined as a theoretical process that enacts minimal change to the environment by recovering an infinitesimal fraction of water from the ambient air. The recovery ratio is defined as the fraction of water vapor that is removed from the available water in the ambient air.

Dew harvesting processes are strongly impacted by the ambient humidity, shown by Fig. 3.2. Both the least work and the dew energy requirement improve near saturation ($\text{RH} = 100\%$) and drastically suffer in arid conditions. Since dew processes aim to cool a mixture to the dew point (saturation temperature), a lower relative humidity results in more cooling of air that is required. In practice, passive and active technologies have trade-offs in meeting the energy requirements.

Membrane processes are most effective in hot and arid regions. The value proposition of this system, like other separation mechanisms, is the ability to avoid cooling ambient air. The ideal membrane system efficiency is nearly constant ($40\text{-}55\%$) over a wide range of ambient conditions ($\text{RH} < 60\%$). At higher humidity, the least work trends to zero while the membrane energy requirement remains stable, thus resulting in low overall efficiency. It should be noted that the process recovery and vacuum pump efficiency strongly affects the system efficiency, as described in B.11, B.12, B.13. To obtain maximum efficiency in membrane-based processes, operation should aim to minimize the membrane-flux and condense all water that passes the membrane. A closed system design may further improve the 2nd law efficiency of membrane processes [68].

Sorbent processes, modelled in this work as open MOF-systems, are mostly influenced by the ambient temperature and the desorption humidity. At low temperatures, the system requires high temperature differences for desorption, thus decreasing the Carnot efficiency. Further, the energy barriers of the enthalpy of adsorption and enthalpy of vaporization make the process fundamentally inefficient. Minimizing the MOF-specific adsorption enthalpy may improve the performance limits. Prior work analyzing such MOF systems showed that a

closed-cycle process with MOF-801 may exhibit a maximum second law efficiency near 20% [30]. While the maximum efficiency limits shown in Fig. 3.2D suggest that sorbent processes are not promising, it should be noted that this process is the only one that is tailored to be driven by heat. The sorbent process may be more cost-competitive if high-grade heat (e.g. solar thermal energy) is cheap to acquire and material costs are low.

The sorbent process complexity and multiple heat transfer interactions make the efficiency trends, relatively unintuitive. The characteristic isotherm, which relates the water uptake to the temperature and humidity, and material-specific adsorption kinetics determine the operating conditions. The maximum uptake capacity increases the theoretical water collection rate but does not significantly impact the specific energy consumption, as shown by B.9. Of the MOF's selected in this work, the two MOFs used for relative humidity values greater than 18% have a desorption relative humidity of 16%. B.8 shows that the desorption humidity is by far the most sensitive parameter in the model, explaining the sudden increase in efficiency at RH=18% in Fig. 3.2. MOFs with higher desorption relative humidity values would extend the region of high efficiency for the MOF to higher ambient humidity conditions. Additionally, while each MOF will require different amounts of desorption heat and experience different uptake dynamics, we show in the supplemental material that these parameters have minimal effect on the system level specific energy consumption. It should be noted that these parameters would strongly impact net energy consumption and real system sizing (B.14).

3.3.2 Fog and saturated humid air mixtures

Fog is liquid water droplets suspended in air and refers to the supersaturated humid air state. Both saturated air (RH = 100%) and fog (RH > 100%) theoretically require no energy to harvest. An ideal fog system requires zero energy because the water is already in the liquid state. On the other hand, an ideal system that condenses 100% humid air has water in the vapor state, but the free energy change of condensation is zero. Such an ideal system can be modeled as a Carnot-driven process operating between reservoirs of saturated

vapor and liquid. This theoretical device is able to supply the latent heat of vaporization at infinite efficiency due to isothermal heat transfer.

The concept can be mathematically supported with Maxwell's relations, where $\frac{dh}{T}|_p = ds$ or $dh = Tds$ at constant pressure. Here, h is the specific enthalpy, s is the specific entropy, T is the temperature, and p is the pressure. Since $dg = dh - Tds$ (g is Gibb's Free Energy) and phase change occurs at constant pressure ($dh = Tds$), then $dg = 0$ and the minimum energy requirements for condensation are thus zero.

Due to these facts, the minimum energy requirements for harvesting water from fog or harvesting water from a water-air mixture at 100% are theoretically equivalent. However, practical technologies for harvesting water from 100% humid air are not equivalent to the thermodynamic minimum. In reality, dew plates, membrane-based systems, and sorbents, must overcome the latent heat of phase change. Fog nets must overcome the free energy barrier associated with forming a new surface. This surface energy is controlled by the surface hydrophobicity and geometry and is orders of magnitude lower than the enthalpy of vaporization.

Where fog is widely available (e.g., Hamilton, NZ; San Francisco, CA; Atacama, Chile; etc.) it may be highly effective to implement fog nets, due to near zero energy requirements. However, the dynamics of fog are complex and therefore unreliable until fog events can be predicted with high accuracy [64]. The optimization of fog collection may enhance surface hydrophilicity to minimize the energy barrier for collection [80], [86]. Additionally, hydrophobic materials can accelerate droplet shedding off the surface for easier collection and distribution [14], [87].

3.3.3 Energy-optimal water recovery

The fractional recovery of water significantly impacts both the cooling load and cooling efficiency (Carnot). When varying recovery ratio, the energy consumption for dew harvesting has a non-zero minimum value, unlike minimum least work. At infinitesimal recovery, the constant energy input to cool air causes the energy per mass of water to asymptotically increase. Therefore, decreasing the temperature of condensation below the dewpoint requires

exponentially lower energy input per unit of water collected until a certain point, as shown by Fig. 3.3. The energy-recovery function for dew harvesting is bounded ($0 < R < 1$) and convex.

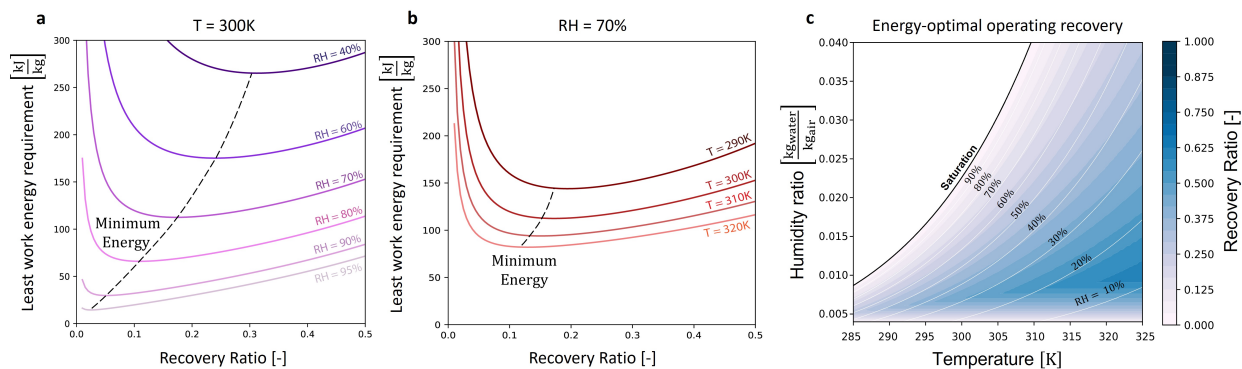


Figure 3.3. Optimal recovery for ideal dew harvesting systems. **a.** The recovery ratio shows the amount of water that is collected in the liquid phase, as a fraction of the total amount of water in the ambient air. The energy requirement of dew harvesting is shown as a function of the recovery from the ambient air for various ambient conditions, where the optimal recovery occurs at the minimum of each frontier. The horizontal axis is stopped at 0.5 to avoid frost-inducing conditions ($T_{\text{cond}} < 273.15K$). **b.** The optimal recovery ratio to minimize energy consumption for dew harvesting is shown on the contour axis of the psychrometric chart. Each point aims to minimize the function shown in a, subject to constraints: $0 < R < 1$ and $T_{\text{cond}} > 273.15K$. R is the recovery ratio and T_{cond} is the condensation temperature (Shown as T_3 in S3). The labelled white lines represent constant relative humidity.

At low absolute humidity, low recovery ratios are required to avoid sub-freezing dew point temperatures (B.4). Conversely, at high humidity, low recovery is ideal to minimize energy requirements. This is shown by Fig 3.3. The optimal recovery, may be used to approximate operational set point conditions for practical water harvesting process. However, specific processes may have inefficiencies that create different economically optimal operating conditions.

Low recovery in MOF systems create large energy requirements, like dew processes. The energy requirements of desorption and regeneration are largely controlled by material properties like heat capacity. A sensitivity analysis on the recovery ratio for the open sorbent cycle showed that the optimal recovery ratio was approximately 65% (B.6). A recovery ratio

in this range provides sufficiently high-water collection, while also using relatively warm condensing temperatures and thus a high Carnot COP for causing the condensation. This optimal recovery ratio in the sorbent process is notably higher than that for the least work.

In general, recovery ratio optimization is highly specific to the driving force and technology. Recovery ratios in ideal fog systems is less straightforward since the energy input is not controlled (passive systems). For the MOF-sorbent open process, the amount of water that enters the system is dependent on the uptake and condenser dynamics, as well the ambient temperature and humidity. For membrane processes, the operating system pressure and energy requirement of the vacuum pump are set by the ambient humidity and selectivity of the membranes. Since the condenser in the membrane process contains pure water vapor, the optimal recovery is 100%. To maintain fair comparison, the water recovery of the membrane process was constrained to be equal to sorbent process. In practical applications, the exergy losses due to friction and pumping will incentivize higher recovery while inefficiencies associated with cooling will push the optimum towards a lower recovery.

3.3.4 Realistic energy comparison

The minimum energy requirement, or least work, decreases with higher humidity and trends towards zero at the saturation point, as shown by Fig. 3.4. Critically, the energy requirements of open system membrane, dew, and sorbent processes with realistic component efficiencies (non-ideal) are over an order of magnitude above the thermodynamic minimum. In this work, realistic efficiencies are modeled by a coefficient of performance (COP) of 3. This has been studied as a reasonable assumption in prior literature [61], [70]. In practice, COPs may be lower at higher temperature differences.

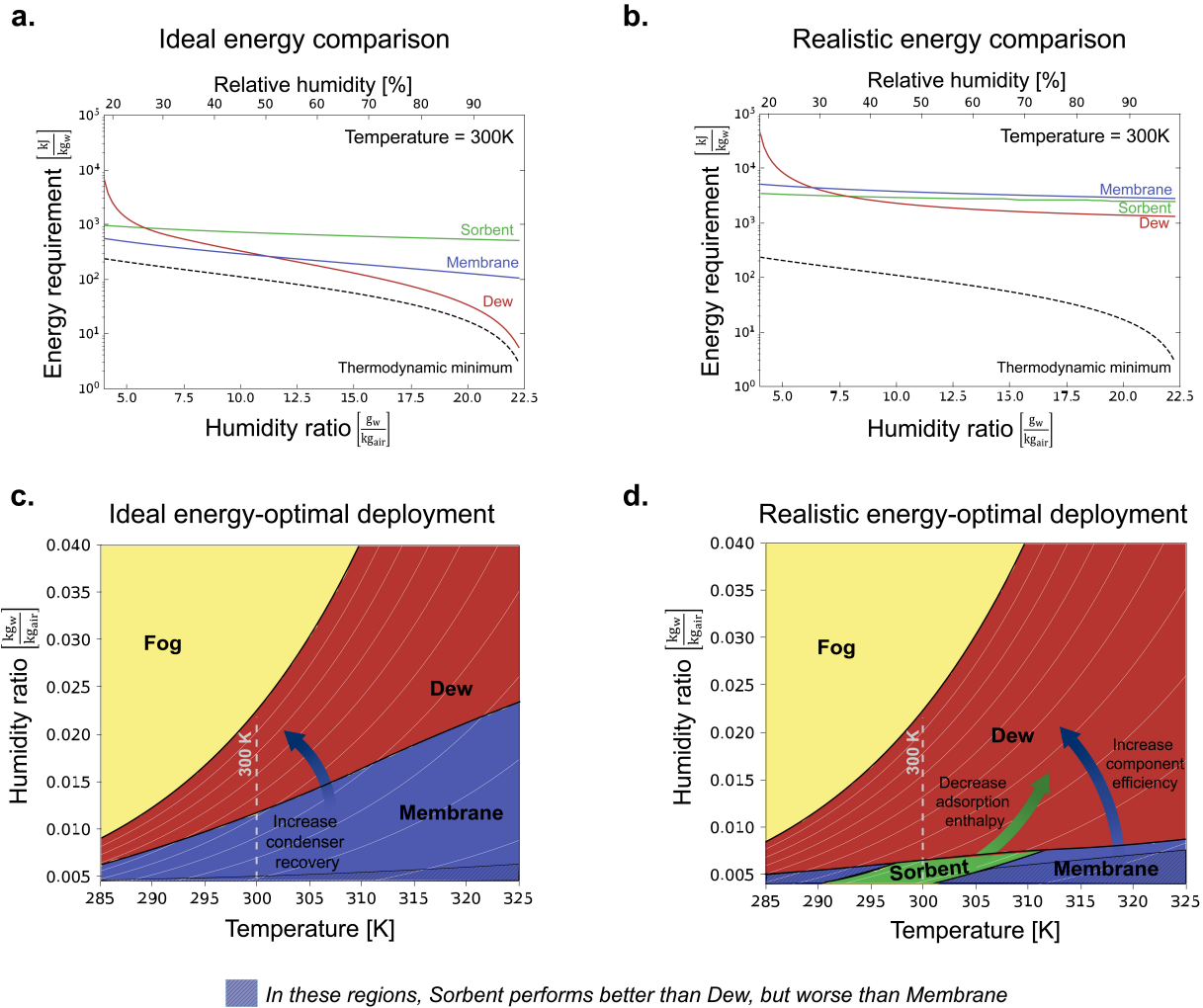


Figure 3.4. The energy-optimal AWH technology, under realistic component-level assumptions, varies with the ambient conditions. **a**, The modelled energy requirements are shown for the three active water harvesting processes, under ideal-component efficiency assumptions. The comparison is shown near room temperature (300K), on a logarithmic scale. The minimum energy requirement (black) refers to the least work at the ambient condition. **a**, The dew, membrane, and sorbent energy consumptions are shown under realistic component-level assumptions with heat transfer COPs of 3, vacuum pump efficiencies of 20%, and compressor efficiencies of 65%. **c**, The ideal processes are compared on the basis of maximum exergy-efficiency, where the membrane process is limited at $r = 65\%$. **d**, The energy-optimal deployment is compared under realistic assumptions.

Dew harvesting is best deployed in high humidity regions; however, it can be competitive with sorbent processes near room-humidity conditions. The dew process efficiency is low

relative to its maximum efficiency in high humidity regions. At high humidity, the temperature is close to the dewpoint, which results in the Carnot COP for cooling being significantly higher than the realistic assumption, 3.

The sorbent process is energy competitive in practical situations near room temperature and low relative humidity. As shown by Fig. 3.4, the sorbent process has a niche operating regime where it is near the desorption humidity. Decreasing the adsorption energy barrier and tailoring the relative humidity of desorption to the environment can significantly increase the system-level efficiency. Furthermore, sorbent systems benefit the least (relative to dew and membrane) from increasing heat transfer efficiency. Here, the Carnot efficiency for cooling is fundamentally low due to large temperature gradients. Sorbent processes may be the most effective when heat is available to drive the process.

Membrane processes could theoretically be always energy-optimal (below saturation) with Carnot cooling, isentropic pumps, and 100% recovery. However, in practice the process is significantly hampered by low vacuum pump efficiency ($\eta_{vac} = 20\%$, $\eta_{comp} = 65\%$ [81]) and finite recovery. Other practical considerations such as the pump and condenser inefficiencies, membrane selectivity, and scaling will further decrease the process efficiency.

Fog harvesting is usually constrained to super-saturated conditions, where water is already in the liquid phase. In these conditions, the energy requirement is minimal and therefore energy-superior to dew, membrane, or sorbent AWH systems.

The COP for cooling devices and vacuum pump efficiency pose large barriers in achieving the maximum process efficiency limits. More efficient cooling increases viability for dew harvesting, while more efficient vacuum pumping makes membrane processes better. S15 shows a comparison of ideal technologies with isentropic pumps, Carnot COPs, but finite recoveries. This results in membranes outperforming other methods in low humidity cases, while dew is best in high humidity conditions.

3.3.5 Geospatial analysis

On Earth, the least work for water harvesting may range from 50-500 $\frac{\text{kJ}}{\text{kg}}$, shown by Fig. 3.5. The lowest energy regions tend to be near the equator and over the oceans, due to high

humidity. The energy requirements tend to increase significantly over landmass, especially inland, and vary significantly over small distances. The overarching trends in least work and humidity may be influenced by patterns resembling Hadley cells [88]. For example, certain regions in Central Africa are highly conducive to water harvesting, whereas the Northern and Southern regions of the continent are averse to atmospheric water harvesting (high least work). Water harvesting on ships, over the Ocean, could be energetically optimal and annually stable, from this cursory analysis. Airborne salt particles near the ocean surface may create additional energy requirements that are not accounted for here.

At high and low latitudes (outside $\pm 60^\circ$), the temperatures are often below the freezing point of water (273.15 K), which may induce icing rather than liquid water collection. The effects of climate change may limit the applicability of the extrapolation of these results [89]. Further analysis should use this framework to evaluate the efficiency of specific technologies and consider long-term climate trends.

3.3.6 Field-wide challenges

AWH technology faces significant process and device-level barriers to being a reliable solution to water production. Current research and development trends in tangential fields such as interfacial physics, membrane science, and thermal hydraulics are crucial to bridge the gap between current processes and the thermodynamic minimum.

Sorbents, particularly MOFs, for water harvesting may benefit from highly tuneable materials, as the efficiency of this technology is the most sensitive to the ambient environment. MOF design is an ongoing research challenge, which aims to increase total water capacity (yield) and capture speed, and decrease the energy barrier for water release, while maintaining material stability over time. Engineering MOFs to desorb in energy-optimal conditions will drastically improve process efficiency.

Membrane-based water harvesting relies on highly vapor-selective membranes and high efficiency water vapor pumps. Ongoing challenges with membranes include defect-free fabrication at scale and achieving highly selective to N_2 and O_2 with highly permeable to H_2O . Vacuum pumps and water vapor compressors that are able to work reliably with nearly sat-

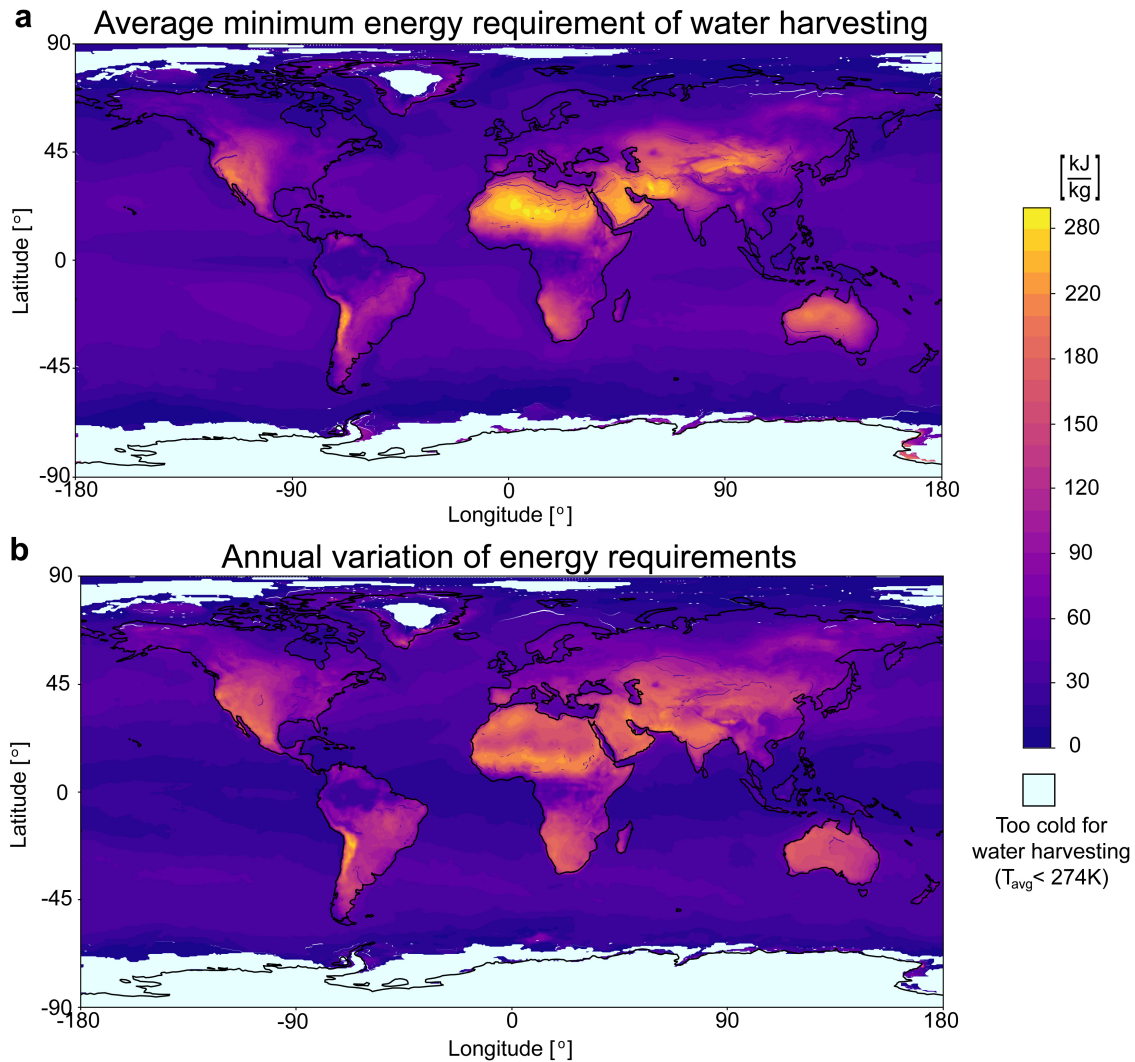


Figure 3.5. The least work for 2021 is computed using hourly satellite re-analysis data. This map shows the geographic distribution of the energy requirements for atmospheric water harvesting. The light-blue shade represents geographic regions where water harvesting may encounter barriers with frost accumulation (average temperature $< 274\text{ K}$). The map uses the surface air temperature, humidity, and pressure in hourly increments at 2m from January 1, 2021 to December 31, 2021. The raw data has a resolution of $0.625^\circ \times 0.5^\circ$ and is from the NASA MERRA-2 reanalysis project [82]

urated water vapor at high efficiencies ($>50\%$) are largely limiting the applicability of this technology.

Dew harvesting technology may best benefit from both process design and material modification. From a process design perspective, closed-loop systems that recirculate air and optimize the condenser temperature and recovery can yield significant efficiency benefits. Further, material and surface modifications – making a surface more hydrophobic or hydrophilic – can be valuable in improving water collection and frost avoidance. However coatings risk quick degradation and often use toxic materials, such as polytetrafluoroethylene (PTFE) [16], [90].

For all technologies, components such as efficient heat pumps and compressors are imperative to reaching the maximum thermodynamic potential. For condensing water, most cooling processes have low efficiencies (3-30% [61]), which then propagate into reducing the system 2nd law efficiency. High efficiency cooling cycles that can operate at a low temperature differences are particularly impactful for dew and membrane processes.

Novel process design that incorporates recirculation, energy reuse, multi-staging, and closed systems may increase the 2nd law efficiency further. Recirculation and energy reuse can allow a system to greatly reduce the energy input requirements for a condenser or pump, by recovering energy from a previous step. Multi-staging allows a process to reduce the driving force within each stage without reducing the total yield [26].

3.4 Chapter conclusions

The thermodynamic efficiency limits of AWH technology creates fundamental understanding for optimizing and tailoring future technology for specific use cases. Idealized analysis shows the efficiency limit for dew harvesting processes (60%), sorbent processes (20%), and membrane processes (50%), and reveals that efficiencies highly vary based on the ambient conditions. Additionally, the recovery ratio most strongly controls the energy requirements of dew and membrane systems. The energy-optimal decision boundary between all processes is tightly linked with the environment (temperature and humidity), and strongly controlled by component-level efficiencies and recovery ratios.

The understanding of process efficiency and the variation of the minimum energy requirements of AWH may be used to imagine novel processes and hybridizations. This work provides a simple computational basis for evaluating the feasibility of AWH against other water technologies like water reuse or desalination. The energy-viability for operating any water harvesting process is largely controlled by the ambient humidity. Regions that consistently experience high humidity (near saturation) may be best for water harvesting, as the least work of water harvesting approaches zero at saturation.

Operationally, systems should aim to tailor the water recovery based on the ambient environment and the efficiency of available components. Below an absolute humidity of approximately $10 \frac{g_w}{kg_{air}}$, the optimal recovery ratio must be reduced to avoid frost accumulation. Below approximately $4 \frac{g_w}{kg_{air}}$, the dew point temperature is comparable to the freezing point of water. In dew processes, recovery should be maximized when low efficiency cooling is used but low recovery at high humidity may be optimal for near-Carnot systems. Energy-optimal membrane processes will minimize vapor flux while maximizing the condenser recovery. Achieving high condenser recovery may require recirculation similar to the design from Bergmair et al. (2014) [68]. Single-stage sorbent-MOF systems consistently have an optimal recovery that lies between 65 to 85%. Additional entropy generation from adverse temperature gradients and frictional effects will increase the energy-optimal recovery of each system.

When comparing ideal processes, dew processes are overwhelmingly more effective in high humidity (RH>50%), while the membrane systems are best in arid regions. When accounting for component inefficiencies, sorbents may have a particular niche in semi-arid regions, while membrane systems are best at low and high temperatures. Dew harvesting is always optimal in high humidity scenarios and fog harvesting is always best when super-saturated conditions are available. Future work may consider hybrid systems (e.g., dew-sorbent, dew-membrane). This approach may take advantage of the high overlap in components and allow for adaptation to regular diurnal and seasonal fluctuations in ambient conditions [4], [89].

Maximum efficiency studies of open systems suggest that sorbent and MOF-based systems suffer thermodynamically but may be effective when high-grade thermal energy is cheaply available. This analysis suggests that reducing energy barriers (adsorption) and large

temperature gradients for desorption can be primary factors for improving the viability of these systems.

Through thermodynamic analysis, we see that current water harvesting processes have room to improve efficiency by over an order of magnitude. This leads us to conclude that future water harvesting technology can improve by selecting optimal operating environments, improving component-level efficiency, and tuning the system-level water recovery. Solutions to field-wide challenges in advanced surface materials, heat pumps, and energy reuse devices will significantly improve the energy efficiency and yield of atmospheric water harvesting technology.

3.5 Chapter acknowledgements

The authors would like to thank Dr. Evelyn Wang and Dr. Hyunho Kim for providing experimental property data for MOF-801. We would also like to thank Dr. Freek Kaptejin, Dr. Tian Li, and Dr. Bikram Bhatia for valuable academic discussions and feedback, as well as Dr. Thomas Beecham for access to supercomputing resources. We thank Geoffery Lenter and staff at the Purdue IT department for providing advice for using high performance computing resources. We would also like acknowledge Anna V. Rausch and Curtis Eckstein for contributions and suggestions about figure and manuscript preparation. Finally, we thank the Purdue department of Mechanical Engineering and the Purdue Center for High Performance Buildings for funding this work.

3.6 Chapter author contributions

Akshay K. Rao: Conceptualization, Methodology, Software, Validation, Formal Analysis, Investigation, Data Curation, Writing, Visualization. Andrew J. Fix: Methodology, Software, Validation, Formal Analysis, Investigation, Data Curation, Writing, Visualization. Yun Chi Yang: Software, Investigation, Data Curation, Visualization. David M. Warsinger: Conceptualization, Writing, Supervision, Project administration, Funding acquisition

4. CONCLUSIONS

4.1 Contributions

Through this work, we provide a general framework for analyzing the thermodynamic limits of water harvesting, with provisions for encapsulating environments where water exists in extreme temperatures and pressures (outside room conditions). This framework was applied to planetary data to obtain the first energy calculation for harvesting water on extraterrestrial environments. Further, it was also for water capture from humid air mixtures at Earth-standard conditions, which resulted in an approach to quickly compute efficiency for atmospheric water harvesting (AWH) technology. This efficiency metric was then applied to compare the performance of AWH approaches on Earth and resulted in identifying technology niches, suggesting mechanisms for energy-optimization, and informing a geographic understanding of the minimum energy requirements.

4.2 Overarching takeaways

The primary, and perhaps obvious, conclusion from studying water harvesting in outer space is that obtaining water from space environments is significantly more energy intense, as opposed to what we are used to on Earth. However, the energy requirements for in-situ approaches are orders of magnitude less than currently feasible methods for transporting water from Earth into Space. When considering extraterrestrial sources, liquid water brines are energy-optimal even when encountering extremely high concentrations. Water vapor sources on many planetary bodies may require more than 4-10x the energy requirement of accessing ice depots. However, the trade-off between using water vapor versus water-ice or liquid water may come down to accessibility, as water vapor may be accessible through decentralized methods.

For water harvesting on Earth, dew harvesting is optimal dew harvesting is optimal in high humidity and membrane systems are better at low humidity. MOFs may be best near room-temperature environments, but only are only competitive with membrane and dew harvesting when the efficiency of heat transfer devices is far below the Carnot efficiency.

Membrane systems that operate with high water recovery and low membrane flux may be significantly better than other approaches to water harvesting in all environments. Current systems for water harvesting are on the order of 5-10% efficient, compared to the thermodynamic minimum. The best way to improve these processes is the implementation of high efficiency pumping and cooling. Additionally, current technologies for accessing water are built for Earth environments and may encounter difficulties in working in sub-freezing temperatures, with complex salt solutions, and at low water vapor pressures (mbar).

4.3 Future work

Future work should consider using the energy efficiency framework to study the performance requirements and viability of new technology trends like liquid sorbents and radiative cooling materials. Additionally, this work highlights the need for understanding the deployment of such gas separation systems in the context of their environment. The approach can be extended to understanding the thermodynamic minimum energy requirements for capturing green house gases like carbon dioxide and methane. Technoeconomic analysis using least work should elucidate decision frontiers associated with the performance-cost trade-off in these low technology readiness level fields.

REFERENCES

- [1] M. M. Mekonnen and A. Y. Hoekstra, “Sustainability: Four billion people facing severe water scarcity,” *Science Advances*, vol. 2, no. 2, 2016, ISSN: 23752548. DOI: [10.1126/sciadv.1500323](https://doi.org/10.1126/sciadv.1500323). [Online]. Available: https://advances.sciencemag.org/content/2/2/e1500323?__hstc=12316075.07430159d50a3c91e72c280a7921bf0d.1520208000163.1520208000164.1520208000165.1&__hssc=12316075.1.1520208000166&__hsfp=998628806.
- [2] L. Castillo, W. Gutierrez, and J. Gore, “Renewable Energy Saves Water and Creates Jobs,” *Scientific American*, pp. 1–17, 2018.
- [3] J. F. Reynolds, D. M. Stafford Smith, E. F. Lambin, *et al.*, *Ecology: Global desertification: Building a science for dryland development*, May 2007. DOI: [10.1126/science.1131634](https://doi.org/10.1126/science.1131634). [Online]. Available: <http://science.sciencemag.org/>.
- [4] UNESCO, “United Nations World Water Development Report 2020 ; Water and Climate Change,” in *UN-Water*, Paris, 2020, ISBN: 9789231003714. DOI: [10.1002/9781118786352.wbieg0793.pub2](https://doi.org/10.1002/9781118786352.wbieg0793.pub2).
- [5] I. Shiklomanov, *Water in crisis: a guide to the world’s fresh water resources*, P. H. Gleick, Ed., 3. New York: Oxford University Press, 1994, vol. 70, pp. 557–557. DOI: [10.2307/2623756](https://doi.org/10.2307/2623756).
- [6] D. M. Warsinger, E. W. Tow, K. G. Nayar, L. A. Maswadeh, and J. H. Lienhard V, “Energy efficiency of batch and semi-batch (CCRO) reverse osmosis desalination,” *Water Research*, vol. 106, pp. 272–282, 2016, ISSN: 18792448. DOI: [10.1016/j.watres.2016.09.029](https://doi.org/10.1016/j.watres.2016.09.029).
- [7] E. Jones, M. Qadir, M. T. van Vliet, V. Smakhtin, and S. mu Kang, *The state of desalination and brine production: A global outlook*, Mar. 2019. DOI: [10.1016/j.scitotenv.2018.12.076](https://doi.org/10.1016/j.scitotenv.2018.12.076).
- [8] D. M. Warsinger, S. Chakraborty, E. W. Tow, *et al.*, “A review of polymeric membranes and processes for potable water reuse,” *Progress in Polymer Science*, vol. 81, pp. 209–237, Jun. 2018, ISSN: 0079-6700. DOI: [10.1016/J.PROGPOLYMSCI.2018.01.004](https://doi.org/10.1016/J.PROGPOLYMSCI.2018.01.004).
- [9] M. Peter-Varbanets, C. Zurbrügg, C. Swartz, and W. Pronk, “Decentralized systems for potable water and the potential of membrane technology,” *Water Research*, vol. 43, no. 2, pp. 245–265, 2009, ISSN: 0043-1354. DOI: <https://doi.org/10.1016/j.watres.2008.10.030>. [Online]. Available: <https://www.sciencedirect.com/science/article/pii/S0043135408004983>.
- [10] K. F. Kaseke and L. Wang, “Fog and Dew as Potable Water Resources: Maximizing Harvesting Potential and Water Quality Concerns,” *GeoHealth*, vol. 2, no. 10, pp. 327–332, Oct. 2018, ISSN: 2471-1403. DOI: [10.1029/2018GH000171@10.1002/\(ISSN\)2169-8996.FOG1](https://doi.org/10.1029/2018GH000171@10.1002/(ISSN)2169-8996.FOG1). [Online]. Available: [https://agupubs.onlinelibrary.wiley.com/doi/full/10.1029/2018GH000171%5C%\\$4010.1002/%5C%\\$28ISSN%5C%\\$292169-8996.FOG1](https://agupubs.onlinelibrary.wiley.com/doi/full/10.1029/2018GH000171%5C%$4010.1002/%5C%$28ISSN%5C%$292169-8996.FOG1).

- [11] B. Teychene, G. Collet, H. Gallard, and J.-P. Croue, “A comparative study of boron and arsenic (III) rejection from brackish water by reverse osmosis membranes,” *Desalination*, vol. 310, Feb. 2013, ISSN: 00119164. DOI: [10.1016/j.desal.2012.05.034](https://doi.org/10.1016/j.desal.2012.05.034).
- [12] R. Enright, N. Miljkovic, J. L. Alvarado, K. Kim, and J. W. Rose, “Dropwise Condensation on Micro- and Nanostructured Surfaces,” *Nanoscale and Microscale Thermophysical Engineering*, vol. 18, no. 3, pp. 223–250, Jul. 2014, ISSN: 1556-7265. DOI: [10.1080/15567265.2013.862889](https://doi.org/10.1080/15567265.2013.862889).
- [13] V. R. S. S. Mokkapati, D. Y. Koseoglu-Imer, N. Yilmaz-Deveci, I. Mijakovic, and I. Koyuncu, “Membrane properties and anti-bacterial/anti-biofouling activity of polysulfone–graphene oxide composite membranes phase inversed in graphene oxide non-solvent,” *RSC Advances*, vol. 7, no. 8, pp. 4378–4386, 2017, ISSN: 2046-2069. DOI: [10.1039/C6RA25015G](https://doi.org/10.1039/C6RA25015G).
- [14] Y. Y. Song, Y. Liu, H. B. Jiang, *et al.*, “A bioinspired structured graphene surface with tunable wetting and high wearable properties for efficient fog collection,” *Nanoscale*, vol. 10, no. 34, pp. 16 127–16 137, Sep. 2018, ISSN: 20403372. DOI: [10.1039/c8nr04109a](https://doi.org/10.1039/c8nr04109a). [Online]. Available: <https://pubs.rsc.org/en/content/articlehtml/2018/nr/c8nr04109a> %20https://pubs.rsc.org/en/content/articlelanding/2018/nr/c8nr04109a.
- [15] F. Fathieh, M. J. Kalmutzki, E. A. Kapustin, P. J. Waller, J. Yang, and O. M. Yaghi, “Practical water production from desert air,” *Science Advances*, vol. 4, no. 6, Jun. 2018, ISSN: 2375-2548. DOI: [10.1126/sciadv.aat3198](https://doi.org/10.1126/sciadv.aat3198).
- [16] Y. Tu, R. Wang, Y. Zhang, and J. Wang, *Progress and Expectation of Atmospheric Water Harvesting*, Aug. 2018. DOI: [10.1016/j.joule.2018.07.015](https://doi.org/10.1016/j.joule.2018.07.015).
- [17] L. Hua, J. Xu, and R. Wang, “Exergy-efficient boundary and design guidelines for atmospheric water harvesters with nano-porous sorbents,” *Nano Energy*, vol. 85, p. 105 977, Jul. 2021, ISSN: 22112855. DOI: [10.1016/j.nanoen.2021.105977](https://doi.org/10.1016/j.nanoen.2021.105977).
- [18] J. Lord, A. Thomas, N. Treat, *et al.*, “Global potential for harvesting drinking water from air using solar energy,” *Nature*, vol. 598, no. 7882, pp. 611–617, Oct. 2021, ISSN: 0028-0836. DOI: [10.1038/s41586-021-03900-w](https://doi.org/10.1038/s41586-021-03900-w).
- [19] S. Pérez-Hoyos, A. Sánchez-Lavega, A. García-Muñoz, *et al.*, “Venus Upper Clouds and the UV Absorber From MESSENGER/MASCS Observations,” *Journal of Geophysical Research: Planets*, vol. 123, no. 1, Jan. 2018, ISSN: 21699097. DOI: [10.1002/2017JE005406](https://doi.org/10.1002/2017JE005406).
- [20] J. D. Toner, D. C. Catling, and B. Light, “Soluble salts at the Phoenix Lander site, Mars: A reanalysis of the Wet Chemistry Laboratory data,” *Geochimica et Cosmochimica Acta*, vol. 136, pp. 142–168, Jul. 2014, ISSN: 00167037. DOI: [10.1016/j.gca.2014.03.030](https://doi.org/10.1016/j.gca.2014.03.030).

- [21] K. H. Mistry, H. A. Hunter, and J. H. Lienhard V, “Effect of composition and nonideal solution behavior on desalination calculations for mixed electrolyte solutions with comparison to seawater,” *Desalination*, vol. 318, pp. 34–47, Jun. 2013, ISSN: 00119164. DOI: [10.1016/j.desal.2013.03.015](https://doi.org/10.1016/j.desal.2013.03.015).
- [22] N. L. Chabot, C. M. Ernst, J. K. Harmon, *et al.*, “Craters hosting radar-bright deposits in Mercury’s north polar region: Areas of persistent shadow determined from MESSENGER images,” *Journal of Geophysical Research E: Planets*, vol. 118, no. 1, pp. 26–36, 2013, ISSN: 01480227. DOI: [10.1029/2012JE004172](https://doi.org/10.1029/2012JE004172).
- [23] J. D. Toner, D. C. Catling, and B. Light, “The formation of supercooled brines, viscous liquids, and low-temperature perchlorate glasses in aqueous solutions relevant to Mars,” *Icarus*, vol. 233, pp. 36–47, May 2014, ISSN: 00191035. DOI: [10.1016/j.icarus.2014.01.018](https://doi.org/10.1016/j.icarus.2014.01.018).
- [24] K. H. Mistry and J. H. Lienhard, “Generalized least energy of separation for desalination and other chemical separation processes,” *Entropy*, 2013, ISSN: 10994300. DOI: [10.3390/e15062046](https://doi.org/10.3390/e15062046).
- [25] S. Lin, *Energy Efficiency of Desalination: Fundamental Insights from Intuitive Interpretation*, 2020. DOI: [10.1021/acs.est.9b04788](https://doi.org/10.1021/acs.est.9b04788). [Online]. Available: <https://pubs.acs.org/sharingguidelines>.
- [26] A. LaPotin, Y. Zhong, L. Zhang, *et al.*, “Dual-Stage Atmospheric Water Harvesting Device for Scalable Solar-Driven Water Production,” *Joule*, vol. 5, no. 1, pp. 166–182, Jan. 2021, ISSN: 25424351. DOI: [10.1016/j.joule.2020.09.008](https://doi.org/10.1016/j.joule.2020.09.008).
- [27] A. Das and D. M. Warsinger, “Batch counterflow reverse osmosis,” *Desalination*, vol. 507, p. 115 008, Jul. 2021, ISSN: 0011-9164. DOI: [10.1016/J.DESAL.2021.115008](https://doi.org/10.1016/J.DESAL.2021.115008).
- [28] K. M. Brodersen, E. A. Bywater, A. M. Lanter, *et al.*, “Direct-drive ocean wave-powered batch reverse osmosis,” *Desalination*, vol. 523, Jul. 2022, ISSN: 00119164. DOI: [10.1016/j.desal.2021.115393](https://doi.org/10.1016/j.desal.2021.115393). arXiv: [2107.07137](https://arxiv.org/abs/2107.07137). [Online]. Available: <https://arxiv.org/abs/2107.07137v1>.
- [29] M. Qin, A. Deshmukh, R. Epsztein, *et al.*, “Comparison of energy consumption in desalination by capacitive deionization and reverse osmosis,” *Desalination*, vol. 455, pp. 100–114, Apr. 2019, ISSN: 00119164. DOI: [10.1016/j.desal.2019.01.003](https://doi.org/10.1016/j.desal.2019.01.003).
- [30] H. Kim, S. R. Rao, A. LaPotin, S. Lee, and E. N. Wang, “Thermodynamic analysis and optimization of adsorption-based atmospheric water harvesting,” *International Journal of Heat and Mass Transfer*, vol. 161, p. 120 253, Nov. 2020, ISSN: 00179310. DOI: [10.1016/j.ijheatmasstransfer.2020.120253](https://doi.org/10.1016/j.ijheatmasstransfer.2020.120253).

- [31] M. K. Dougherty, K. K. Khurana, F. M. Neubauer, *et al.*, “Identification of a dynamic atmosphere at Enceladus with the Cassini magnetometer,” *Science*, vol. 311, no. 5766, pp. 1406–1409, Mar. 2006, ISSN: 00368075. DOI: [10.1126/science.1120985](https://doi.org/10.1126/science.1120985).
- [32] P. R. Christensen, D. L. Anderson, S. C. Chase, *et al.*, “Results from the Mars global surveyor thermal emission spectrometer,” *Science*, vol. 279, no. 5357, pp. 1692–1696, Mar. 1998, ISSN: 00368075. DOI: [10.1126/science.279.5357.1692](https://doi.org/10.1126/science.279.5357.1692). [Online]. Available: <http://science.sciencemag.org/>.
- [33] W. M. Folkner, R. D. Kahn, R. A. Preston, *et al.*, “Mars dynamics from Earth-based tracking of the Mars Pathfinder lander,” *Journal of Geophysical Research: Planets*, vol. 102, no. E2, pp. 4057–4064, Feb. 1997, ISSN: 2156-2202. DOI: [10.1029/96JE02125@10.1002/\(ISSN\)2169-9100.MPATHMISS1](https://doi.org/10.1029/96JE02125@10.1002/(ISSN)2169-9100.MPATHMISS1).
- [34] C. B. Farmer, D. W. Davies, and D. D. Laporte, “Mars: Northern summer ice cap - Water vapor observations from Viking 2,” *Science*, vol. 194, no. 4271, pp. 1339–1340, Dec. 1976, ISSN: 00368075. DOI: [10.1126/science.194.4271.1339](https://doi.org/10.1126/science.194.4271.1339). [Online]. Available: <https://science.sciencemag.org/content/194/4271/1339%20https://science.sciencemag.org/content/194/4271/1339.abstract>.
- [35] J. S. Lewis, “The clouds of Jupiter and the NH₃—H₂O and NH₃—H₂S systems,” *Icarus*, vol. 10, no. 3, pp. 365–378, May 1969, ISSN: 0019-1035. DOI: [10.1016/0019-1035\(69\)90091-8](https://doi.org/10.1016/0019-1035(69)90091-8). [Online]. Available: <https://www.sciencedirect.com/science/article/pii/0019103569900918>.
- [36] C. C. Porco, P. Helfenstein, P. C. Thomas, *et al.*, “Cassini observes the active south pole of enceladus,” *Science*, vol. 311, no. 5766, pp. 1393–1401, Mar. 2006, ISSN: 00368075. DOI: [10.1126/science.1123013](https://doi.org/10.1126/science.1123013). [Online]. Available: <http://science.sciencemag.org/>.
- [37] J. I. Lunine, “Ocean worlds exploration,” *Acta Astronautica*, vol. 131, pp. 123–130, Feb. 2017, ISSN: 00945765. DOI: [10.1016/j.actaastro.2016.11.017](https://doi.org/10.1016/j.actaastro.2016.11.017).
- [38] J. I. Lunine and D. M. Hunten, “Moist convection and the abundance of water in the troposphere of Jupiter,” *Icarus*, vol. 69, no. 3, pp. 566–570, Mar. 1987, ISSN: 0019-1035. DOI: [10.1016/0019-1035\(87\)90025-X](https://doi.org/10.1016/0019-1035(87)90025-X). [Online]. Available: <https://www.sciencedirect.com/science/article/pii/001910358790025X>.
- [39] C. J. Hansen, D. E. Shemansky, L. W. Esposito, *et al.*, “The composition and structure of the Enceladus plume,” *Geophysical Research Letters*, vol. 38, no. 11, Jun. 2011, ISSN: 00948276. DOI: [10.1029/2011GL047415](https://doi.org/10.1029/2011GL047415). [Online]. Available: <https://agupubs.onlinelibrary.wiley.com/doi/full/10.1029/2011GL047415%20https://agupubs.onlinelibrary.wiley.com/doi/abs/10.1029/2011GL047415%20https://agupubs.onlinelibrary.wiley.com/doi/10.1029/2011GL047415>.

- [40] B. A. Smith, L. A. Soderblom, R. Beebe, *et al.*, “The galilean satellites and Jupiter: Voyager 2 imaging science results,” *Science*, vol. 206, no. 4421, pp. 927–950, 1979, ISSN: 00368075. DOI: [10.1126/science.206.4421.927](https://doi.org/10.1126/science.206.4421.927).
- [41] B. Bézard and C. de Bergh, “Composition of the atmosphere of Venus below the clouds,” *Journal of Geophysical Research E: Planets*, vol. 112, no. 4, E04S07, Apr. 2007, ISSN: 01480227. DOI: [10.1029/2006JE002794](https://doi.org/10.1029/2006JE002794). [Online]. Available: <http://doi.wiley.com/10.1029/2006JE002794>.
- [42] P. D. Spudis, D. B. J. Bussey, S. M. Baloga, *et al.*, “Evidence for water ice on the Moon: Results for anomalous polar craters from the LRO Mini-RF imaging radar,” *Journal of Geophysical Research: Planets*, vol. 118, no. 10, pp. 2016–2029, Oct. 2013, ISSN: 21699097. DOI: [10.1002/jgre.20156](https://doi.org/10.1002/jgre.20156). [Online]. Available: <http://doi.wiley.com/10.1002/jgre.20156>.
- [43] D. P. Cruikshank, “Near-infrared studies of the satellites of Saturn and Uranus,” *Icarus*, vol. 41, no. 2, pp. 246–258, 1980, ISSN: 10902643. DOI: [10.1016/0019-1035\(80\)90008-1](https://doi.org/10.1016/0019-1035(80)90008-1).
- [44] D. C. Shallcross, “Preparation of psychrometric charts for water vapour in Martian atmosphere,” *International Journal of Heat and Mass Transfer*, vol. 48, no. 9, pp. 1785–1796, Apr. 2005, ISSN: 0017-9310. DOI: [10.1016/J.IJHEATMASSTRANSFER.2004.11.015](https://doi.org/10.1016/J.IJHEATMASSTRANSFER.2004.11.015).
- [45] A. K. Rao, A. J. Fix, and D. M. Warsinger, “Thermodynamic limits of atmospheric water harvesting technology,” *Pending review in Energy and Environmental Science.*, vol. xx, no. xx, p. xx, 2021.
- [46] J. D. Toner and D. C. Catling, “Water activities of NaClO₄, Ca(ClO₄)₂, and Mg(ClO₄)₂ brines from experimental heat capacities: Water activity >0.6 below 200 K,” *Geochimica et Cosmochimica Acta*, vol. 181, pp. 164–174, May 2016, ISSN: 00167037. DOI: [10.1016/j.gca.2016.03.005](https://doi.org/10.1016/j.gca.2016.03.005).
- [47] B. S. Krumgalz, A. Starinsky, and K. S. Pitzer, “Ion-interaction approach: Pressure effect on the solubility of some minerals in submarine brines and seawater,” *Journal of Solution Chemistry*, vol. 28, no. 6, pp. 667–692, 1999, ISSN: 00959782. DOI: [10.1023/a:1021711926908](https://doi.org/10.1023/a:1021711926908). [Online]. Available: <https://link.springer.com/article/10.1023/A:1021711926908>.
- [48] T. B. McCord, G. B. Hansen, and C. A. Hibbitts, “Hydrated salt minerals on Ganymede’s surface: Evidence of an ocean below,” *Science*, vol. 292, no. 5521, pp. 1523–1525, May 2001, ISSN: 00368075. DOI: [10.1126/science.1059916](https://doi.org/10.1126/science.1059916). [Online]. Available: <http://science.sciencemag.org/content/292/5521/1523>.
- [49] B. Henin, *Exploring the Ocean Worlds of Our Solar System*. 2018, pp. 79–96, ISBN: 9783319934761. DOI: [10.1007/978-3-319-93476-1](https://doi.org/10.1007/978-3-319-93476-1).

- [50] A. L. Bruce, “A General Quadrature Solution for Relativistic, Non-relativistic, and Weakly-Relativistic Rocket Equations,” Apr. 2015. arXiv: [1504.07205](https://arxiv.org/abs/1504.07205). [Online]. Available: <https://arxiv.org/abs/1504.07205v1>.
- [51] A. Bejan, *Entropy generation minimization: the method of thermodynamic optimization of finite-size systems and finite-time processes*. Boca Raton, FL: CRC press, 2013.
- [52] G. C. Lordos, J. A. Hoffman, and S. E. Summers, “Towards a sustainable industrial development of mars: Comparing novel ISRU / ISM architectures using lifetime embodied energy,” in *2018 AIAA SPACE and Astronautics Forum and Exposition*, American Institute of Aeronautics and Astronautics Inc, AIAA, 2018, ISBN: 9781624105753. DOI: [10.2514/6.2018-5125](https://doi.org/10.2514/6.2018-5125). [Online]. Available: <https://arc.aiaa.org/doi/abs/10.2514/6.2018-5125>.
- [53] G. B. Sanders, “Advancing in situ resource utilization capabilities to achieve a new paradigm in space exploration,” in *2018 AIAA SPACE and Astronautics Forum and Exposition*, American Institute of Aeronautics and Astronautics Inc, AIAA, 2018, ISBN: 9781624105753. DOI: [10.2514/6.2018-5124](https://doi.org/10.2514/6.2018-5124).
- [54] M. Rezaei, A. Alsaati, D. M. Warsinger, F. Hell, and W. M. Samhaber, “Long-Running Comparison of Feed-Water Scaling in Membrane Distillation,” *Membranes 2020, Vol. 10, Page 173*, vol. 10, no. 8, p. 173, Jul. 2020. DOI: [10.3390/MEMBRANES10080173](https://doi.org/10.3390/MEMBRANES10080173). [Online]. Available: <https://www.mdpi.com/2077-0375/10/8/173/htm%20https://www.mdpi.com/2077-0375/10/8/173>.
- [55] S. R. Charlton and D. L. Parkhurst, “Modules based on the geochemical model PHREEQC for use in scripting and programming languages,” *Computers and Geosciences*, vol. 37, no. 10, pp. 1653–1663, Oct. 2011, ISSN: 00983004. DOI: [10.1016/j.cageo.2011.02.005](https://doi.org/10.1016/j.cageo.2011.02.005).
- [56] K. Klein and F. A. .-. Middleton, *Ees-engineering equation solver*, 2004.
- [57] I. H. Bell, J. Wronski, S. Quoilin, and V. Lemort, “Pure and pseudo-pure fluid thermophysical property evaluation and the open-source thermophysical property library cool-prop,” *Industrial and Engineering Chemistry Research*, vol. 53, no. 6, pp. 2498–2508, Feb. 2014, ISSN: 08885885. DOI: [10.1021/ie4033999](https://doi.org/10.1021/ie4033999). [Online]. Available: <https://pubs.acs.org/sharingguidelines>.
- [58] A. L. Buck, “New equations for computing vapour pressure and enhancement factor.,” Tech. Rep. 12, 1981, pp. 1527–1532. DOI: [10.1175/1520-0450\(1981\)020<1527:nefcvp>2.0.co;2](https://doi.org/10.1175/1520-0450(1981)020<1527:nefcvp>2.0.co;2). [Online]. Available: https://journals.ametsoc.org/view/journals/apme/20/12/1520-0450_1981_020_1527_nefcvp_2_0_co_2.xml.

- [59] B. Gido, E. Friedler, and D. M. Broday, “Assessment of atmospheric moisture harvesting by direct cooling,” *Atmospheric Research*, vol. 182, pp. 156–162, 2016, ISSN: 01698095. DOI: [10.1016/j.atmosres.2016.07.029](https://doi.org/10.1016/j.atmosres.2016.07.029). [Online]. Available: <http://dx.doi.org/10.1016/j.atmosres.2016.07.029>.
- [60] J. Steven Brown and P. A. Domanski, “Review of alternative cooling technologies,” *Applied Thermal Engineering*, vol. 64, no. 1-2, pp. 252–262, Mar. 2014, ISSN: 1359-4311. DOI: [10.1016/J.APPLTHERMALENG.2013.12.014](https://doi.org/10.1016/J.APPLTHERMALENG.2013.12.014).
- [61] O. Labban, T. Chen, A. F. Ghoniem, J. H. Lienhard, and L. K. Norford, “Next-generation hvac: Prospects for and limitations of desiccant and membrane-based dehumidification and cooling,” *Applied Energy*, vol. 200, pp. 330–346, Aug. 2017, ISSN: 0306-2619. DOI: [10.1016/J.APENERGY.2017.05.051](https://doi.org/10.1016/J.APENERGY.2017.05.051).
- [62] M. Dong, Z. Zhang, Y. Shi, X. Zhao, S. Fan, and Z. Chen, “Fundamental Limits of the Dew-Harvesting Technology,” *Nanoscale and Microscale Thermophysical Engineering*, vol. 24, no. 1, pp. 43–52, Jan. 2020, ISSN: 15567273. DOI: [10.1080/15567265.2020.1722300](https://doi.org/10.1080/15567265.2020.1722300). arXiv: [1909.05757](https://arxiv.org/abs/1909.05757). [Online]. Available: <https://www.tandfonline.com/doi/full/10.1080/15567265.2020.1722300>.
- [63] O. Klemm, R. S. Schemenauer, A. Lummerich, *et al.*, “Fog as a Fresh-Water Resource: Overview and Perspectives,” *AMBIO*, no. 41, pp. 221–234, 2012. DOI: [10.1007/s13280-012-0247-8](https://doi.org/10.1007/s13280-012-0247-8). [Online]. Available: www.marienberg.cl.
- [64] A. Torregrosa, C. Combs, and J. Peters, “GOES-derived fog and low cloud indices for coastal north and central California ecological analyses,” *Earth and Space Science*, vol. 3, no. 2, pp. 46–67, Feb. 2016, ISSN: 2333-5084. DOI: [10.1002/2015EA000119](https://doi.org/10.1002/2015EA000119). [Online]. Available: <https://onlinelibrary.wiley.com/doi/full/10.1002/2015EA000119%20https://onlinelibrary.wiley.com/doi/abs/10.1002/2015EA000119%20https://agupubs.onlinelibrary.wiley.com/doi/10.1002/2015EA000119>.
- [65] A. Entezari, M. Ejeian, and R. Wang, “Modifying water sorption properties with polymer additives for atmospheric water harvesting applications,” *Applied Thermal Engineering*, vol. 161, p. 114 109, Oct. 2019, ISSN: 13594311. DOI: [10.1016/j.applthermaleng.2019.114109](https://doi.org/10.1016/j.applthermaleng.2019.114109).
- [66] M. W. Logan, S. Langevin, and Z. Xia, “Reversible Atmospheric Water Harvesting Using Metal-Organic Frameworks,” *Scientific Reports*, vol. 10, no. 1, pp. 1–11, Dec. 2020, ISSN: 20452322. DOI: [10.1038/s41598-020-58405-9](https://doi.org/10.1038/s41598-020-58405-9). [Online]. Available: <https://doi.org/10.1038/s41598-020-58405-9>.
- [67] H. Kim, S. R. Rao, E. A. Kapustin, *et al.*, “Adsorption-based atmospheric water harvesting device for arid climates,” *Nature Communications*, vol. 9, no. 1, Dec. 2018, ISSN: 20411723. DOI: [10.1038/s41467-018-03162-7](https://doi.org/10.1038/s41467-018-03162-7).

- [68] D. Bergmair, S. J. Metz, H. C. De Lange, and A. A. van Steenhoven, “System analysis of membrane facilitated water generation from air humidity,” *Desalination*, vol. 339, no. 1, pp. 26–33, Apr. 2014, ISSN: 00119164. DOI: [10.1016/j.desal.2014.02.007](https://doi.org/10.1016/j.desal.2014.02.007).
- [69] D. E. Claridge, C. Culp, W. Liu, *et al.*, “A new approach for drying moist air: The ideal Claridge-Culp-Liu dehumidification process with membrane separation, vacuum compression and sub-atmospheric condensation,” *International Journal of Refrigeration*, vol. 101, pp. 211–217, May 2019, ISSN: 01407007. DOI: [10.1016/j.ijrefrig.2019.03.025](https://doi.org/10.1016/j.ijrefrig.2019.03.025).
- [70] A. J. Fix, J. E. Braun, and D. M. Warsinger, “Vapor-selective active membrane energy exchanger for high efficiency outdoor air treatment,” *Applied Energy*, vol. 295, 2021, ISSN: 03062619. DOI: [10.1016/j.apenergy.2021.116950](https://doi.org/10.1016/j.apenergy.2021.116950).
- [71] J. Woods, *Membrane processes for heating, ventilation, and air conditioning*, May 2014. DOI: [10.1016/j.rser.2014.01.092](https://doi.org/10.1016/j.rser.2014.01.092).
- [72] O. R. Al-Jayyousi and M. S. Mohsen, “Evaluation of Fog Collection in Jordan,” *Water and Environment Journal*, vol. 13, no. 3, pp. 195–199, Jun. 1999, ISSN: 1747-6585. DOI: [10.1111/j.1747-6593.1999.tb01034.x](https://doi.org/10.1111/j.1747-6593.1999.tb01034.x). [Online]. Available: <https://doi.org/10.1111/j.1747-6593.1999.tb01034.x>.
- [73] Y. Tai, H. Liang, A. Zaki, *et al.*, “Core/Shell Microstructure Induced Synergistic Effect for Efficient Water-Droplet Formation and Cloud-Seeding Application,” *ACS Nano*, vol. 11, no. 12, pp. 12 318–12 325, Dec. 2017, ISSN: 1936086X. DOI: [10.1021/acsnano.7b06114](https://doi.org/10.1021/acsnano.7b06114). [Online]. Available: www.acsnano.org.
- [74] H. Vuollekoski, M. Vogt, V. A. Sinclair, *et al.*, “Estimates of global dew collection potential on artificial surfaces,” *Hydrology and Earth System Sciences*, vol. 19, no. 1, pp. 601–613, Jan. 2015, ISSN: 16077938. DOI: [10.5194/hess-19-601-2015](https://doi.org/10.5194/hess-19-601-2015).
- [75] F. Bagheri, “Performance investigation of atmospheric water harvesting systems,” *Water Resources and Industry*, vol. 20, pp. 23–28, Dec. 2018, ISSN: 22123717. DOI: [10.1016/j.wri.2018.08.001](https://doi.org/10.1016/j.wri.2018.08.001).
- [76] B. Zhao, L. Y. Wang, and T. S. Chung, “Enhanced membrane systems to harvest water and provide comfortable air via dehumidification moisture condensation,” *Separation and Purification Technology*, vol. 220, pp. 136–144, Aug. 2019, ISSN: 18733794. DOI: [10.1016/j.seppur.2019.03.034](https://doi.org/10.1016/j.seppur.2019.03.034).
- [77] W. Xu and O. M. Yaghi, “Metal-Organic Frameworks for Water Harvesting from Air, Anywhere, Anytime,” *ACS Central Science*, vol. 12, p. 20, Aug. 2020, ISSN: 23747951. DOI: [10.1021/acscentsci.0c00678](https://doi.org/10.1021/acscentsci.0c00678). [Online]. Available: <http://pubs.acs.org/journal/acscii>.

- [78] X. Zhou, H. Lu, F. Zhao, and G. Yu, *Atmospheric water harvesting: A review of material and structural designs*, Jul. 2020. DOI: [10.1021/acsmaterialslett.0c00130](https://doi.org/10.1021/acsmaterialslett.0c00130). [Online]. Available: www.acsmaterialsletters.org.
- [79] ASHRAE, “2009 ASHRAE Fundamentals,” *ASHRAE*, Chapter 1, 2009. [Online]. Available: [http://tecdigital.tec.ac.cr/file/2718369/\(Sist._Ingl%7B%5C'%7Be%7D%7Ds\)_Ashrae_-_Fundamentals.pdf](http://tecdigital.tec.ac.cr/file/2718369/(Sist._Ingl%7B%5C'%7Be%7D%7Ds)_Ashrae_-_Fundamentals.pdf).
- [80] X. Liu, X. Wang, and F. Kapteijn, “Water and Metal–Organic Frameworks: From Interaction toward Utilization,” *Chemical Reviews*, vol. 120, no. 16, pp. 8303–8377, Aug. 2020, ISSN: 0009-2665. DOI: [10.1021/acs.chemrev.9b00746](https://doi.org/10.1021/acs.chemrev.9b00746). [Online]. Available: <https://doi.org/10.1021/acs.chemrev.9b00746>.
- [81] T. D. Bui, Y. Wong, M. R. Islam, and K. J. Chua, “On the theoretical and experimental energy efficiency analyses of a vacuum-based dehumidification membrane,” *Journal of Membrane Science*, vol. 539, pp. 76–87, Oct. 2017, ISSN: 0376-7388. DOI: [10.1016/J.MEMSCI.2017.05.067](https://doi.org/10.1016/J.MEMSCI.2017.05.067).
- [82] G. Modeling and A. O. (GMAO), *Merra-2 inst1₂d_lf_{o_n}x: 2d,1-hourly,instantaneous,single-level,assimilation,land surface forcings v5.12.4*, 2015. DOI: [10.5067/RCMZA6TL70BG](https://doi.org/10.5067/RCMZA6TL70BG).
- [83] S. Khodakarami, L. Li, and N. Miljkovic, “Ultra-efficient and ultra-rapid solar cell de-icing and de-snowing,” <https://doi.org/10.1117/12.2598078>, vol. 11824, pp. 33–42, Aug. 2021. DOI: [10.1117/12.2598078](https://doi.org/10.1117/12.2598078). [Online]. Available: <https://www.spiedigitallibrary.org/conference-proceedings-of-spie/11824/118240C/Ultra-efficient-and-ultra-rapid-solar-cell-de-icing-and/10.1117/12.2598078.full%20https://www.spiedigitallibrary.org/conference-proceedings-of-spie/11824/118240C/Ultra-efficient-and-ultra-rapid-solar-cell-de-icing-and/10.1117/12.2598078.short%20https://www.spiedigitallibrary.org/conference-proceedings-of-spie/11824/118240C/Ultra-efficient-and-ultra-rapid-solar-cell-de-icing-and/.full>.
- [84] A. J. Mahvi, K. Boyina, A. Musser, S. Elbel, and N. Miljkovic, “Superhydrophobic heat exchangers delay frost formation and enhance efficiency of electric vehicle heat pumps,” *International Journal of Heat and Mass Transfer*, vol. 172, p. 121 162, Jun. 2021, ISSN: 0017-9310. DOI: [10.1016/J.IJHEATMASSTRANSFER.2021.121162](https://doi.org/10.1016/J.IJHEATMASSTRANSFER.2021.121162).
- [85] E. W. Tow, D. M. Warsinger, A. M. Trueworthy, *et al.*, “Comparison of fouling propensity between reverse osmosis, forward osmosis, and membrane distillation,” *Journal of Membrane Science*, vol. 556, pp. 352–364, 2018, ISSN: 18733123. DOI: [10.1016/j.memsci.2018.03.065](https://doi.org/10.1016/j.memsci.2018.03.065). [Online]. Available: https://www.sciencedirect.com/science/article/pii/S0376738818303247?casa_token=vDH00E27Bv0AAAAA:qA9ai-_505BMkaS4UXxjbQ5wETBiNuzQlhPFUgcHLEHpWtqPvFYX7u1Nq2yE_ogg34v2hnpVmg.

- [86] H. Yang, H. Zhu, M. M. Hendrix, *et al.*, “Temperature-triggered collection and release of water from fogs by a sponge-like cotton fabric,” *Advanced Materials*, vol. 25, no. 8, pp. 1150–1154, Feb. 2013, ISSN: 09359648. DOI: [10.1002/adma.201204278](https://doi.org/10.1002/adma.201204278).
- [87] D. E. Warsinger, J. Swaminathan, L. A. Maswadeh, and J. H. Lienhard, “Superhydrophobic condenser surfaces for air gap membrane distillation,” *Journal of Membrane Science*, vol. 492, pp. 578–587, Oct. 2015, ISSN: 18733123. DOI: [10.1016/j.memsci.2015.05.067](https://doi.org/10.1016/j.memsci.2015.05.067). [Online]. Available: <https://www.sciencedirect.com/science/article/pii/S0376738815005050>.
- [88] D. M. Frierson, J. Lu, and G. Chen, “Width of the Hadley cell in simple and comprehensive general circulation models,” *Geophysical Research Letters*, vol. 34, no. 18, p. 18 804, Sep. 2007, ISSN: 1944-8007. DOI: [10.1029/2007GL031115](https://doi.org/10.1029/2007GL031115). [Online]. Available: <https://onlinelibrary.wiley.com/doi/full/10.1029/2007GL031115%20https://onlinelibrary.wiley.com/doi/abs/10.1029/2007GL031115%20https://agupubs.onlinelibrary.wiley.com/doi/10.1029/2007GL031115>.
- [89] E. Jansen, J. H. Christensen, T. Dokken, *et al.*, “Past perspectives on the present era of abrupt Arctic climate change,” *Nature Climate Change*, vol. 10, no. 8, Aug. 2020, ISSN: 1758-678X. DOI: [10.1038/s41558-020-0860-7](https://doi.org/10.1038/s41558-020-0860-7).
- [90] Y. Gurumukhi, S. Chavan, S. Sett, *et al.*, “Dynamic Defrosting on Superhydrophobic and Biphilic Surfaces,” *Matter*, vol. 3, no. 4, pp. 1178–1195, Oct. 2020, ISSN: 25902385. DOI: [10.1016/j.matt.2020.06.029](https://doi.org/10.1016/j.matt.2020.06.029).
- [91] A. Wexler, “VAPOR PRESSURE FORMULATION FOR ICE.,” *J Res Natl Bur Stand Sect A Phys Chem*, vol. 81 A, no. 1, pp. 5–20, 1977, ISSN: 0022-4332. DOI: [10.6028/jres.081A.003](https://doi.org/10.6028/jres.081A.003).

A. APPENDIX: OBTAINING WATER IN THE SOLAR SYSTEM

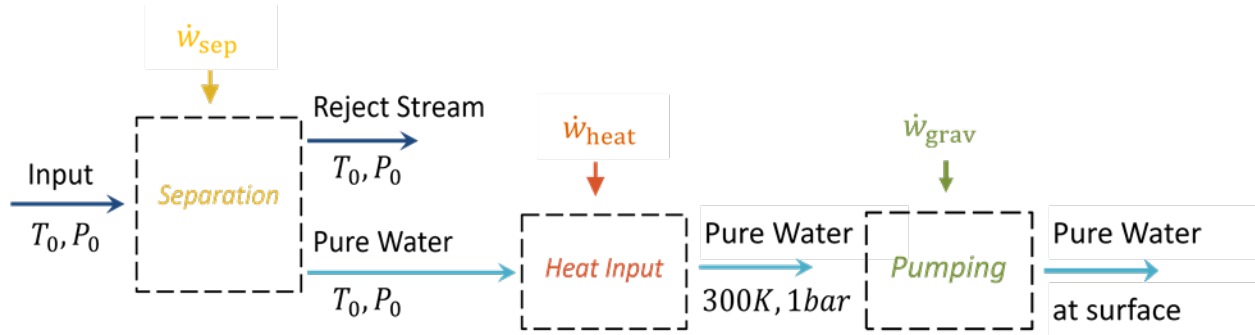


Figure A.1. Extended least work model visualization: The least work can be modeled as a staged, fully reversible process. The input and reject streams represent the feed and brine. These are evaluated the natural temperature of the source. The pure water from the input mixture is separated, isothermally using the minimum separation work. It is then brought to the Earth standard conditions, via the work due to heating. A third stage can be similarly added when gravitational potential is applicable.

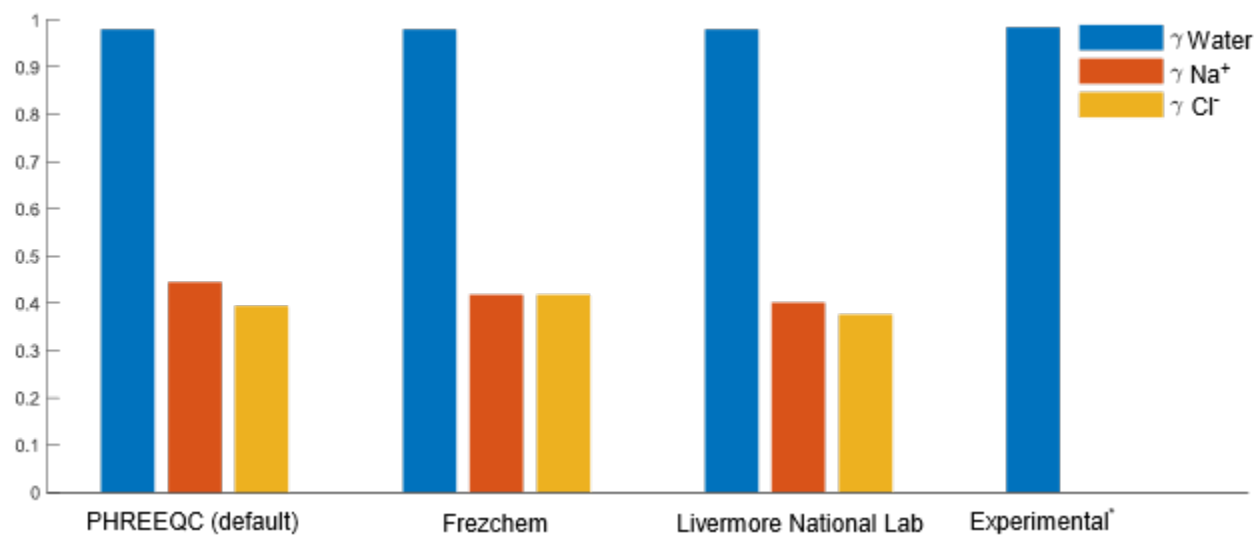


Figure A.2. PHREEQC model validation: A comparison of activity coefficient values to validate the thermochemical property models in PHREEQC is shown [CITE 1,2]. The activity of water, Na⁺, and Cl⁻ are compared to prior literature for the thermochemical databases used in this study. The comparison was done at 300K and 0.596M (seawater salinity). The PHREEQC (default) and Livermore National Lab (LLNL) databases are publicly available at USGS. The Frezchem database is provided by Professor David Catling and Dr. Jon Toner [20], [23], [46]. Experimental values are provided at M = 0.6 from Chirife and Resnik (1984).

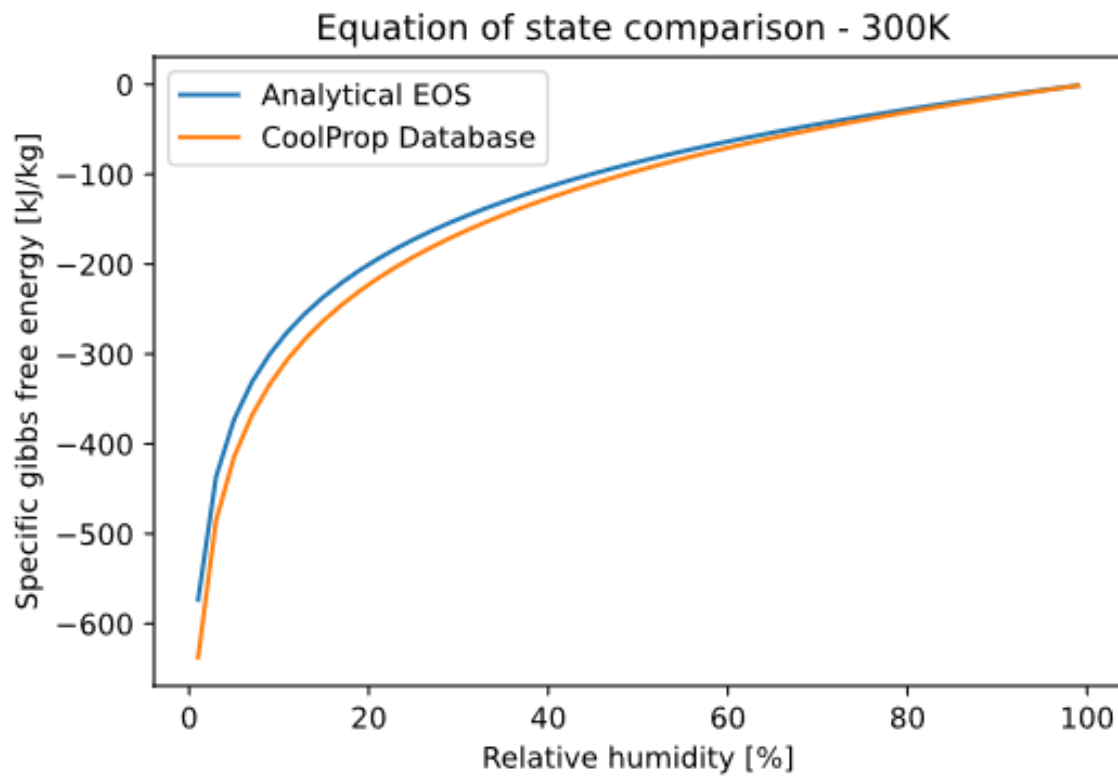


Figure A.3. Equation of state specific Gibbs free energy validation. The analytical EOS represents the property calculations based on the compressibility factor correlations, presented in methods. The CoolProp database of properties is validated against ASHRAE property standards [57].

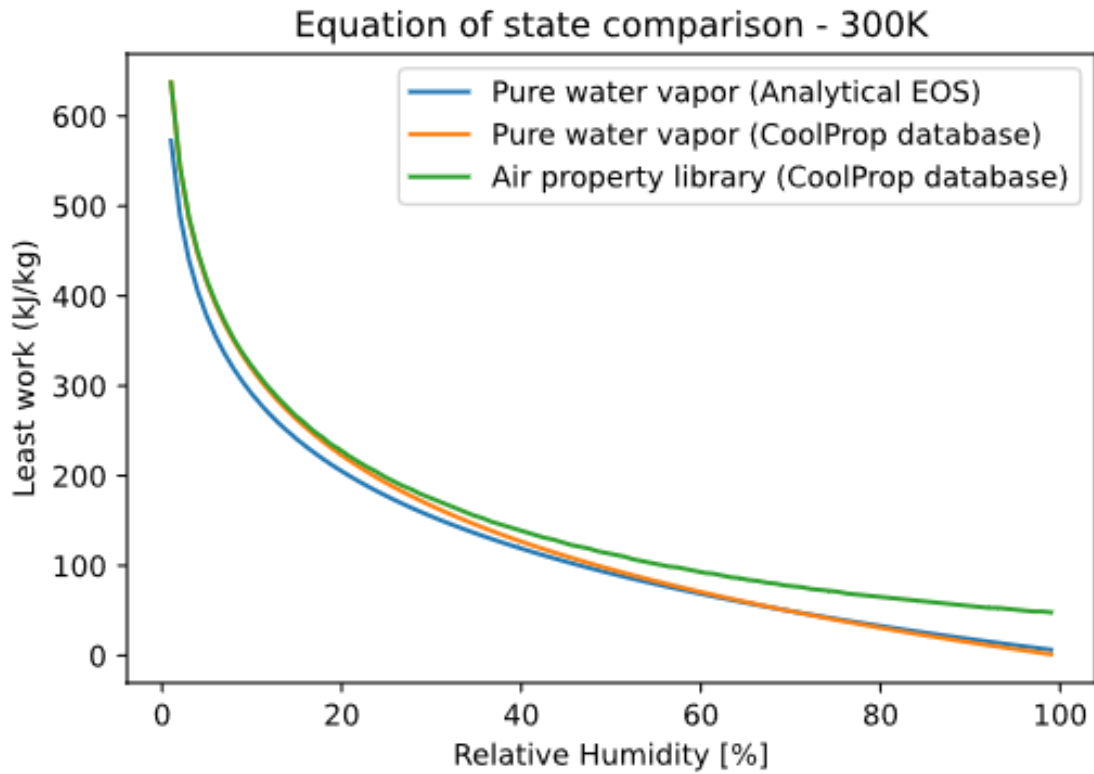


Figure A.4. Equation of state least work of separation validation. The calculation assumes an isothermal process at the thermodynamic dead state temperature (300K) to isolate the separation energy. The analytical equation of state (blue) and CoolProp property database (orange) are used for pure water vapor. The CoolProp database for humid air properties (green) is additionally used for comparison [57].

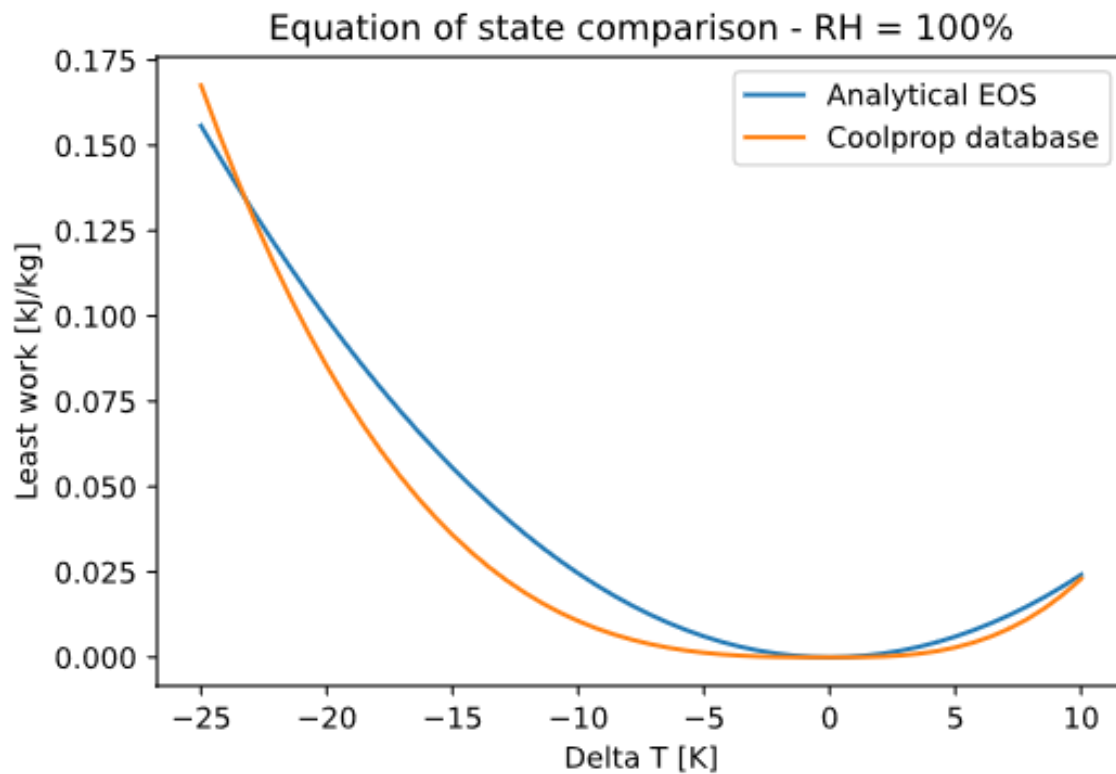


Figure A.5. Equation of state least work of heating validation. The calculation assumes an isobaric process at saturation ($RH = 100\%$). The analytical equation of state (blue) and CoolProp database (orange) are used for pure water vapor. Regardless of the equation of state, the least work approaches zero at the thermodynamic dead state.

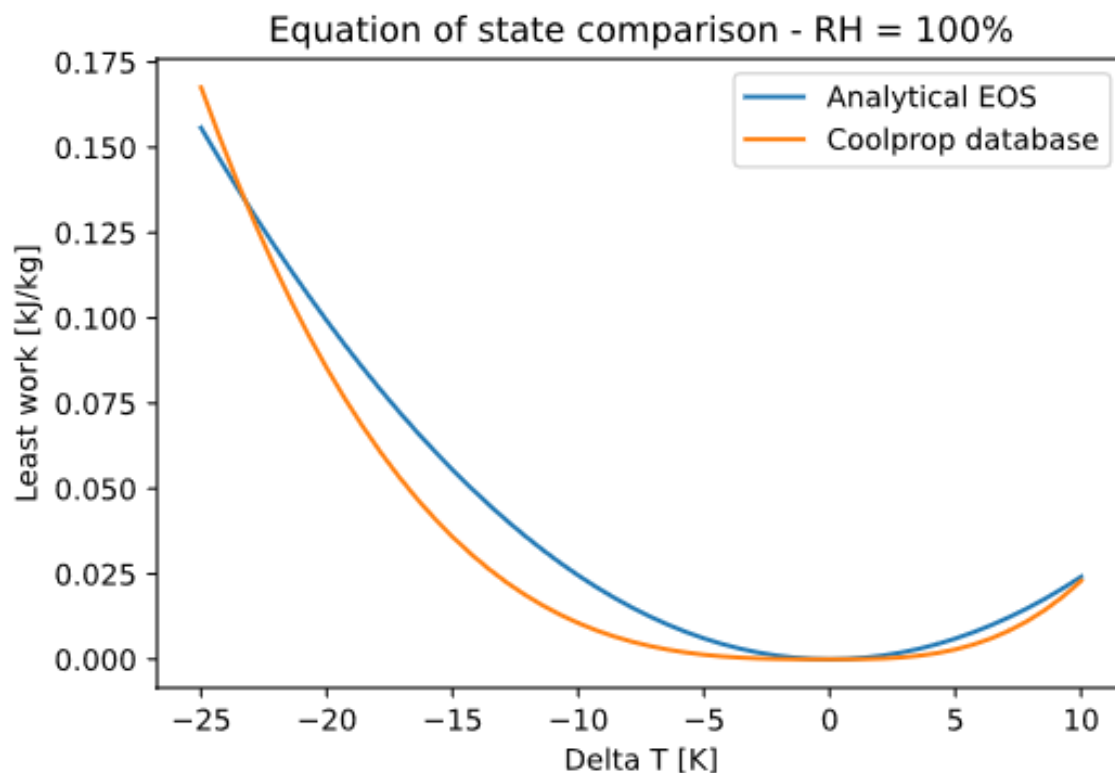


Figure A.6. Equation of state least work of heating validation. The calculation considers the total least work at ambient conditions that are well defined by the CoolProp database [57]. The relative error is calculated by $err = 100 \left(\frac{W_{analytical} - W_{CoolProp}}{w_{analytical}} \right)$. The majority of the error may be attributed to the compressibility factor correlations since a 1st order Taylor series expansion in pressure was used. As shown by Wexler (1977) [91] this error is reduced to less than 1% at temperatures below 273K 8, and therefore the range of this plot show the conditions of maximum model error.

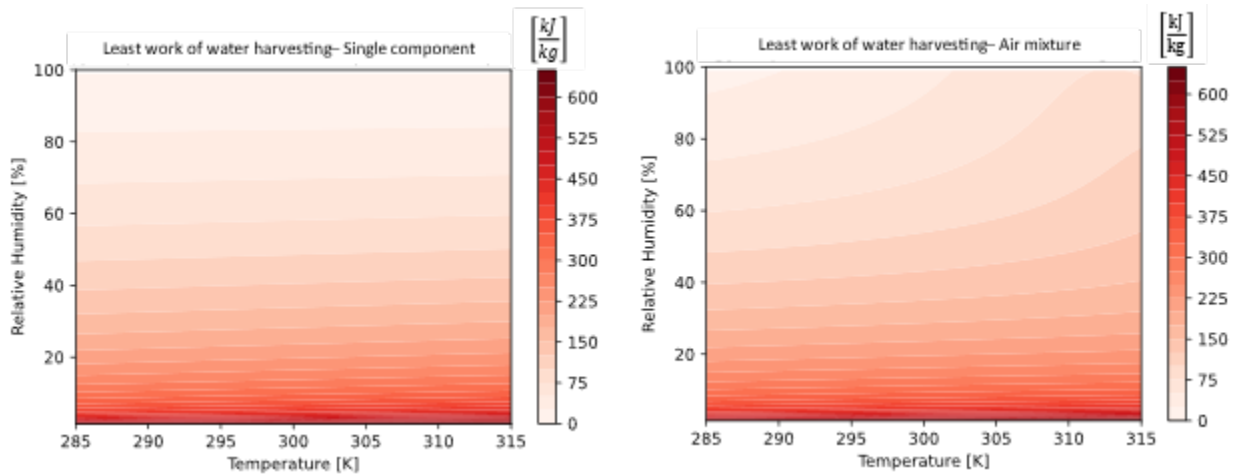


Figure A.7. Water harvesting from air and pure water vapor mixtures. This considers the full parametric sweep for water harvesting. The single-component version (left) assumes Dalton’s law and ignores other components in the mixture. The air version (right) assumes water is in a standard air mixture and accounts for energy interactions between mixture components. Nearly inert water vapor mixtures, like air, can behave as an ideal gas at low humidity. Water vapor on other planets is often found at low vapor pressures and concentrations. This suggests that the least work at low temperatures and humidity behaves similarly when computed with full mixture properties and water vapor partial properties.

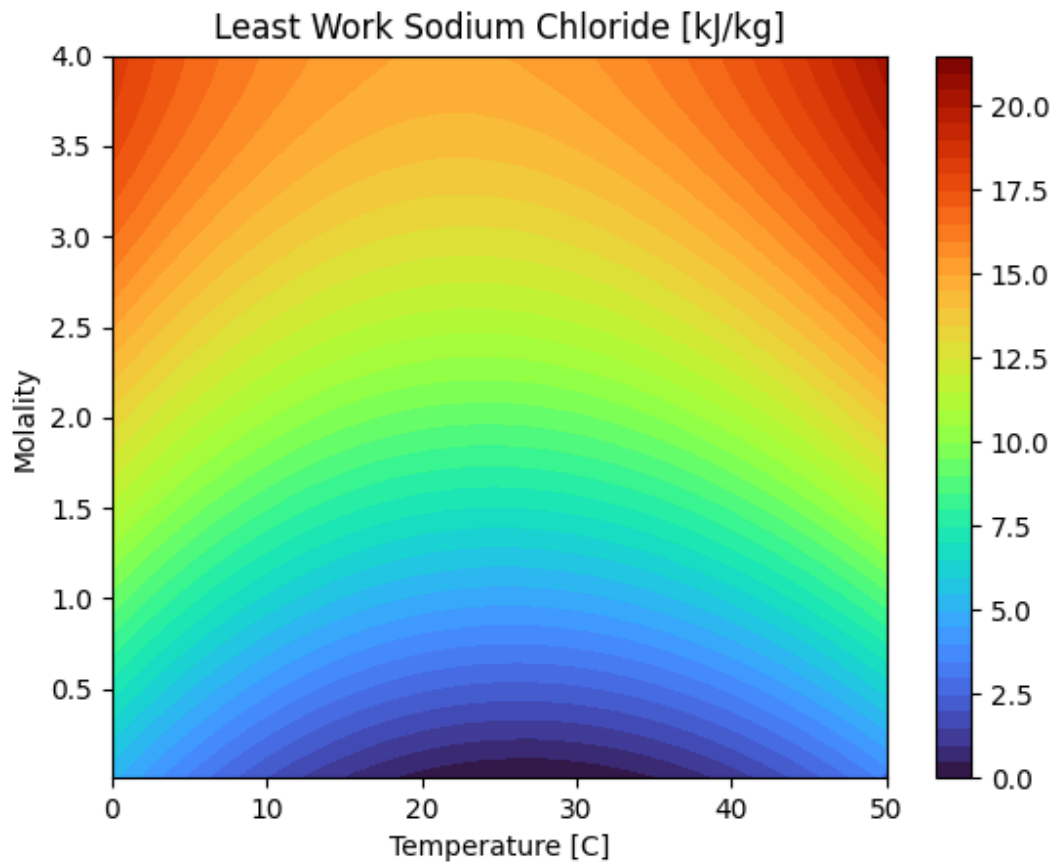


Figure A.8. Extended model of NaCl brine separation. Axes bounds represent the range of model validity. NaCl properties resemble water solutions on Earth and fall in between the upper and lower bounds shown in the manuscript Fig 2.1. For reference, most conventional waters on Earth are less than 1m.

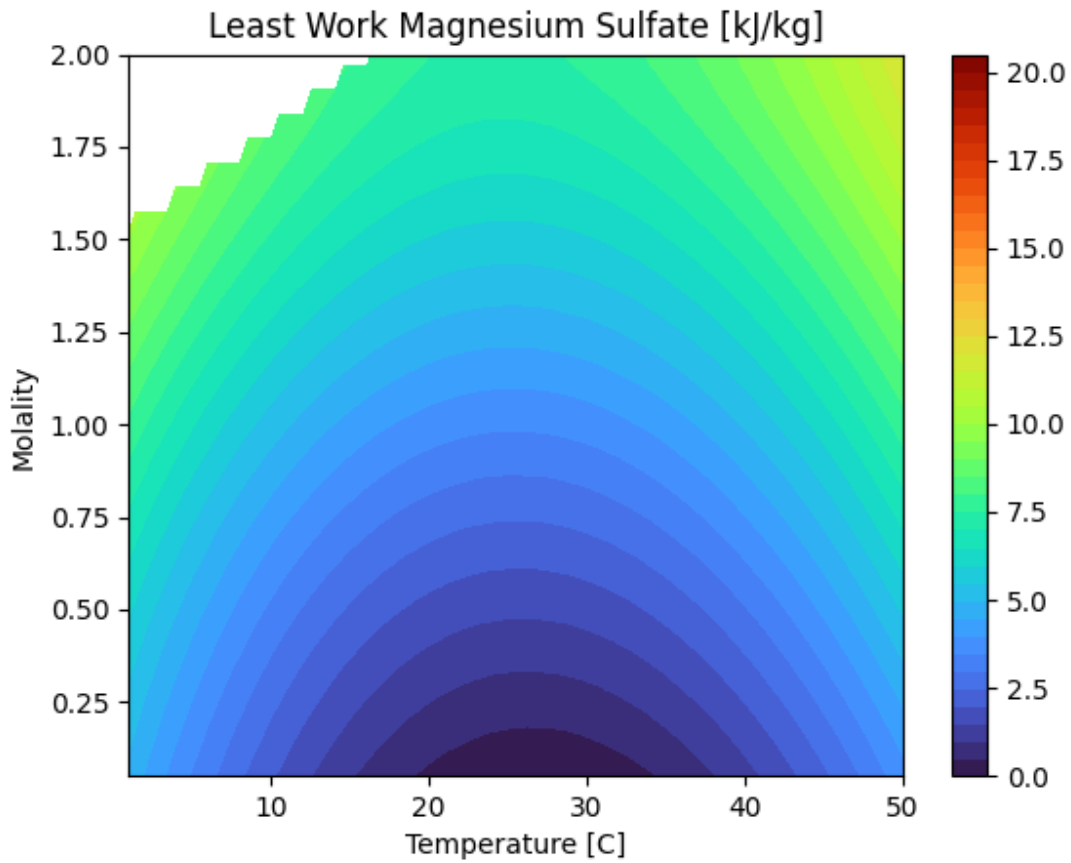


Figure A.9. Extended model for magnesium sulfate brine separation. Axes bounds represent the range of model validity. White space signifies supersaturation. Magnesium sulfate solutions fall in between the upper and lower bounds shown in the manuscript.

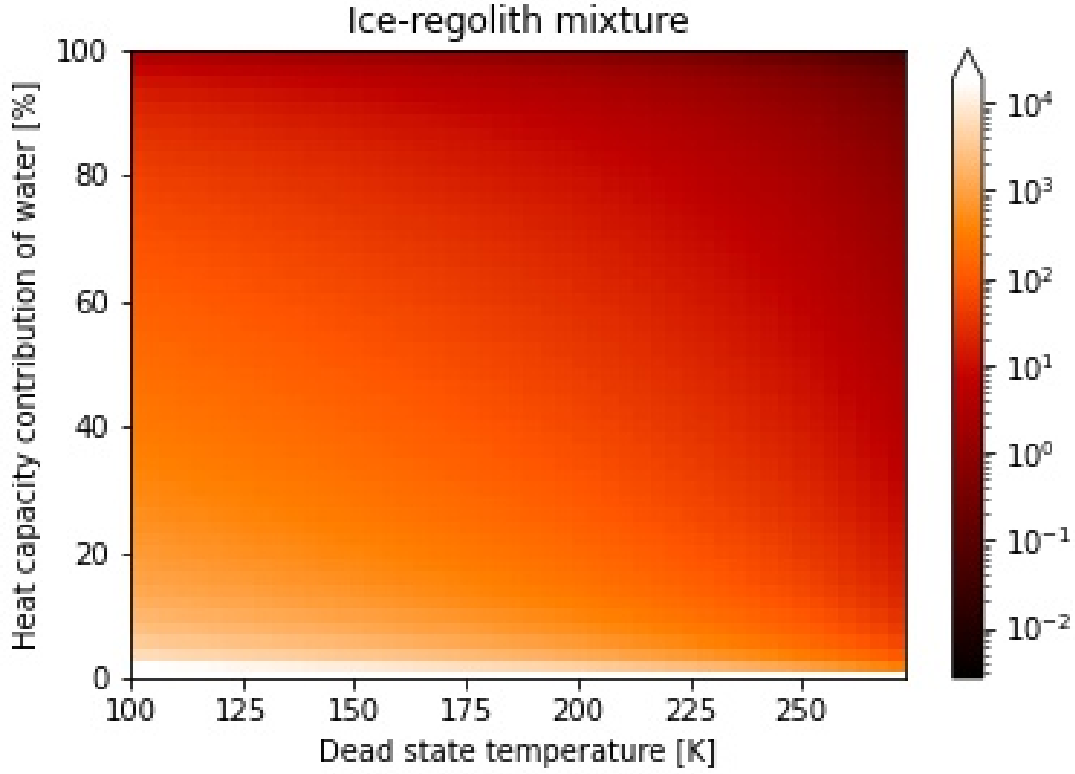


Figure A.10. Irreversibility of transient heating in physical mixtures like regolith. The heat capacity contribution of water encompasses the relative mass and specific heat capacity of water and the other species in the physical mixture.

The irreversible energy input is computed via the following equation:

$$\tilde{W}_{phys} = \int_{T_0}^{300K} \left(1 - \frac{T_0}{T}\right) C_{reg} dT \quad (\text{A.1})$$

Here, T_0 is the dead state temperature and C_{reg} is the constant pressure heat capacity of the non-water portion of the sample, on a per mass of water basis.

$$C_{ratio} = \frac{C_{ice}}{C_{ice} + C_{reg}} \rightarrow \frac{C_{reg}}{m_{ice}} = c_{ice} \left(\frac{1}{C_{ratio}} - 1 \right) \quad (\text{A.2})$$

The specific heat ratio, C_{ratio} , is shown on the y axis of the contour plot in S11 and represents the extensive heat capacity contribution of water-ice. Rearranging the equation for the heat capacity of regolith, C_{reg} , on a per mass of ice basis, m_{ice} , allows for a simple estimate in terms of just the specific heat capacity of ice, c_{ice} . This equation assumes the ratio of specific heats is constant through the heating process, with $c_{\text{ice}} = 2.108 \text{ kJ/kg-K}$. This is a reasonable assumption due to the incompressibility of solids within the shown temperature range.

Table A.1. Water-Ice ranges of conditions

Planetary Body	Temperature [K]	Depth [km]
Mercury	90 – 155	0
Earth	184 – 273	0
Moon	95 – 110	0
Mars	184 – 237	0
Europa	116 – 122	0
Ganymede	130 – 138	0
Enceladus	65 – 125	0
Tethys	75 – 85	0
Uranus	100 – 250	200-300
Jupiter	230 – 250	20-50

Table A.2. Liquid water ranges of conditions

Planetary Body	Temperature [km]	Depth [km]	Concentration	Species Present
Earth	273 – 310	0	0.5 – 0.65	Na, Cl
Mars	271 – 285	0 – 0.75	0.4 – 1.2	Na, Mg, SO_4
Europa	272 – 325	10 – 30	0.9 – 1	Mg, SO_4
Ganymede	0 – 278	800	0.1 – 0.8	Na, Cl, HCO_3 , CO_2 , K
Enceladus	273 – 300	35	2.5 – 12	Na, Cl, Mg, K, Ca, ClO_4

Table A.3. Water vapor ranges of conditions. Vapor pressure is used to represent mixing fraction and ambient pressure due to the ideal gas relationship. The depth is considered for both accessing water at the mean planetary solid surface and the 1bar pressure level. Due to the extreme low pressure on Mars, water is able to stay in the vapor state below 273.15K.

Planetary Body	Temperature	Depth	Vapor Pressure*
	[K]	[km]	[kPa]
Venus	430 – 740	0 – 50 **	0.006 – 0.5
Earth	273 – 325	0	0.2 - 13
Mars***	250 – 337	0	0.00005 – 0.0002

Table A.4. All simulations, except for ZnSO_4 , use the FREZCHEM thermochemistry database provided by Professor David Catling. Zinc solutions are simulated using the LLNL database. Each trial is simulated at 0.5 molality and 300 K. Trends are validated with prior literature on NaCl and ZnSO_4 studies of least work and compared to the least work trends of five other relevant binary electrolyte solutions: KCl, MgCl_2 , CaCl_2 , Na_2SO_4 , MgSO_4 . This comparison can be found in Figure 11 of Mistry, Hunter, Lienhard (2013) [21].

Binary electrolyte solution	Least work [kJ/kg]
NaCl	2.42
NaClO ₄	2.35
MgClO ₄	4.02
Ca(ClO ₄) ₂	3.97
ZnSO ₄	1.55

Table A.5. Compressibility factor validation. The calculation of the compressibility factor for sub-freezing temperatures is compared to the compressibility factor presented in Wexler (1997) [91]. The maximum percent difference between the two is 0.01%

Temperature [K]	This work	Wexler, 1977
273.16	0.999624	0.999624
273.15	0.999624	0.999624
263.15	0.999807	0.999907
253.15	0.999907	0.999958
243.15	0.999959	0.999982
232.15	0.999982	0.999993
213.15	0.999999	0.999999
193.15	0.999999	1
173.15	0.999999	1

B. APPENDIX: ATMOSPHERIC WATER HARVESTING

The least work formulation begins with a steady-state balance of exergy for an irreversible open system.

$$\sum^{in} \dot{m}\tilde{e} - \sum^{out} \dot{m}\tilde{e} - \dot{W} + \dot{Q} \left(1 - \frac{T_0}{T}\right) = 0 \quad (\text{B.1})$$

Where \tilde{e} is the flow exergy, \dot{m} is the mass flow rate, \dot{W} is the thermodynamic work and \dot{Q} is the heat transfer. T_0 represents the temperature of the thermodynamic dead state and T is the system boundary temperature. By considering a system without entropy generation that is driven by work, we find that the least work is only a function of the ambient environmental conditions.

$$\dot{W}_{least} = \sum_0^{in} \dot{m}\tilde{e} - \sum_0^{out} \dot{m}\tilde{e} \quad (\text{B.2})$$

$$\tilde{e} = (h - h_0) - T_0(s - s_0) \quad (\text{B.3})$$

Where h_0 and s_0 are the enthalpy and entropy evaluated at the thermodynamic dead state. Expanding this form to include a conservation of mass, the least work is equivalent to the mass flow weighted sum of flow exergy. The equation is written on a basis of mass of water collected, which is equivalent to the change in absolute humidity of the ambient air. The infinitesimal change in bulk properties yields the theoretical minimum least work [24], [30], as shown by Eq. 3.1.

We define the maximum 2nd law efficiency as a function of the theoretical minimum least work and the work input from any given system, normalized by time or mass.

$$\eta_{II, \max} = \frac{w_{\min, \text{least}}}{w_{\text{real}}} \quad (\text{B.4})$$

Where $\eta_{II, \max}$ signifies the maximum second law efficiency of a given system and w_{real} is the specific energy consumption of a process (e.g., dew, membrane, or MOF) on a basis of the

mass of permeate produced. This definition of efficiency can be used as a generalized form to analyze all water harvesting systems on a consistent basis.

Extending this derivation, we model the energy consumption of an ideal dew collection process by assuming that a finite amount of water is separated from the bulk mixture and collected at the dewpoint temperature. This is shown by Eq. [3.2](#)

The MOF system depends on the adsorption characteristics of the material. In order to provide a robust analysis of the potential for MOFs, four MOFs with varying properties were considered. These MOFs, and their key properties are shown in Table [B.1](#).

Table B.1. RH_{desorb} is the relative humidity needed to induce desorption, W_{max} is the maximum water uptake for the MOF, and Δh_{adsorb} is the enthalpy of adsorption for a given MOF. $RH_{\text{inflection}}$ is the relative humidity “inflection point” at which the water uptake is 50% of the maximum water uptake (W_{max}). Given the added complexity of considering numerous MOFs, our modeling framework assumes a step-wise increase in water uptake from near-zero to W_{max} at $RH_{\text{inflection}}$. This enables easy modification of the model for new MOF materials so other researchers can make use of the model. It also presents an idealized scenario for the MOFs. All information and assumptions are used from prior work [30], [80].

Material [-]	Desorption RH [%]	Inflection RH [%]	W_{max} [kg/kg]	Δh_{adsorb} [kJ/kg]
MOF-801	5.5	9	0.41	58.8
MOF-303	5.5	13	0.45	49
MIP-200(Zr)	16	18	0.45	55
Al-Fumarate	16	27	0.45	50

There are several mass terms needed to evaluate the thermodynamics of the system, however, we would like to generalize the analysis by having everything in terms of the mass of water ultimately collected, m_w . Thus, the MOF, adsorbed water, desorbed water, and desorption air masses are all defined per kilogram of collected water.

$$\frac{m_{\text{ad}}}{m_w} = \frac{w_{\text{ad}}}{w_{\text{ad}} - w_{\text{des}}} \left(\frac{\omega_{\text{cs}} - \omega_{\text{air}}}{\omega_{\text{cs}} - \omega_{\text{cond}}} \right) \quad (\text{B.5})$$

$$\frac{m_{\text{des}}}{m_w} = \frac{\omega_{\text{cs}} - \omega_{\text{air}}}{\omega_{\text{cs}} - \omega_{\text{cond}}} \quad (\text{B.6})$$

$$\frac{m_{\text{air}}}{m_w} = \frac{1}{\omega_{\text{cs}} - \omega_{\text{cond}}} \quad (\text{B.7})$$

$$\frac{m_{\text{MOF}}}{m_w} = \frac{1}{w_{\text{ad}} - w_{\text{des}}} \left(\frac{\omega_{\text{cs}} - \omega_{\text{air}}}{\omega_{\text{cs}} - \omega_{\text{cond}}} \right) \quad (\text{B.8})$$

m_{ad} and m_{des} represent the mass of water that is adsorbed and desorbed in a cycle. w_{ad} and w_{des} are the water uptake values for the adsorption and desorption conditions, respectively. The subscript cs signifies the air after water is desorbed into it. The subscript cond represents the state of the condenser. To evaluate the outlet humidity from the desorption, the integral average method was employed, as has been done in other modeling work [30].

$$\omega_{\text{cs}} = \omega_{\text{des,outlet}} = \frac{\int_{T_{a,i}}^{T_{\text{des}}} \omega(RH_{\text{des}}, T) dT}{T_{\text{des}} - T_{a,i}} \quad (\text{B.9})$$

Here, $T_{a,i}$ is an ‘‘intermediate temperature’’ at which the relative humidity of the heated air is equal to the desorption relative humidity condition for the MOF. T_{des} is the high temperature used for desorption. To determine the humidity at the outlet of the desorption process, the humidity ratio is integrated along the line of constant relative humidity and then divided by the total temperature difference, giving somewhat of an ‘‘average’’ outlet humidity condition.

The recovery ratio is the ratio of mass of humidity collected to the total mass of the humidity in the desorption air stream. Essentially, this gives the relative amount of water collected compared to the total amount of water vapor in the air entering the condenser.

$$r = \frac{\omega_{cs} - \omega_{cond}}{\omega_{cs}} \quad (\text{B.10})$$

Here, everything is fixed except ω_{cond} . Thus, the recovery ratio controls the setpoint for the humidity of the air leaving the condenser. This implicitly controls the temperature of the condenser, as well as the condenser efficiency in the Carnot case.

The heat transfer terms for desorption, condensation, and regeneration were originally described in Kim, et al (2020) [30] and repeated below.

$$q_{des} = \left(\frac{m_{MOF}}{m_w} c_{p,MOF} + \frac{m_{ad}}{m_w} c_{p,w} + \frac{m_{air}}{m_w} c_{p,air} \right) (T_{des} - T_{air}) + \frac{m_{des}}{m_w} \Delta h_{ad} \quad (\text{B.11})$$

$$q_{cond} = h_{fg} + c_p (T_{des} - T_{sat}(\omega = \omega_{cs})) + \frac{m_{air}}{m_w} (c_{p,air} + \omega_{cond} c_p) (T_{des} - T_{cond}) \quad (\text{B.12})$$

$$q_{regen} = \frac{m_{MOF}}{m_w} c_{p,MOF} (T_{des} - T_{air}) \quad (\text{B.13})$$

A c_p of 1 kJ/kg-K was used as the baseline (being very similar to that of MOF-801, $C_p = 1.14$). The sensitivity to this assumption is covered in this material.

The open membrane system is modeled as a Claridge-Culp-Liu process and was assumed to have constant membrane parameters: 5000GPU permeability to water vapor and 0GPU permeability to N_2 and O_2 [68], [69]. For consistency, the membrane area was taken to be 1 m² since the water flux scales linearly with area when concentration polarization is not considered. The flux through the membrane is defined by a force balance of water vapor at the membrane surface.

$$\dot{m}_{vapor} = BA_m (p_v - p_{sys}) \quad (\text{B.14})$$

Where \dot{m}_{vapor} is the vapor flowrate into the system, B is the membrane permeability to water vapor, and A_m is the membrane area. p is the partial pressure of water vapor and subscripts v and sys signify the ambient vapor and the internal system. The membrane system model in this work was based off of the process proposed by Claridge et al. (2019) whereby the water vapor pulled across the membrane is compressed close to the saturation pressure at the ambient temperature by a separate water vapor compressor. A vacuum pump is also included to keep the whole system near-vacuum and to expel non-condensed gases back to the environment. Including this intermediate compression stage requires less sub-cooling to induce condensation. The pressure of this intermediate condensation stage (p_{ICS}) was chosen as 95% of the saturation pressure of water for the given ambient temperature. This models the aspect of minimizing the driving force.

$$p_{ICS} = 0.95p_{sat}(\text{water}, T_{amb}) \quad (\text{B.15})$$

The heat required for the condenser is equivalent to the change in enthalpy between the ICS state and a pre-set quality at the saturation temperature.

$$\dot{q}_{cond} = h_{in}(T_{amb}, p_{ICS}) - h_{out}(T_{sat}, x) \quad (\text{B.16})$$

Where h is the enthalpy of water vapor and subscripts in and out represent the inlet and outlet of the condenser. T is the temperature. Subscript amb represents ambient air and sat represents the saturation temperature at the system pressure. x is the desired quality exiting the condenser. Conversely this is related to the fractional recovery where x=1 signifies no condensation and x=0 means that all incoming vapor is converted to liquid. The power consumption of the vacuum pump and compressor can be similarly calculated with enthalpy balances.

$$\dot{W}_{membrane} = \left(\frac{\dot{Q}}{\text{COP}_c} + \dot{W}_{vac} + \dot{W}_{comp} \right) \quad (\text{B.17})$$

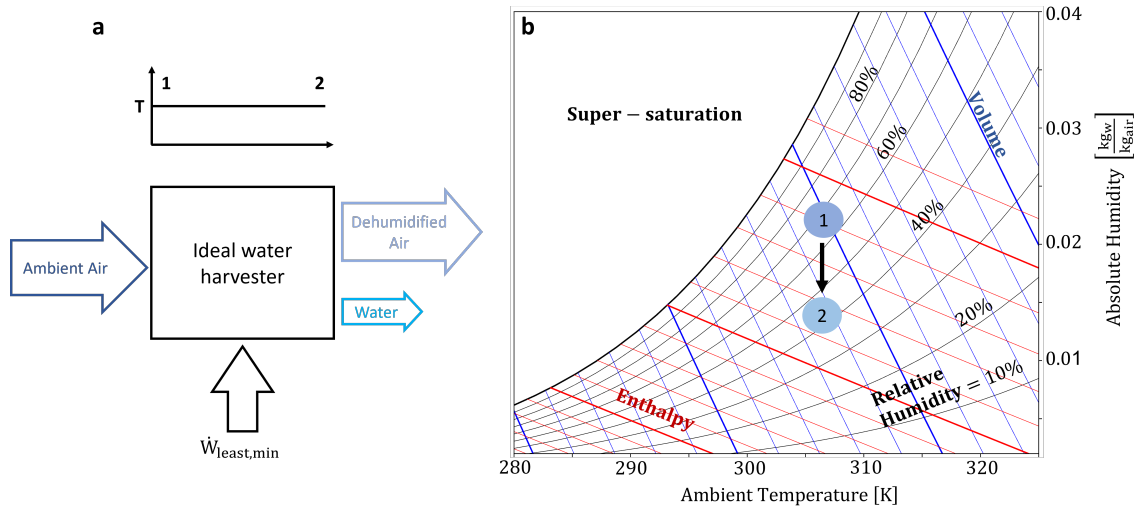


Figure B.1. a, Process schematic describing ambient air (1) flow being dehumidified (2) through an ideal atmospheric water device. The definition of the thermodynamic minimum represents a steady state, isothermal process. The thickness of each arrow qualitatively represents the relative magnitude of the mass flow rate. The color of each arrow represents the amount of water in the given stream, with more saturated colors signifying more water. The graph qualitatively describes the temperature (vertical axis) along the ideal process (horizontal axis). b, The thermodynamic state of the air stream is described on the psychrometric chart. Beginning at high humidity, and isothermally moving to low humidity. The change in absolute humidity between states 1 and 2 corresponds to the mass of water collected.

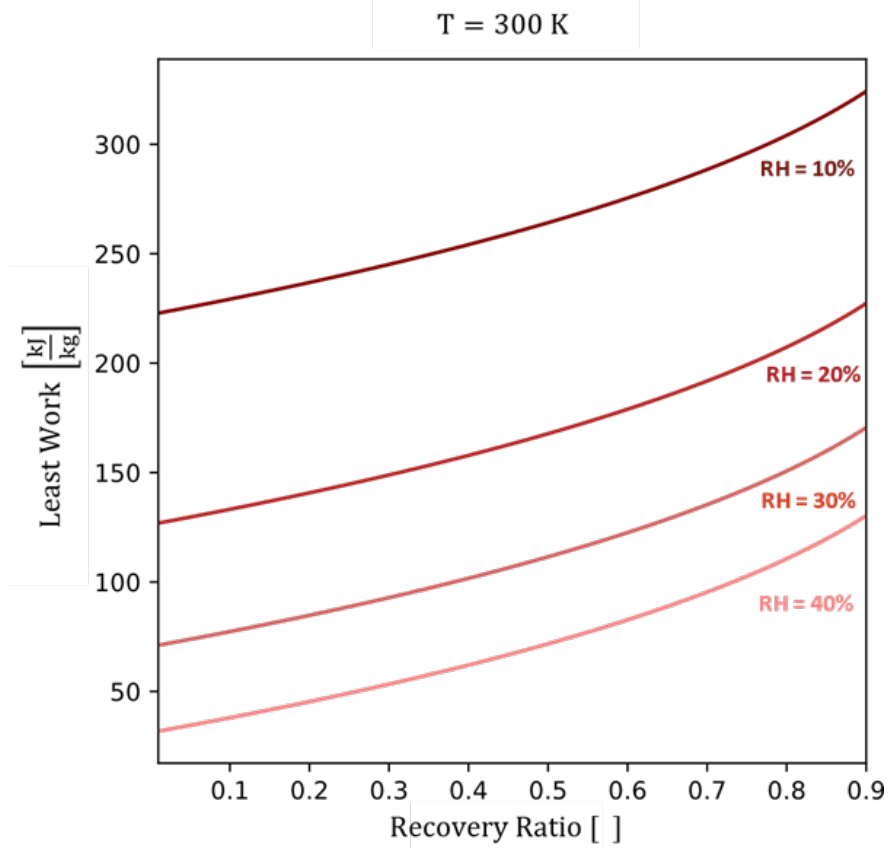


Figure B.2. The least work trends are similar to those shown in previous analyses in desalination and with thermal-MOF systems [21], [24], [30]. The minimum least work is evaluated with the limit as recovery goes to zero. This trend varies significantly by the relative humidity.

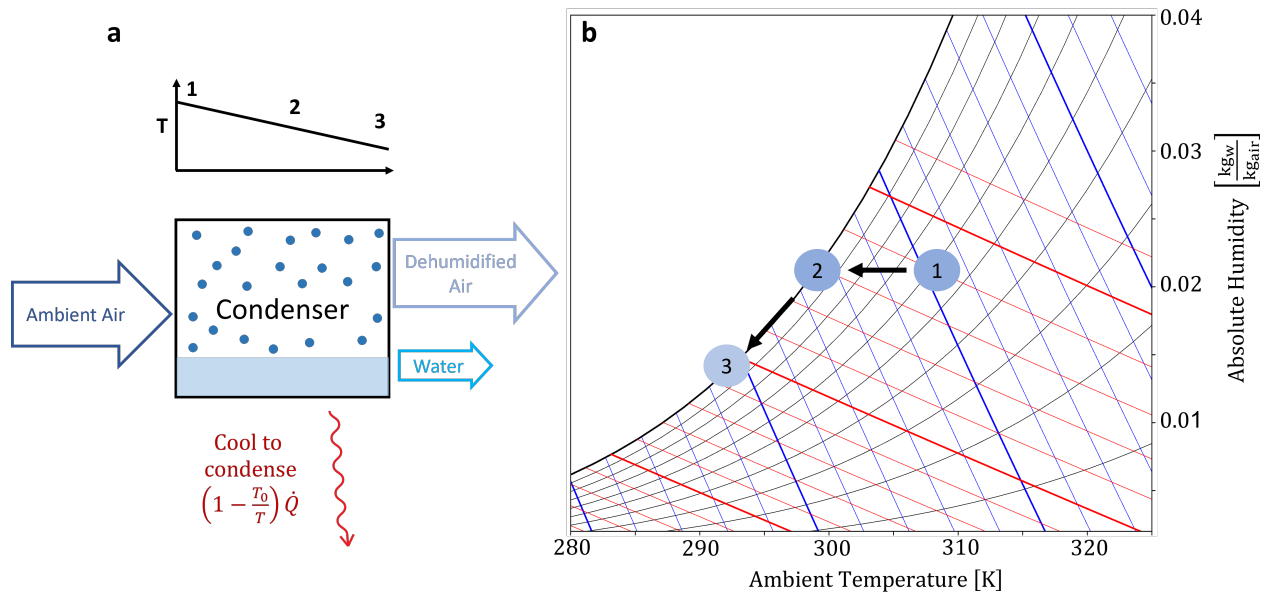


Figure B.3. a, The process schematic describes an ideal dew water harvesting device. Ambient air enters at the ambient temperature (1), is cooled to the dew point for condensation (2) (by a Carnot-like device), and then exits at a saturated state at the condenser temperature (3). The graph qualitatively describes the temperature of the air (vertical axis) along the dew harvesting process (horizontal axis). b, The dew process for the humid air stream is visualized on the psychrometric chart. The difference in humidity between (1) and (3) represents the mass of water collected.

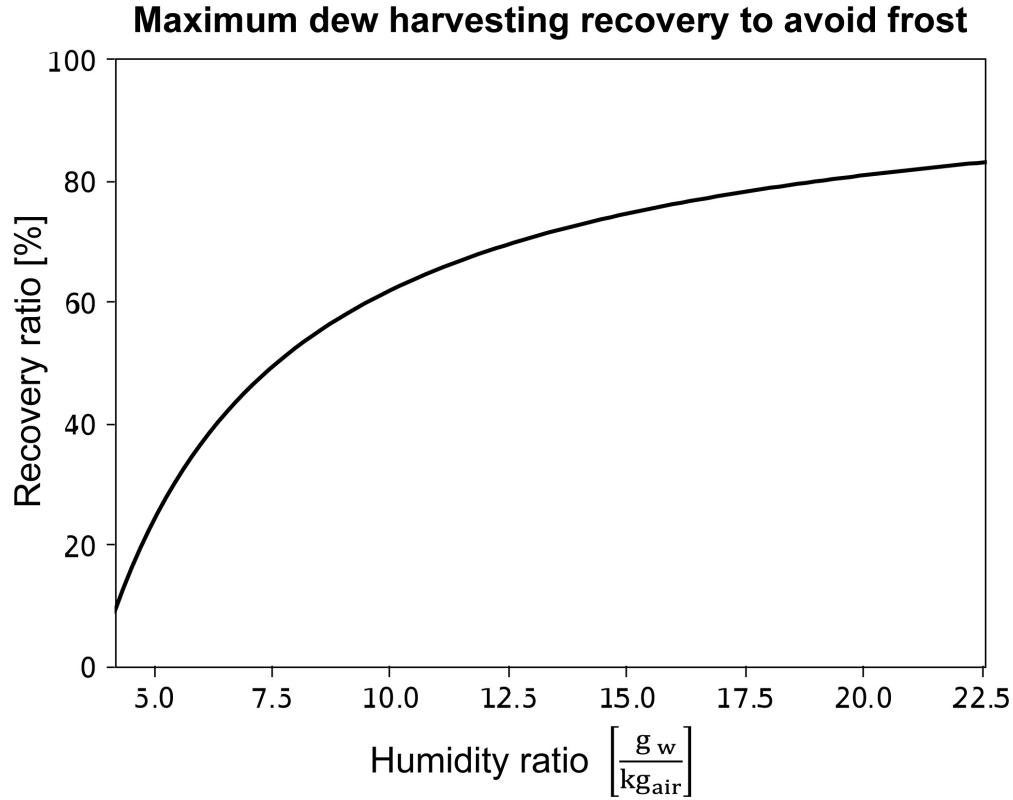


Figure B.4. The figure shows the recovery associated with subcooling a humid air mixture to the frost accumulation temperature. The lower bound of condenser temperature is limited by frost accumulation, and here is set to 273.15K. Lower condenser temperatures, or larger subcooling, induces higher recoveries and yields. In the case of a constant COP with respect to temperature, maximizing the recovery also maximizes the process efficiency. However, as shown by Fig 3.3 in the main text, when the COP is inversely proportional to the temperature difference, as is the case with a Carnot-device and many practical cooling systems, there is a trade-off between maximizing yield and efficiency.

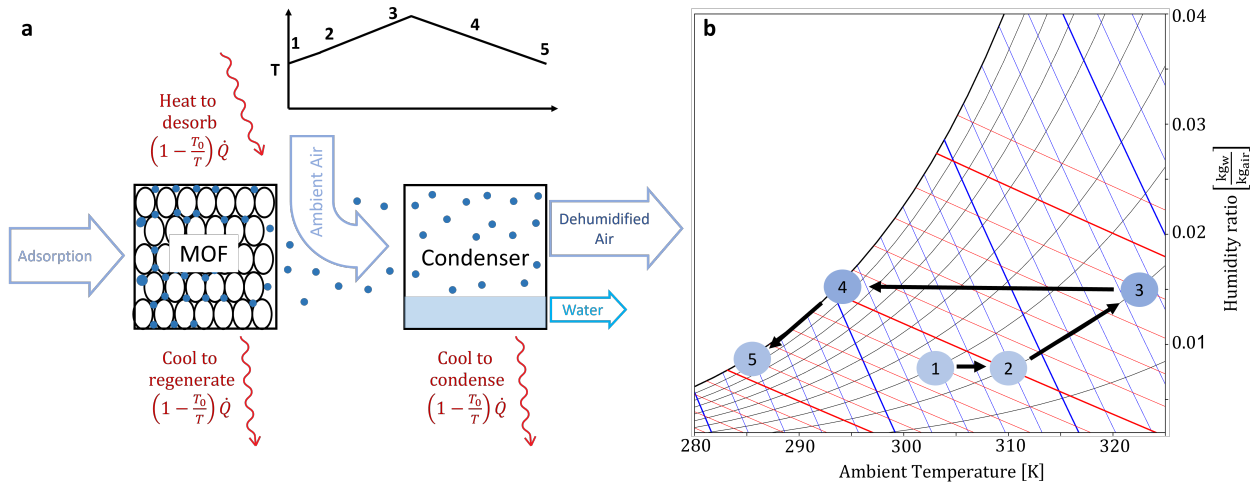


Figure B.5. a, The MOF process aims to concentrate water vapor within a structure in cycles, to increase the humidity for more efficient condensation. The psychrometric chart represents the humid air states in the process. Ambient air (1) is heated to a low relative humidity (2) where it can desorb the water contained within the MOF. To facilitate desorption, the MOF must be heated to a pre-defined relative humidity. The humidified air (3) is then sent to a condenser to extract water similar to the dew harvesting process. The graph qualitatively describes the temperature (vertical axis) along the desorption and condensation process (horizontal axis). b, The humid air states of the MOF process are described on the psychrometric chart. The process begins at an arbitrary inlet ambient air temperature and humidity. The collected mass of liquid water corresponds to the difference in humidity between (4) and (5).

Table B.2. Comparison of assumptions to prior literature

Assumption	Kim et al. (2020)	This work
System type	Closed system with recirculation	Open system
Condensation temperature	Occurs at ambient temperature and not accounted for in efficiency calculation	Occurs at a recovery-specified condenser temperature and modeled as a Carnot-device
Desorption process	Determines a minimum temperature, exceeds the minimum temperature, uses integral method to determine desorption outlet humidity ratio.	Uses integral method to determine outlet humidity RH of desorption is set by material properties.

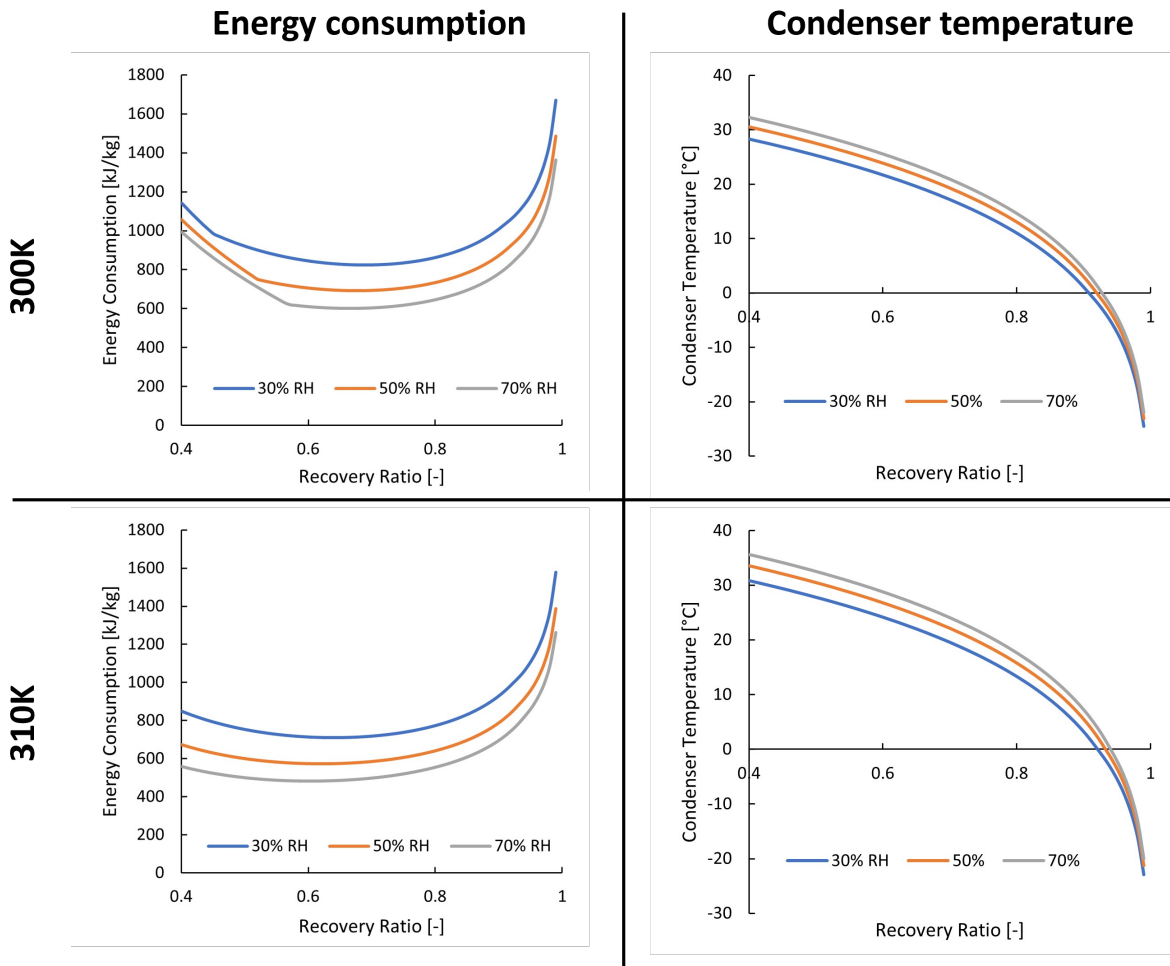


Figure B.6. a, The MOF process aims to concentrate water vapor within a structure in cycles, to increase the humidity for more efficient condensation. The psychrometric chart represents the humid air states in the process. Ambient air (1) is heated to a low relative humidity (2) where it can desorb the water contained within the MOF. To facilitate desorption, the MOF must be heated to a pre-defined relative humidity. The humidified air (3) is then sent to a condenser to extract water similar to the dew harvesting process. The graph qualitatively describes the temperature (vertical axis) along the desorption and condensation process (horizontal axis). b, The humid air states of the MOF process are described on the psychrometric chart. The process begins at an arbitrary inlet ambient air temperature and humidity. The collected mass of liquid water corresponds to the difference in humidity between (4) and (5).

In this work, four MOF materials with ranging adsorption properties were implemented. In order to simplify the analysis, given the broad scope of this work, each MOF was assumed to experience a stepwise increase in water vapor uptake at the inflection humidity. In other words, for any ambient relative humidity greater than the inflection humidity, the MOF experiences the tabulated maximum uptake. This assumption has represents the behavior of an idealized MOF isotherm. By implementing four different MOFs, the model can decide which MOF properties to use based on the ambient relative humidity. The breakdown of when each MOF is used is summarized as follows.

Table B.3. One calculation that is carried out in the same manner between both models is the minimum desorption temperature. Both models can take a known/assumed absolute humidity of the incoming air stream and determine the temperature for which that absolute humidity is 10% relative humidity. This work heats ambient air to attain the desorption relative humidity, whereas Kim et al. (2020) uses a saturated air stream at 25°C from the recirculation process. By setting the ambient condition to 25°C and 100% RH in our model, we confirmed that our model would calculate a desorption temperature of 71°C, which is the minimum temperature determined by Kim et al. (2020). While this is only a small portion of the models, it is nonetheless a shared calculation between the two models which were matched. Furthermore, the cycle model for the single-cycle recirculation system presented by Kim et al. (2020) was replicated for MOF-801 B.7. The foundational assumptions about operating conditions for both models match and can reproduce results of the prior published work.

Condition	Tailored MOF
$\text{RH} \leq 13\%$	MOF-801
$13\% < \text{RH} \leq 18\%$	MOF-303
$18\% < \text{RH} \leq 27\%$	MIP-200(Zr)
$27\% < \text{RH}$	Al-fumarate

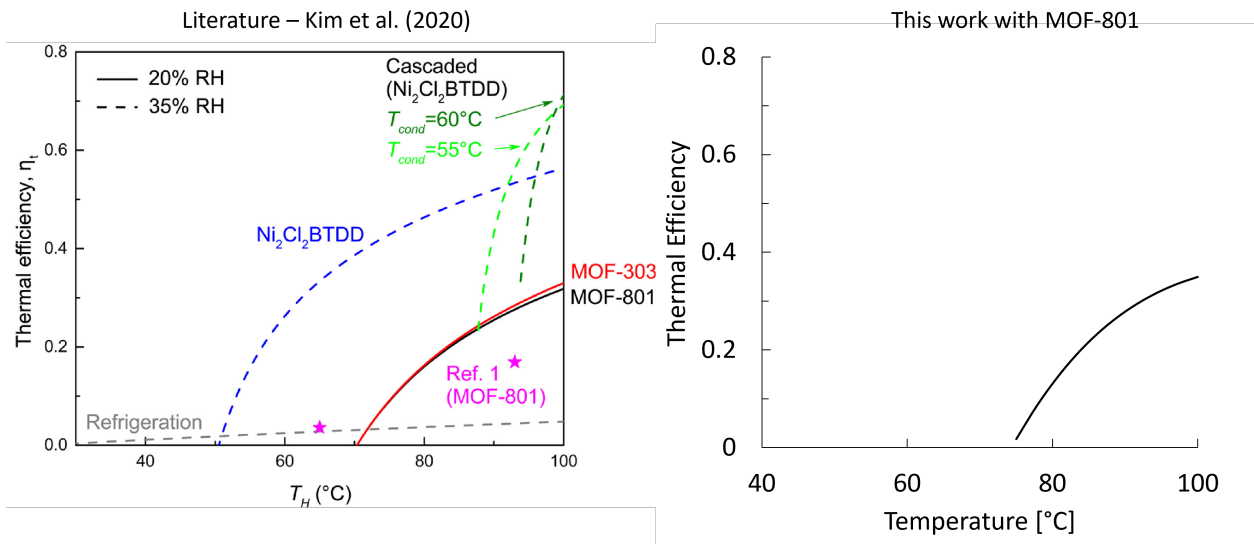


Figure B.7. The open system was chosen as it is the simpler option that is more robust and flexible to adapt to different MOF's and operating conditions. Additionally, it is the most comparable system to the other AWH systems modeled in this work (dew, membrane, and least work). So, while the two systems are different in several aspects, they also share many similarities as discussed above. The framework developed in this work is developed with a very similar approach.

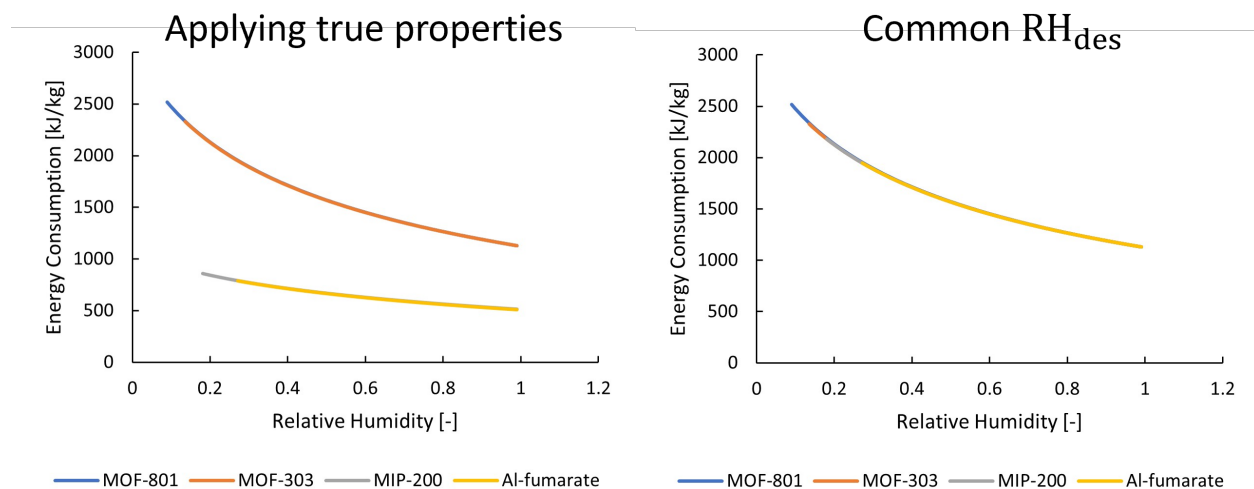


Figure B.8. We further demonstrate this with the plots below. These plots show the specific energy consumption of water harvesting at an ambient temperature of 300K. The left plot employs the MOF assumptions exactly, whereas the right plot employs a constant desorption relative humidity to each MOF. It can be seen that when all MOFs use the same desorption relative humidity, the energy consumption across the range of humidity values is nearly identical. In the main text, we use all 4 MOFs while employing a constant desorption humidity across all MOFs.

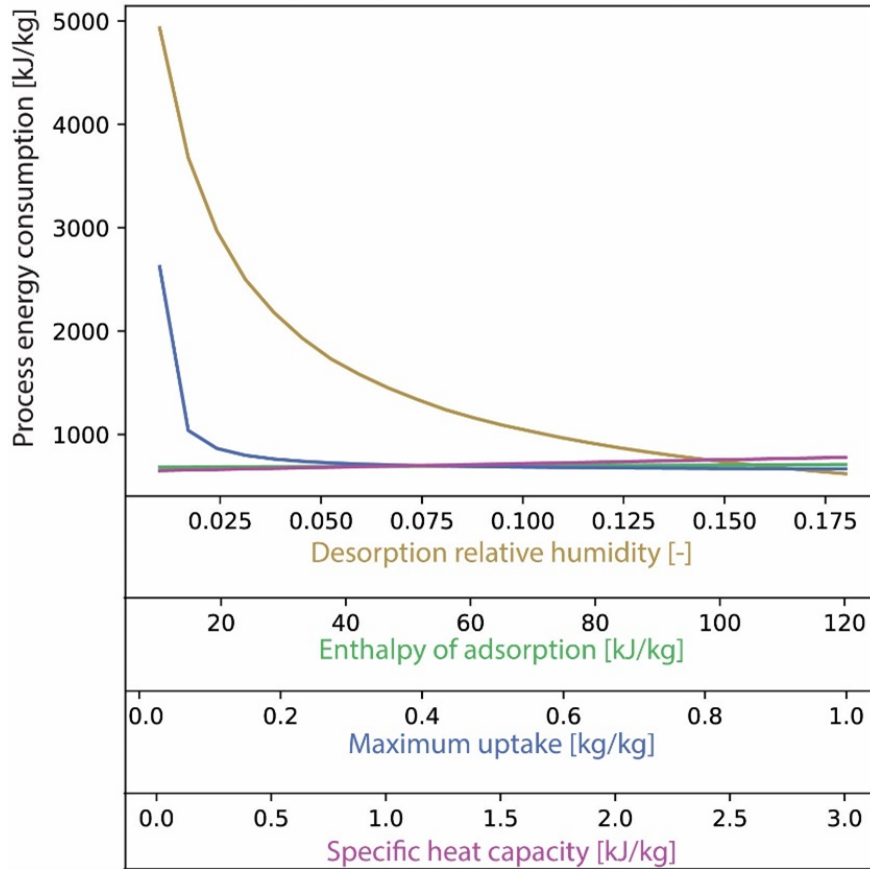


Figure B.9. A sensitivity analysis was conducted with assumed parameters in the MOF model, to show the relative effects on the energy consumption. The default analysis conditions include the ambient relative humidity of 50%, the specific heat capacity (1 kJ/kg K), and recovery ratio of 65%, and MOF-specific properties in presented previously. As can be seen, the specific heat capacity, adsorption energy, and maximum water uptake of the MOF have very minimal impact on the specific energy consumption. However, these variables may significantly impact the non-normalized energy consumption, which may be important in practical systems with size and form factor constraints. The most significant factor affecting the specific energy consumption for water harvesting is the desorption relative humidity. Due to the integral method used to determine the outlet humidity ratio from the desorption process, even small increases in the desorption relative humidity led to significant increases in the outlet humidity ratio. Thus, for a constant recovery ratio, a significant increase in desorption outlet humidity ratio leads to a higher condenser temperature and cooling COP, greatly improves the specific energy consumption of the system.

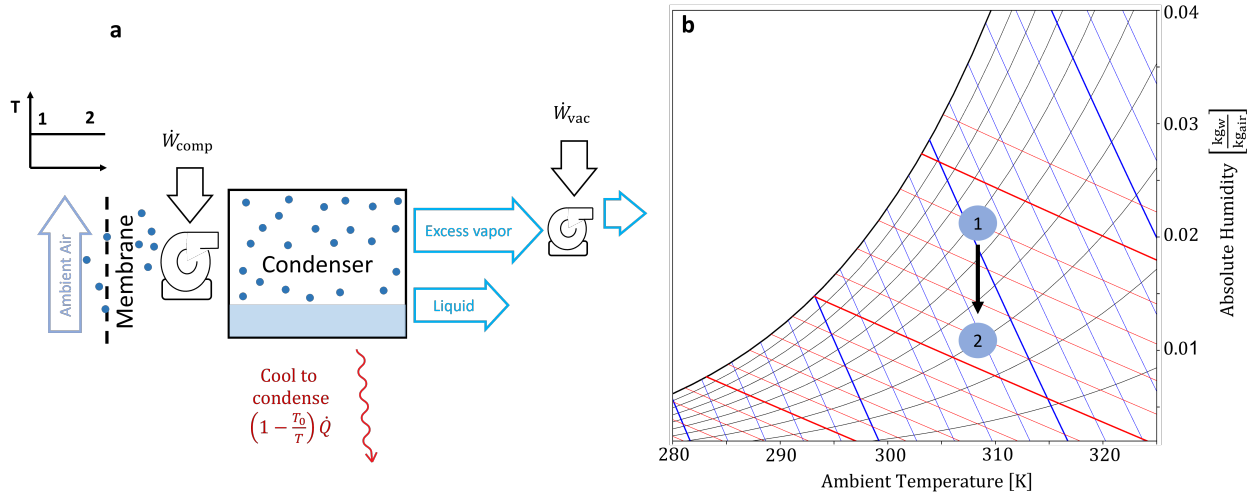


Figure B.10. The membrane process employs a membrane to isothermally concentrate water vapor before condensation. This is a depiction of the original Claridge-Culp-Liu dehumidification process [69]. The psychrometric chart represents the humid air states in the process. Ambient air (1) is concentrated (2) where now it has a lower energy requirement for condensation. The water vapor is condensed and then is pumped back to atmospheric pressure. Note: only the air states are shown in the psychrometric chart. Since the membrane is assumed to be perfectly selective, only water vapor enters the condenser. b, The humid air states of the membrane process are described on the psychrometric chart. The process begins at an arbitrary inlet ambient air temperature and humidity. The collected mass of liquid water corresponds to the difference in absolute humidity between 1 and 2 minus the amount of excess vapor that is rejected from the system.

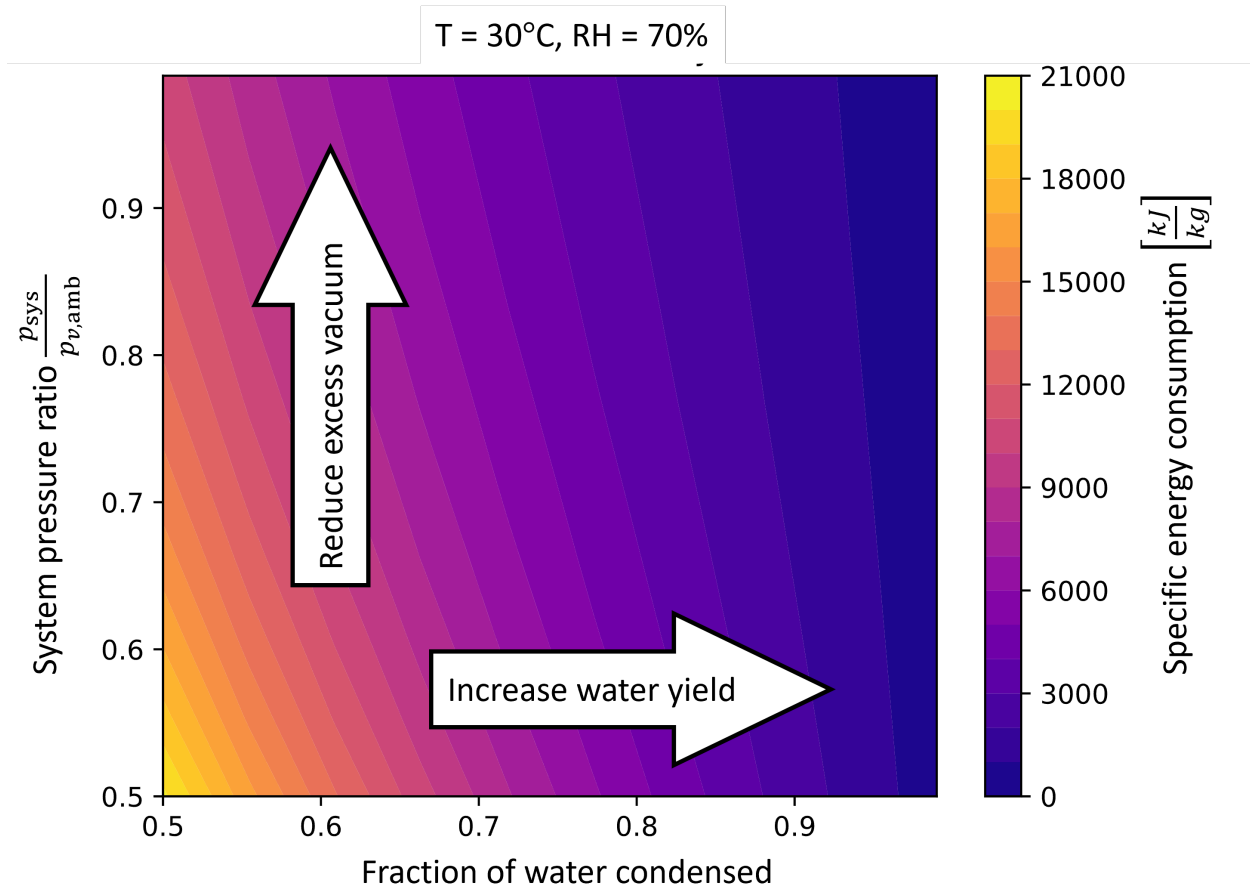


Figure B.11. The fraction of water condensed represents the recovery ratio at the condenser of the membrane. The system pressure ratio represents the ratio between the system operating pressure and the ambient vapor pressure of water. This calculation is done for 30°C and RH = 70%. A perfectly ideal membrane system will have a system pressure approaching 1 (infinitesimal flux) and a recovery ratio nearing 100%. For the analysis in this work, the recovery ratio, or fraction of water condensed, is set to 65% to create a fair comparison with the other processes. Optimizing this process with recirculation could artificially increase the true recovery ratio, thus enabling higher efficiencies.

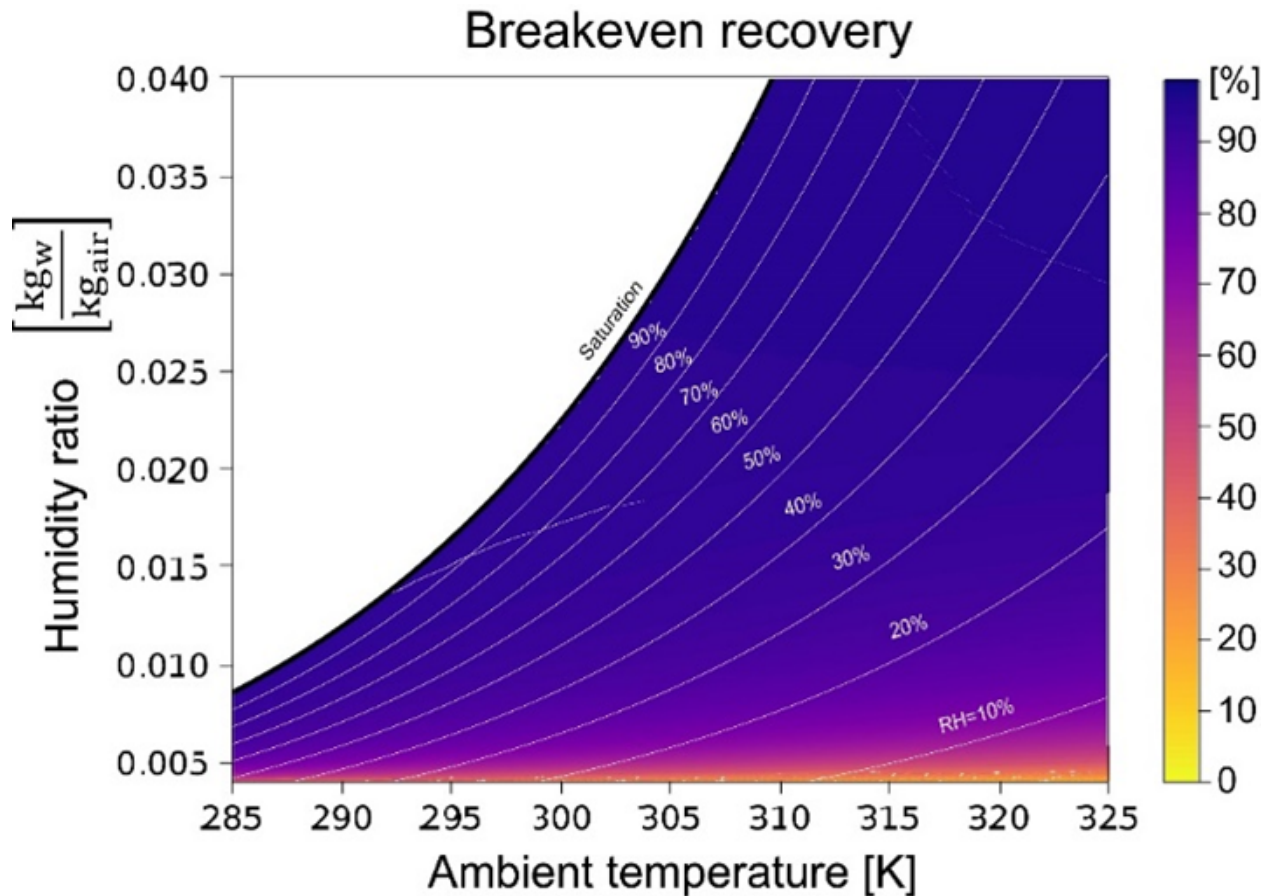


Figure B.12. The breakeven recovery represents the recovery ratio at which the membrane must operate to be energy-equivalent to dew harvesting. In the membrane system, it is always optimal to condense all the water vapor that passes through the membrane. In the case that this happens, the membrane system will require less energy than dew. However, achieving high recovery through heat exchangers may have practical limitations such as scaling and frost.

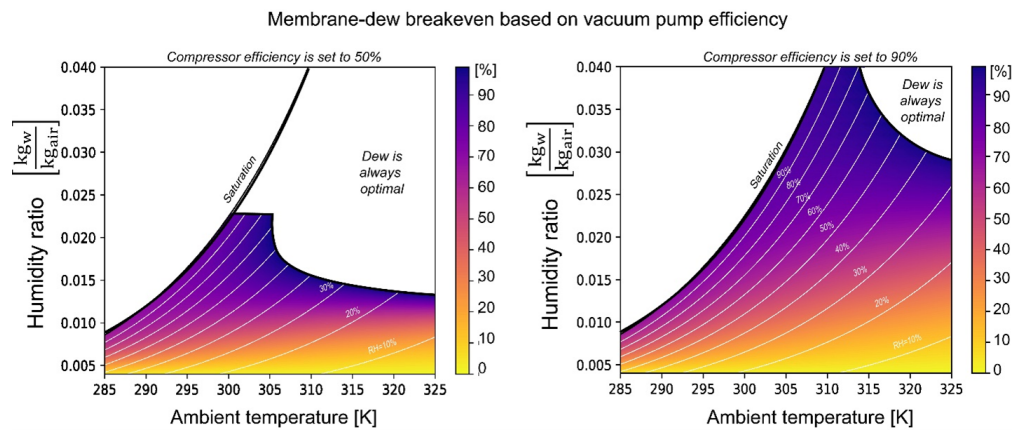


Figure B.13. The breakeven efficiency refers to the isentropic efficiency of the vacuum pump in the membrane system that allows the membrane to be energy-equivalent to the dew harvesting process. The figure on the left assumes a compressor efficiency of 50%, while the figure on the right sets the compressor efficiency to 90%. The sub-saturated region in white represents the area where dew is better than the membrane even with isentropic vacuum pumping. This white region becomes larger with lower compressor efficiency and lower recovery. The default recovery for the membrane system is 65%, which was chosen to create a fair comparison on the basis of yield with the MOF-sorbent process.

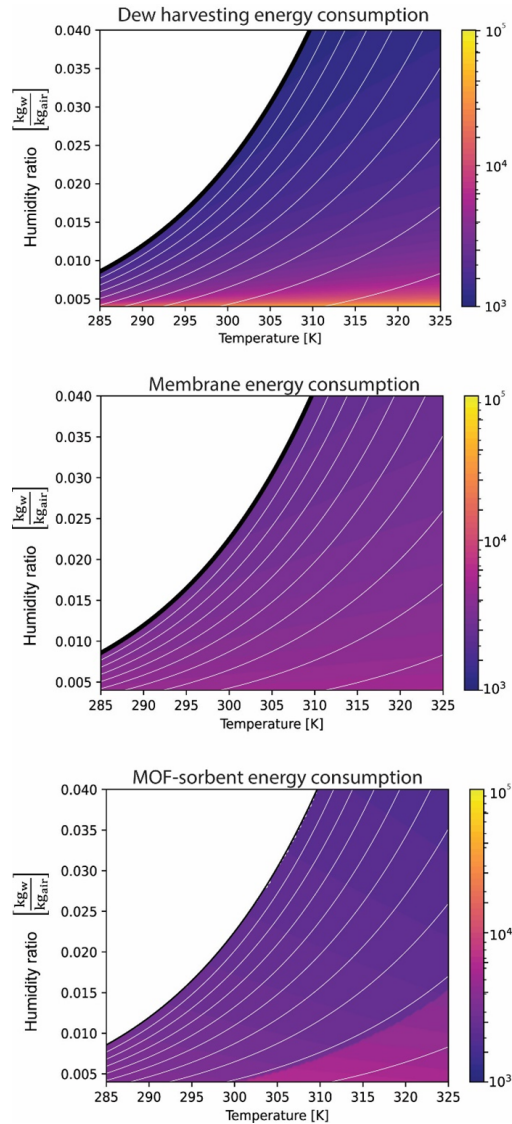


Figure B.14. Dew harvesting, membrane, and sorbent processes are modeled with cooling and heating coefficient of performances of 3 and pump isentropic efficiencies of 65% (compressor) and 20% (vacuum pump) [61], [70], [81]. This represents a first order estimate of current heating and cooling technologies, although in practice larger temperature differences will yield lower efficiency components and technologies for near-saturation pumping may encounter additional issues. The contour axis is represented on a log scale in units of kJ/kg.

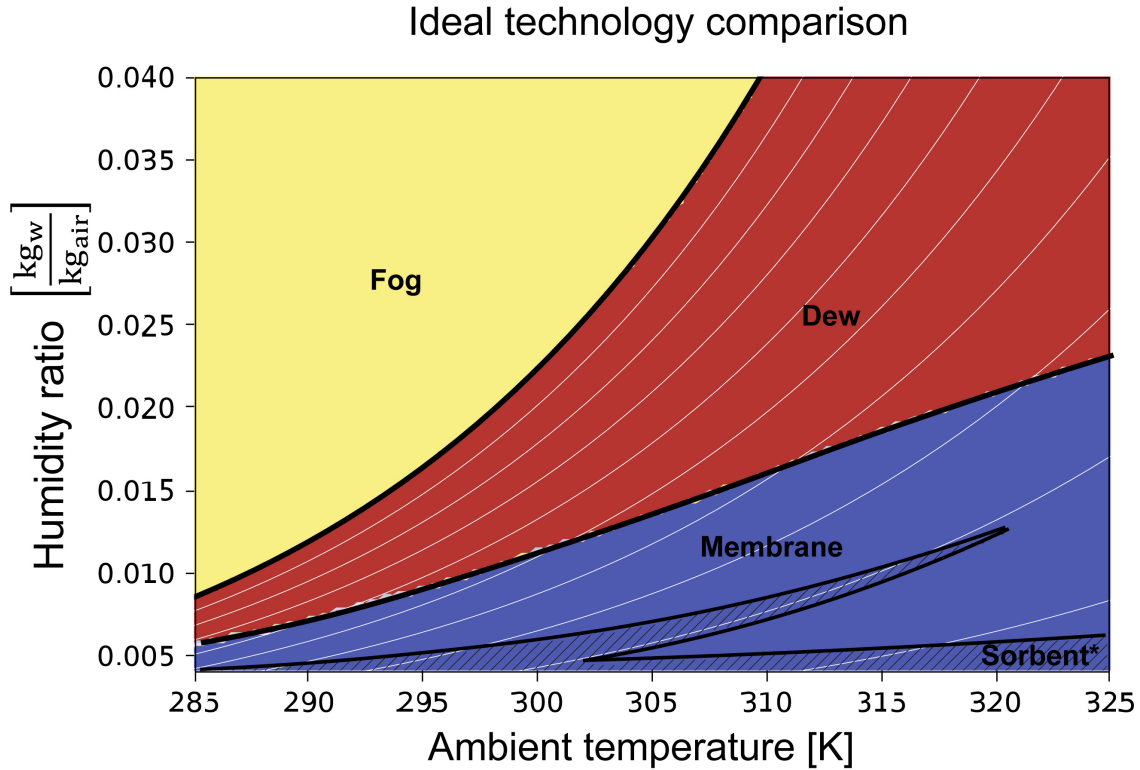


Figure B.15. Ideal processes are compared on the basis of energy efficiency. All heating and cooling are assumed to be conducted by a Carnot-like device. Fog harvesting (yellow) is optimal in supersaturated conditions. Dew harvesting (red) is optimal in high-humidity conditions. Membrane processes (blue) are optimal in low relative humidity conditions. Ideal sorbent systems are always sub-optimal when compared to membrane systems, however the dashed region shows where sorbent processes are better than dew harvesting. Furthermore, as the COP decreases (real systems may be 3 or less), the membrane processes become optimal at higher relative humidity. Additionally, the region where sorbent systems outperform dew harvesting also increases in area on the temperature-humidity plane. This analysis is conducted for open system processes and only consider thermodynamic optimality. Other factors may influence deployment such as technology cost and accessibility.

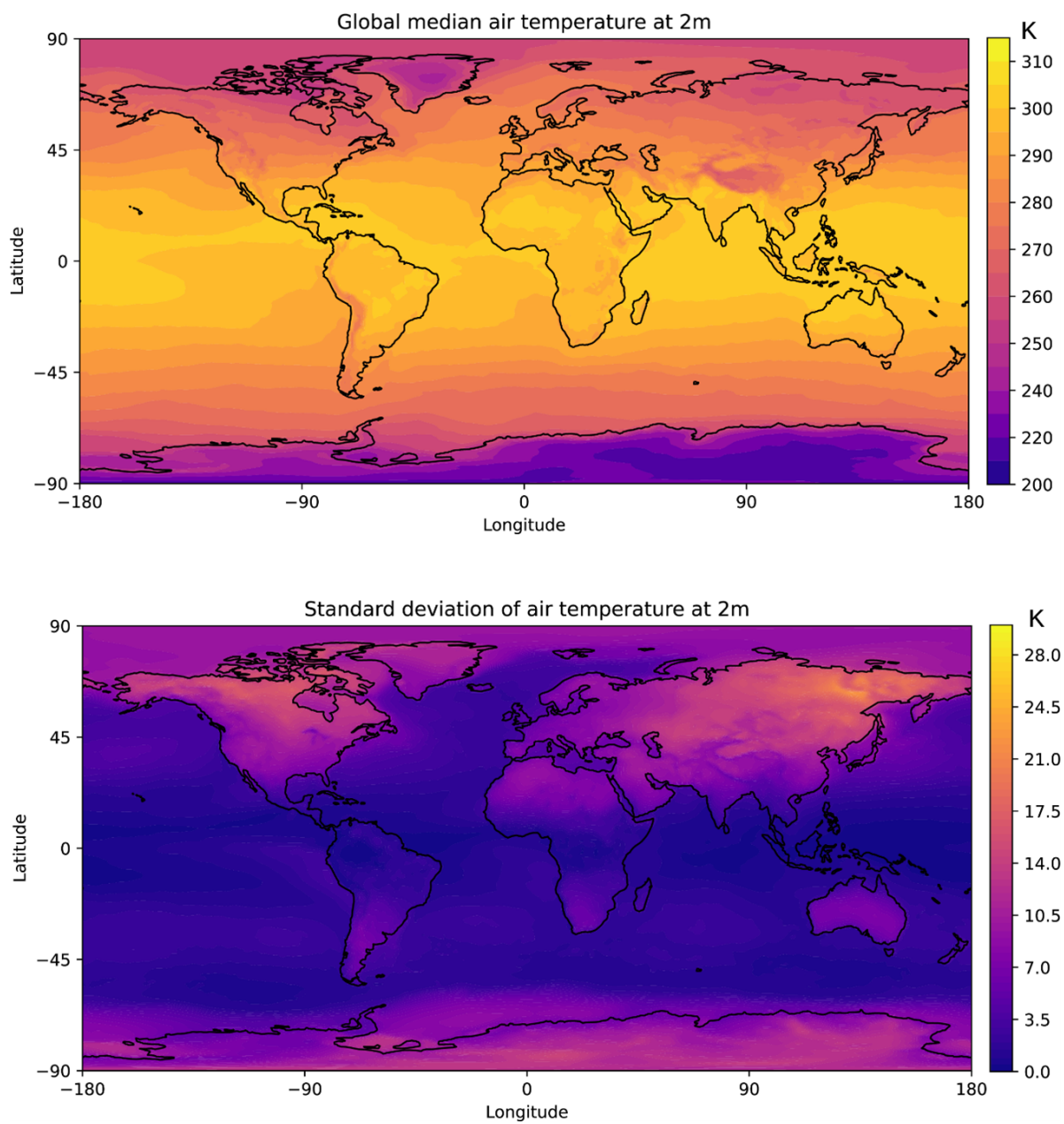


Figure B.16. The air temperature at 2m above the surface is mapped, based on the monthly NASA MERRA2 database [82]. The median and standard deviation are taken from monthly mean temperatures (January 2019 to January 2021).

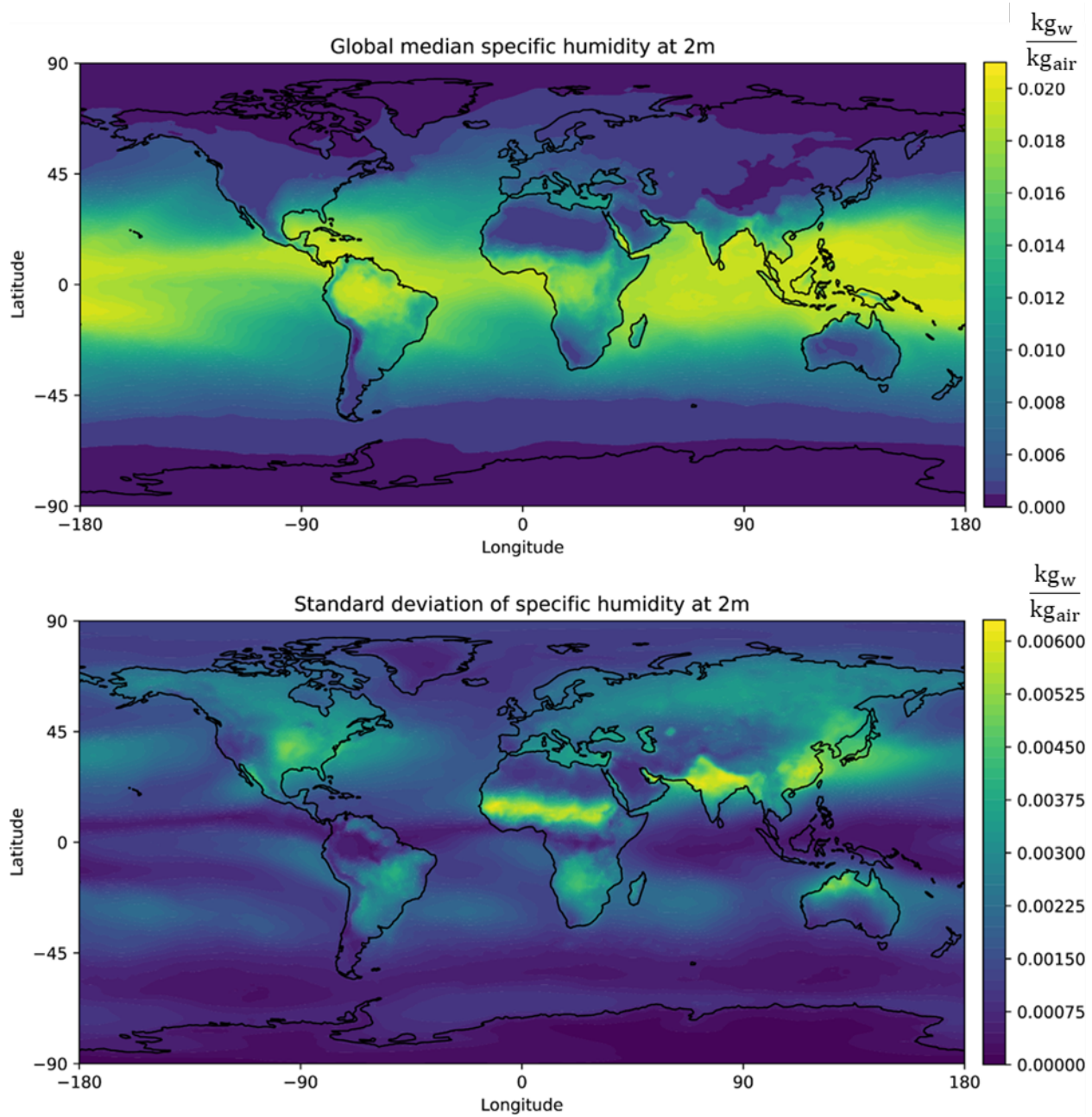


Figure B.17. The specific humidity at 2m above the surface is mapped, based on the monthly NASA MERRA2 database [82]. The median and standard deviation are taken from monthly mean temperatures (January 2019 to January 2021).

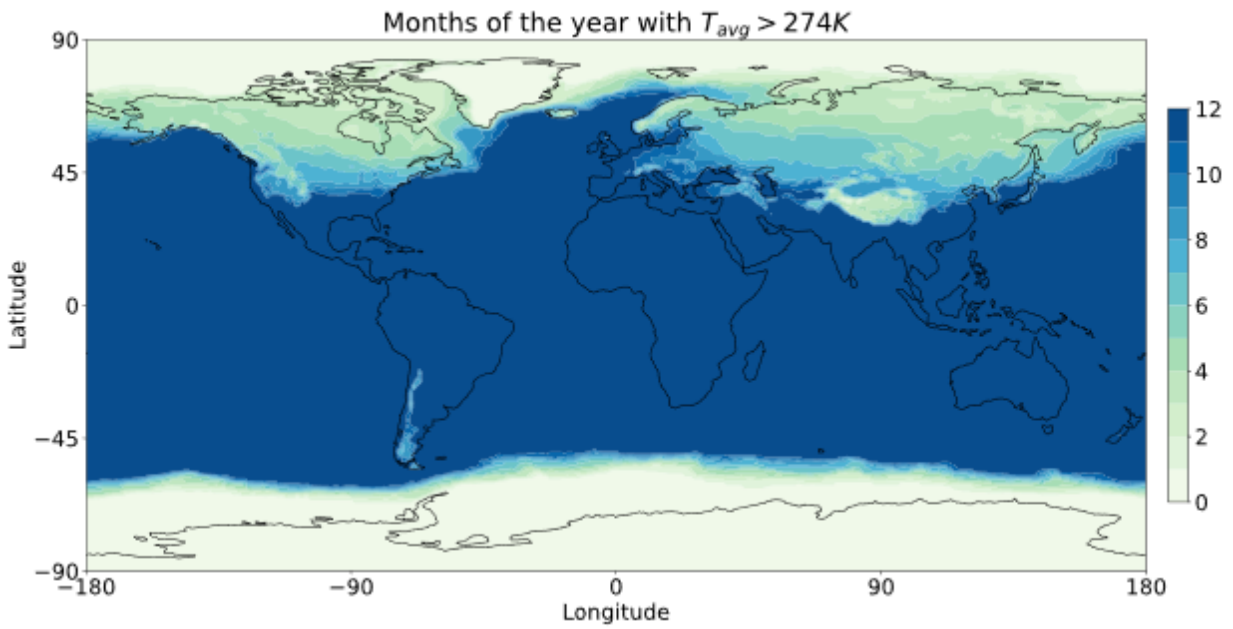


Figure B.18. The number of months in a year where the monthly average surface temperature is above 274K is mapped, based on the monthly NASA MERRA2 database [82]. This is averaged over 2019 and 2020. The evidence of global temperature rise should be noted [89].